Atlas of Bofedales in the Southern Tropical Andes: Spatial Distribution and Spatiotemporal Analysis

Dissertation

Presented in Partial Fulfillment of the Requirements for the Degree Doctor of Philosophy in the Graduate School of The Ohio State University

By

Gabriel Zeballos Castellon

Graduate Program in Geography

The Ohio State University

2022

Dissertation Committee

Dr. Bryan Mark, Advisor

Dr. Karina Yager

Dr. Alvaro Montenegro

Dr. Desheng Liu

Dr. Michael Durand

Abstract

Bofedales are ecologically defined as an Andean mountain wetland and peatland system, which constitute one of the most highly biodiverse and important hydroecological systems of the high Andes. Their geographic distribution is scattered across high mountain plateaus and glacier valleys across the Andean Cordilleras. Bofedales provide key environmental, social, and cultural services for pastoralist communities, including critical habitat for a wide range of wild flora and fauna, including livestock animals and endemic birds. Alterations to the regional climate processes, land use change, and rapid glacier retreat are affecting the sustainability and equilibrium of bofedales, leading to their degradation. Despite their importance for ecosystem services, there is a substantial gap about the geographical distribution of bofedales, which is a critical need in order to understand current threats and vulnerabilities to these systems, and a dearth of information about the range of biophysical patterns regarding the classes of bofedales and differing bio-geographical characteristics of bofedales across Andean region, including the seasonal to interannual patterns of vegetation productivity. In this research, I developed and applied new methodologies utilizing state-of-the-knowledge Earth Observation Systems analysis with extensive ground truthing, archival research of published studies, and mixed botanical field methods to create an Atlas of bofedales in the Southern Tropical Andes, including the countries of Peru, Bolivia, Chile, and Argentina. In particular this research has resulted in

the development of mapping products to address the academic gaps in bofedal distribution including 1) A baseline inventory of varying bofedal classes and a regional map of their distribution and size of bofedales for the Southern Tropical Andes, and 2) A comparative geo-botanical analysis of bofedal classes in three regions of the Bolivian Altiplano, and 3) An examination of the annual to seasonal trends of the vegetation indices of bofedales (i.e. Normalized Difference Vegetation Index), and an evaluation of the potential climatological drivers of their degradation to assess the degree of risk to their conservation.

Dedication

Dedico este documento a mi padre, Humberto Zeballos Flores, y a mi madre, Martha Luz Castellon Chávez. De ambos aprendí que las metas más importantes en la vida se logran con tenacidad, amor y dulce dedicación.

Acknowledgments

Agradezco a la Madre Tierra, a los Apus y Achachilas que nos protegen desde las alturas. Al Padre Chullunkhu y a la Madre Uma. A Tata Sajama, Illampu, Jankho Uma, Huayna Potosí, y a las Payachatas. Guardianes de los bofedales.

Agradezco a mi padre y a mi madre por todo el amor, dedicación, y cariño que me dieron durante toda su vida. Su apoyo y ejemplo fueron determinantes en el cumplimiento de mis sueños.

A mis hermanas Ximena y Patricia, por su cariño y por su apoyo. Ustedes fueron mis primeras maestras.

Agradezco a mi compañera de vida, de bailes, y aventuras, Thalía Pacheco Fernández, el amor de mi vida, porque con tu sonrisa, chispa, y dulzura también sacaste la mejor versión de mí.

Agradezco a mi asesor, amigo, y mentor Bryan Mark por su conocimiento, apoyo, amistad, y humildad. Gracias, Bryan, por tu motivación a cuestionarme y conducir mi investigación a mi propio modo y ritmo, por recordarme que todos somos seres humanos antes que estudiantes o profesores, por apostar por mí cuando yo me veía rendido, por tener las puertas de tu casa siempre abiertas, y por el hacky sack.

A Karina Yager por invitarme siempre a investigar, a indagar, y a ser curiosos de una manera divertida y por confiar en mí desde el principio.

A Rosa Isela Meneses Quisbert por la amistad, las enseñanzas, los viajes, y por mostrarme que el camino para entender los bofedales es a través del corazón tanto como la mente.

Agradezco al Parque Nacional Sajama, sus autoridades tradicionales, todos los compañeros locales, y al equipo de brillantes guardaparques.

I want to thank the Byrd Polar and Climate Research Center and to its fabulous team of researchers and staff and extend my gratitude to the Department of Geography of the Ohio State University.

I want to thank to all teachers and professors that trusted me, and shared their time with me, gave me advice, and taught me their knowledge, including Alvaro Soruco, Clea Paz Rivera, Kendra McSweeney, Ana Del Sarto, Elvia Andia Grajeda, Alvaro Montenegro, Desheng Liu, Manuel Molina, Miguel Angel Vera, Aaron Wilson, Ian Howat, Mike Durand, y Lonnie Thompson.

Agradezco a la Sociedad para el Avance de Hispanos/Chicanos y Nativos Americanos en la Ciencia y a los amigos y amigas que forman parte de este fantástico grupo.

A Kevin Guzmán Armijo y Sergio Paredes Noya por su inmensa ayuda. No hubiera llegado ni a la mitad sin Ustedes.

I want to thank to my colleagues who advanced with me side by side during different phases of my time at The Ohio State University: Rohit Mukherjee, Forrest Schoessaw, Tal Shutkin, Jeff Gunderson, Emily Sambuco, Emilio Mateo, and Bridget McGovern.

A los amigos y amigas en Bolivia que participaron en los viajes y las aventuras: Javier Maldonado, Filemón Quenallata, Estefanía Quenta-Herrera, Ana Patricia Sandoval, Humber Alberto, Diego Cusicanqui, Fabricio Medina Viscarra, René Cerezo.

Agradezco a los amigos y amigas que ya son mi familia de los Yunaites: Rohit Mukherjee, Sara Riva, Laura Rivas Burgos, Guille Bervejillo, Gabriel Guzman, Lorena Quiroga, Estelí Puente, Alfonso Gomez Urquiza Garcia, Laura Neese, Nora Sylvander, Ariel Rawson, Endya Clark. Gracias por todas las tardes en la biblioteca, por las jornadas de zumba, por las parrilladas, y las noches de cervezas. Soy millonario por contar con su amistad.

Curriculum Vitae

Gabriel Zeballos Castellon

Education

The Ohio State University, Columbus, OH
Ph.D. Geography, Expected in July 2022

Escuela Militar de Ingeniería, La Paz, Bolivia
Engineer in Geographic Systems, 2014

Universidad Mayor de San Andrés, La Paz, Bolivia
B.Sc. Biology, 2007

Work Experience

Department of Geography, The Ohio State University, OH
Instructor — Summer 2018, Summer 2020
Graduate Teaching Assistant — August 2016 – May 2020

Escuela Militar de Ingeniería, La Paz, Bolivia
Instructor — February 2014 – July 2016

Wildlife Conservation Society
GIS Consultant — August 2015 – July 2016

- Elaboration of the Conservation Management Plan for the Pampas del Yacuma Protected Area in Bolivia
- Organization of workshops with local communities in the Protected Area
- Geographic Information System Analysis and Mapping

Publications

Peer-reviewed Journal Articles

2019 K. Yager et al. "Socio-ecological dimensions of Andean pastoral landscape change: bridging traditional ecological knowledge and satellite image analysis in Sajama National Park, Bolivia." Regional Environmental Change (2019): 1-17.

2017 Mark, B.; Stansell, N.; Zeballos, G. The last deglaciation of Peru and Bolivia. Cuadernos de Investigación Geográfica. (0211-6820), 43 (2), p. 591. DOI: 10.18172/cig.3265

2017 O. Dangles et al. Ecosystem sentinels for climate change? Evidence of wetland cover changes over the last 30 years. PLoS ONE. DOI10.1371/journal.pone.0175814

2014 Zeballos, G., Soruco, et al. Uso de imágenes satelitales, modelos digitales de elevación y sistemas de información geográfica para caracterizar la dinámica espacial de glaciares y humedales de alta montaña en Bolivia. Ecología en Bolivia, 49(3), 14-26.

Chapters in Edited Books

2015 Meneses R., Ortuño, T., Loza Herrera, S., Domic, A. Palabral-Aguilera, A. & G. Zeballos. (2015). Bofedales altoandinos. Pp: 190 – 205. En: M. Isabel Moya, Meneses, R. & J. Sarmiento (Eds.). 2015. Historia Natural de un Valle en Los Andes: La Paz (2a Edición). Museo Nacional de Historia Natural, La Paz, Bolivia. 801 p.

Fields of Study

Major Field: Physical Geography

Research Specialties: Remote Sensing, GIS, Bofedales, Mountain Regions, Andes

Table of Contents

List of Tables

List of Figures

Chapter 1. Inventory of bofedales of the Southern Tropical Andes

Introduction

Bofedales are a group of high Andean wetlands, peatlands, and wet meadows situated along glacier valleys and high plateaus at altitudes above 3,200 m a.s.l. (Squeo, Warner et al. 2006, Maldonado Fonkén 2014, Meneses, Rosa, Ortuño et al. 2015, Yager, Prieto et al. 2021). Bofedales occur in Andean regions that are associated with diverse vegetation classes including arid grasslands, shrublands, salt flats and deserts, and they have year-round biomass productivity, are a habitat and source of food and water to a wide range of domesticated animals and wild life (Oyague, Cooper 2020, Maldonado Fonkén 2014) (Figure 1). These oasis-like characteristics were key for the survival of native wildlife and native human populations in the high Andes over several millennia, and especially since the peak of aridity of the Mid-Holocene (8.0 – 4.0 kyr BP) (Vining, Steinman et al. 2019). Today, the importance of bofedales relates to different aspects; they are the main component of the social-ecological landscape of the pastoral communities (Maldonado Fonkén 2014, Yager, Valdivia et al. 2019, Squeo, Warner et al. 2006); they have one of the highest carbon sequestration rate among other types of peatlands in the world (Earle, Warner et al. 2003, Hribljan, J. A., Cooper et al. 2015); and they support the regulation of hydrological cycles, thanks to their ability to absorb, retain, and clean water from glacier

melting, underground aquifers, snow, and rainfall (Yager, Prieto et al. 2021, Meneses, Rosa, Ortuño et al. 2015, Maldonado Fonkén 2014, Izquierdo, Foguet et al. 2015).

Figure 1. Bofedales of the Southern Tropical Andes supporting camelid livestock. A) A flat peatland in Sajama National Park, Bolivia, one of the largest bofedales in the Central Andes, B) An example of a small slope peatland in the Cordillera Real, Bolivia, C) An example of a basin bofedal in the Wila Llojeta glacier in Bolivia at 5050 m asl, one of the highest bofedal sites in the region, D) Bofedal ecosystems serve as refuge

to numerous wild species including the Andean goose (Chloephaga melanoptera) and the Andean flamingo (Pheonicoparrus jamesii).

Considering that most of the tropical glaciers in the Andes will significantly retreat in the next decades (Rabatel, Francou et al. 2013, Veettil, Bijeesh Kozhikkodan, Wang et al. 2017), the importance of bofedales as reservoirs of water in the Andes is likely to increase in the future (Maldonado Fonkén 2014). However, a combination of factors, related to the alterations to the climate, land use changes, and the rapid glacier retreat itself, is affecting bofedales, causing their degradation, accelerating their area loss (Yager, Valdivia et al. 2019). Multiple observations indicate a potential link between droughts, degradation of bofedales, and the death of animals that depend on them as a source of food and water (Figure 2B and 2C).

Figure 2. Peatland degradation in the Bolivian Altiplano. A) Healthy cushions of Distichia muscoides rise above the saturated soils. B) Example of an unhealthy

peatland. The organic matter beneath the vegetation became visible. C) During the El Niño drought of 2015 – 2016, thousands of camelids died due to the desiccation of peatlands (Photo credit: Pastoralist from Sajama National Park in Bolivia).

To understand the degree of damage and risk that these ecosystems face and to develop adequate management guidelines, it is first necessary to identify a baseline of the number, size, and geographic distribution of these ecosystems. Yet, this information is incomplete for large portions of the Southern Tropics of the Andes. Complete inventories of bofedales are only available for the Northern Chile and Northwestern Argentina (Izquierdo, Foguet et al. 2015, Chávez, Christie et al. 2019) and over some portions of Peru and Bolivia. However, the methods of quantification of peatlands vary greatly among these different studies, which becomes a problem when trying to compare the results and distribution maps. The gaps of information and discordance of methods are due in part to the bofedales' remoteness and inaccessibility, and also for lack of effectively integrating remote sensing tools with extensive ground assessments recognizing their occurrence at multiple scales.

Remote sensing (RS) tools and systems are the most common tool to map wetlands at multiple scales in many regions of the world (Guo, Li et al. 2017, Amani, Ghorbanian et al. 2020, Kandus, Minotti et al. 2018) and have shown to be effective to delineate bofedales in the Andes (Dangles, Rabatel et al. 2017, Otto, M., Höpfner et al. 2016, Garcia, E., Otto 2015, Yager, Valdivia et al. 2019, Polk, Young et al. 2017, Navarro, C. 2020). However, mapping bofedales at large scales with RS tools introduces additional challenges regarding the precision and quality of the data. In this study, I combined state-of-the-knowledge satellite image analysis with thorough field botanical observations, literature review, and ground truthing assessments to produce a comprehensive map and inventory of the

bofedales in the Southern Tropical Andes in order to create a baseline atlas with updated information of their spatial distribution. Such information would allow decision-makers, stakeholders, local communities, and conservation groups that work or depend on bofedales for their livelihoods to make informed policy and land management actions towards their conservation and sustainability.

Background

Bofedales

In a broad sense, bofedales refer to any alpine wet meadow in the tropical and subtropical Andes, dominated by peat-forming, densely packed, vascular plants that are arranged in complex hydrological networks (Meneses, Rosa, Ortuño et al. 2015, Yager, Valdivia et al. 2019, Maldonado Fonkén 2014). Bofedales are azonal ecosystems, which means that their occurrence depends on the availability of water and nutrients with little influence from the regional climatic characteristics (Yager, Valdivia et al. 2019). For this reason, bofedales occur along a great latitudinal gradient among the different ecoregions that comprise the alpine belt of the Andes (See the section on Southern Tropical Andes). The ecoregions where bofedales can be found are the *Paramo* and *Jalca* (i.e. the wetter Northern Andes), and the *Puna* (i.e. the drier Southern Andes) (Britto 2017). Consequently, bofedales will potentially occur in either of these ecoregions with four main geophysical conditions: freezing temperatures, continuous availability of water, availability of nutrients, and the presence of seed-dispersing animals (Squeo, Warner et al. 2006). Bofedales found in lower altitudinal ranges (from 3,200 m to 4,000 m), occur depending on the latitude and ecoregion (Squeo, Warner et al. 2006, Izquierdo, Foguet et al. 2015). Above these elevations they

occupy two altitudinal tiers: Altiplano and Puna, (< 4,100 m asl), and *Altoandino* (> 4,100 m a.s.l.) (Squeo, Warner et al. 2006, Izquierdo, Foguet et al. 2015).

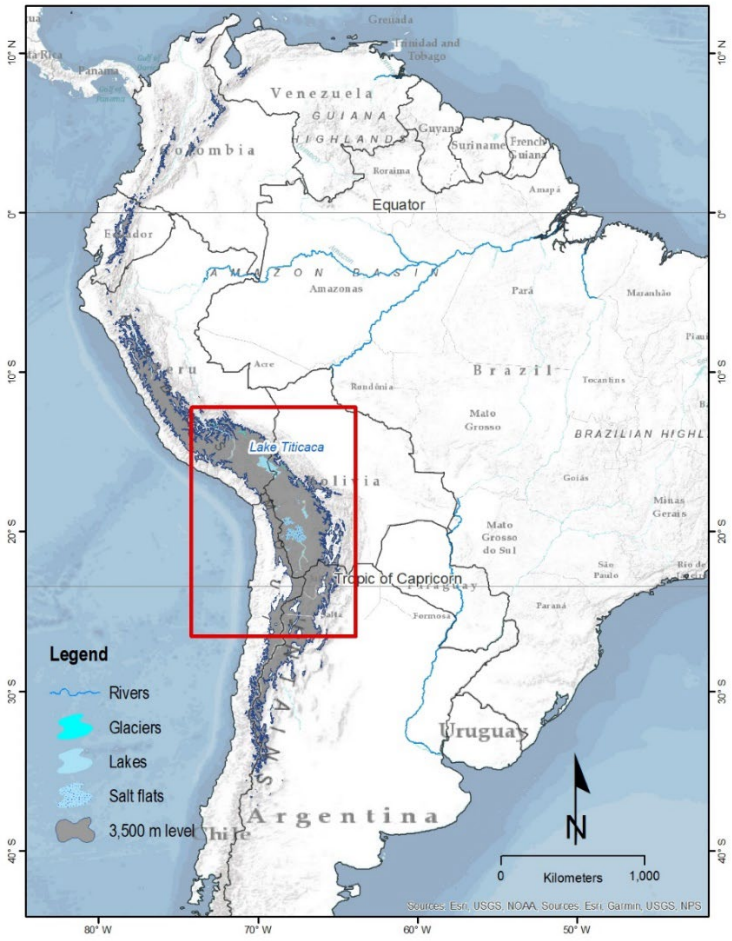

Figure 3. Map of the High Andes. Bofedales occur on the Alpine belt, above 3,200 to 3,800 m a.s.l. The Southern tropics, between 14 ° and 25 ° South, are shown in the red box .

The characteristics used to define and classify bofedales include, but are not limited to, the plant species composition, characteristics of the soil (regarding the texture, structure or organic matter percentage), their hydrological and ecological function, and the local traditional use (White-Nockleby, Prieto et al. 2021). From an exclusively botanical

perspective, the dominant plant species that define the occurrence of Andean bofedal peatlands include the cushion-like peat-forming *Distichia muscoides* (Figure 4A), *D. filamentosa, Oxychloe andina* (Figure 4B), and *Patosia clandestine* (Squeo, Warner et al. 2006, Yager, Prieto et al. 2021). These species belong to the Juncaceous family and are well adapted to water saturated conditions and daily freeze-thaw cycles, common climatic characteristic of the subglacial landscapes in the high Andes (White-Nockleby, Prieto et al. 2021, Yager, Prieto et al. 2021, Beck, Stephan, Domic et al. 2010) (Korner 2003). Vascular species like these, which require constant water saturation, are called wetland obligate species (Mitsch, Gosselink 2015) (Figure 5A).

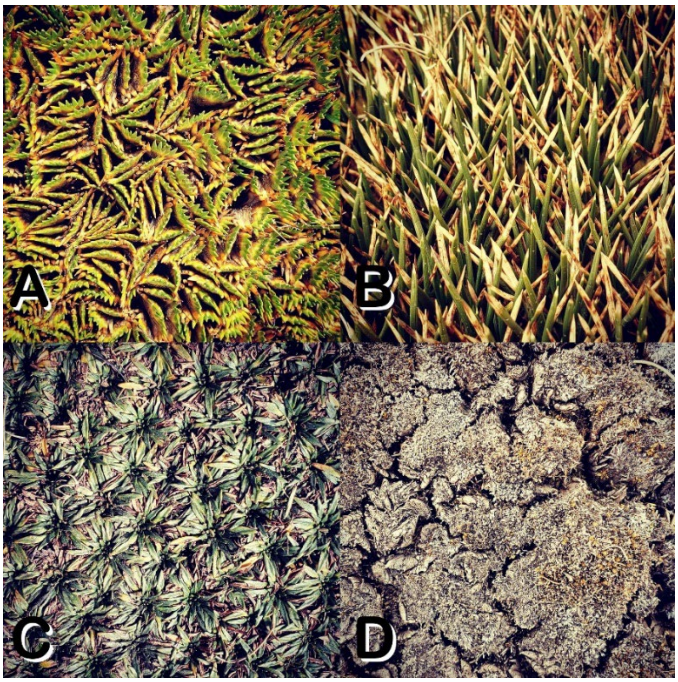

Figure 4. Bofedal predominant species. A) Distichia muscoides, B) Oxychloe andina, C) Plantago tubulosa, and D) a dead individual of Distichia muscoides.

Another group of plant species typically associated with Andean wet meadows and in drier classes of bofedales include *Plantago tubulosa* (Figure 4C), and other species less adapted

to water saturation (wetland facultative species), belonging to the Cyperaceae, Plantaginaceae, and Gramineae families, which may occur interstitially or peripherally to the wetland obligate species. Together, obligate, and facultative species form mosaics where the dominance of a particular species may vary between sites (Yager, Prieto et al. 2021) (Figure 5C and 5D). In general, facultative species are stronger in temporally saturated soils and drier conditions. They play an important role in the transition (called succession) between the wetland and the upland boundaries (Mitsch, Gosselink 2015). When the peatland mosaics lack any of the obligate wetland species, the facultative species may only form wet meadows, locally known as *vegas*, or in association with mixed dry Gramineae species locally termed *porqe* (Beck, Stephan, Domic et al. 2010, Yager, Valdivia et al. 2019) (Figure 5B). Vegas have less percentage of organic matter in the soil, they don't form peat, and have a lower capability to retain water. On the other hand, the bofedales dominated by wetland obligate species form peat, which are often several meters in depth, make them important carbon sinks (Hribljan, J. A., Cooper et al. 2015, Cooper, Kaczynski et al. 2015). Peat-forming bofedales have the largest percentages of organic matter in the soil, compared to vegas or other types of Andean vegetation classes (Earle, Warner et al. 2003) and can hold water for longer periods (Valois, Schaffer et al. 2020).

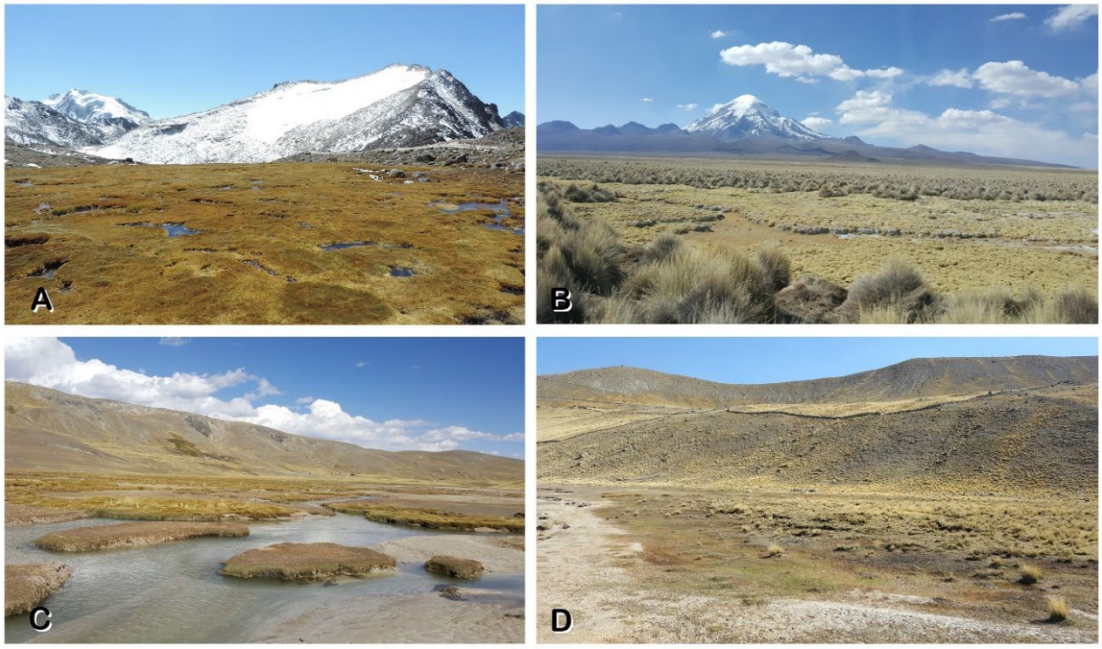

Figure 5. Varying types of bofedales found in the tropical Andes. A) Dense bofedal dominated by Distichia sp., a peat forming juncaceous plant (Cordillera Real), B) Dry bofedal with increasing presence of Deyeuxia curvula, a non-peat forming graminoid (Sajama National Park), C) and D) Mixed bofedales forming mosaics of peat and non-peat forming plants (Cordillera Real).

Use of satellite sensors to study bofedales

The identification and mapping of vegetation cover using satellite sensors is a widely spread practice (Jensen 2009). While remote sensing techniques may have some limitations discriminating specific features of the landscape, they are very powerful when studying ecosystems at various scales or periods. Satellite sensors vary in terms of spatial, temporal, spectral, and radiometric resolutions (Table 1).

Table 1. Summary of the main satellite sensors used in the study of bofedales.

Parameters	Landsat 5 (Thematic Mapper)		Landsat 7 (Enhanced Thematic Mapper)		Landsat 8-9 (Operational Land Imager)		Sentinel-2 (MultiSpectral Instrument)	
Spectral Bands [µm]	1 (blue)	0.45-0.52	1 (blue)	0.45–0.52	1 (blue)	0.43-0.45	B1 (blue)	0.43-0.45
	2 (green)	0.52-0.60	2 (green)	0.52–0.60	2 (blue)	0.45–0.52	B2 (blue)	0.46–0.52
	3 (red)	0.63-0.69	3 (red)	0.63–0.69	3 (green)	0.52–0.60	B3 (green)	0.54–0.58
					4 (red)	0.63–0.68	B4 (red)	0.65-0.68
							B5 (red edge)	0.70-0.71
							B6 (red edge)	0.73-0.75
							B7 (red edge)	0.77-0.79
	4 (NIR)	0.76-0.90	4 (NIR)	0.76–0.90			B8 (NIR)	0.78-0.90
					5 (NIR)	0.84-0.88	B8a (NIR)	0.86-0.88
							B9 (water vapor)	0.93-0.95
					9 (cirrus)	1.36-1.39	B10 (cirrus)	1.37-1.39
	5 (SWIR1)	1.55-1.75	5 (SWIR1)	1.55–1.75	6 (SWIR1)	1.56-1.66	B11 (SWIR1)	1.57-1.66
	7 (SWIR2)	2.08-2.35	7 (SWIR2)	2.08–2.35	7 (SWIR2)	2.10-2.30	B12 (SWRIR2)	2.10-2.28
	6 (TIR)	10.40-12.50	6 (TIR)	10.4–12.5	10 (TIR1)	10.3-11.3		
					11 (TIR2)	11.5-12.5		
Spatial resolution [m]	30	VNIR	30	VNIR	30	VNIR	10	(B2, B3, B4, B8)
			15	Panchromatic	15	Panchromatic	20	(B5, B6, B7, B8a, B11, B12)
	120	TIR	60	TIR	100	TIR	60	(B1, B9, B10)
Radiometric resolution [bit]	8		8		16		12	
Temporal resolution [days]	16		16		8		5	
FOV	Up to 7.2°off nadir		Up to 7.5°off nadir		Up to 7.5°off nadir		Up to 10.3° off nadir	
Orbit [km]	705		705		705		786	
Frame width [km]	185		185		185		290	
Architecture	Cross-track scanner (Whiskbroom)		Cross-track scanner (Whiskbroom)		Pushbroom		Pushbroom	

In addition, some satellite sensors have wide accessibility and provide reliable data to map and monitor peatlands. Low spatial resolution sensors (250 to 1000 m/pixel), such as the Moderate Resolution Imaging Spectroradiometer (MODIS), or the Advanced Very High Resolution Radiometer (AVHRR), are too coarse to delineate peatlands (Zorogastúa-Cruz

2012, Ozesmi, Bauer 2002), but have been successfully used to perform multitemporal analysis of peatlands thanks to their very high temporal resolution (1 day frequency) (Baldassini, Volante et al. 2012, Polk, Mishra et al. 2020, Casagranda, Navarro et al. 2019, García, C. L., Teich et al. 2019, Moreau, Bosseno et al. 2003) (Figure 6). On the other hand, moderate resolution sensors (10 to 60 m/pixel) have a more balanced trade-off between temporal and spatial resolutions for both, mapping and change analysis studies. Among these sensors, the most reliable for long-term monitoring of vegetation are available from NASA's Landsat program (See Table 1). Since the launch of the Thematic Mapper (TM) sensor in 1984, the Landsat program have kept strong consistency in their orbital geometry, spatial and temporal resolutions, and multispectral characteristics (Rocchio, Connot et al. 2018). Thus, Landsat imagery have been used to generate multi-decadal spatiotemporal analysis of Andean peatlands at a local and regional scale (Mazzarino, Finn 2016, Casagranda, Navarro et al. 2019, Dangles, Rabatel et al. 2017, Hartman, Bookhagen et al. 2016, Bury, Mark et al. 2013, Postigo, Young et al. 2008, Garcia, E., Otto 2015, Soto, Román-Figueroa et al. 2019, Yager, Valdivia et al. 2019). In-between Low and Moderate resolution sensors is the Landsat's Multispectral Scanner Systems (MSS). The Landsat MSS provide sparse images since 1972 but only two studies used this data (Zorogastúa-Cruz 2012, Washington-Allen, Ramsey et al. 1998) because, in general, the MSS's spatial resolution (80 m, resampled to 60 m) is not suitable to detect individual wetland systems (Zorogastúa-Cruz 2012, Guo, Li et al. 2017).

Since its launch in 2015, some researchers have used the Sentinel-2 Multispectral Instrument (MSI) (10m/pixel) to study high Andean peatlands (Jara, Delegido et al. 2019,

Araya-López, Lopatin et al. 2018). Sentinel-2 is a constellation of two satellites (Sentinel-2A launched in 2015, and Sentinel-2B in 2017) with identical geometry and a temporal resolution (10 days each). Sentinel-2A/B imagery has equivalent geometric characteristics with those from Landsat, which technically allows combining both datasets to monitor the landscape on wetland ecosystems (Pahlevan, Chittimalli et al. 2019, Wang, Wan et al. 2018, Mandanici, Bitelli 2016). Furthermore, when compared with Landsat to delineate bofedales, Sentinel-2A/B has shown to have better accuracy (Jara, Delegido et al. 2019).

Finally, high-resolution sensors have only been applied for mapping small study areas (Dangles, Rabatel et al. 2017, Araya-López, Lopatin et al. 2018, Fonseca, Godoy et al. 2012). In their comparison of Sentinel-2 and Worldview-2 (0.46 m/pixel), Araya-Lopez et al. (2018) showed similar results monitoring Andean wetlands in the Altiplano. However, high-resolution imagery can be also used as control data to classify moderate-resolution products. For instance, Dangles et al. (2017) combined PLEIADES imagery with Landsat TM to determine an accurate NDVI (Normalized Difference Vegetation Index) threshold of multitemporal imagery. In some cases, high-resolution imagery obtained from Google Earth Pro was also used as validation data to classify wetlands on Landsat imagery (Izquierdo, Foguet et al. 2015). In addition, Google Earth Pro's 'History' tool and high-resolution products are very helpful for planning mapping projects and spatiotemporal analysis. However, the geometrical and radiometrical quality of their products is not specified and may vary between regions (Tooth 2015).

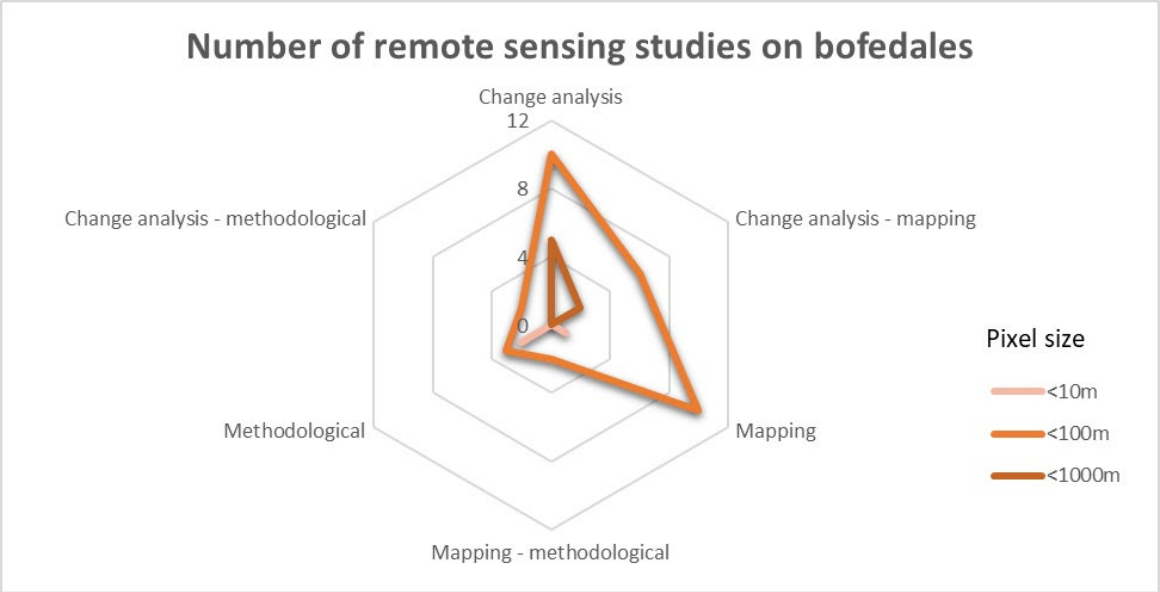

Figure 6. Number of satellite sensors used in detection of bofedales in relation to objective and spatial scale.

Bofedales' delineation

From the use of vegetation indices to supervised and unsupervised classifications, the methods applied to delineate peatlands in the high Andes often vary from study to study. Vegetation indices are the most widespread method to identify all wetlands in general, and, among them, the Normalized Difference of Vegetation Index (NDVI) is the most used index for mapping and detecting changes in peatlands. The NDVI was developed in the 1970s to detect the presence and intensity of photosynthetic activity on the land surface (Tucker 1979). The NDVI is a dimensionless, radiometric measure that helps differentiate the abundance of photosynthetic activity of the landscape. This index consists of dividing the difference between the surface reflectivity values of the Near-Infrared and the Red electromagnetic bands with the sum of both (Bhandari, Kumar et al. 2012).

$$NDVI = \frac{\rho_{nir} - \rho_{red}}{\rho_{nir} + \rho_{red}}$$

As a result, NDVI values span from -1 to +1 (low or non- reflectance (little to sparse vegetation) to high reflectivity (vegetation). A positive NDVI value may correspond to different types of vegetation cover, and thresholds can be applied to differentiate the spectral signatures of the referred type of vegetation. These threshold values vary depending on the plant species, phenological state, or health conditions, but also are influenced by the climate, presence of water, shading & elevation, type of sensor, or the position of the sun (Rojo, Arzamendia et al. 2019). Usually, the threshold value of a particular type of vegetation cover is determined by 1) using field control data, 2) comparing the NDVI image with higher resolution images, or 3) adopting and testing threshold values existing in the literature, or 4) collecting sampled spectral reflectance values from instruments in the field.

The physical principles of the NDVI concept apply ideally for detecting and delineating peatlands, especially if less dense and drier vegetation surrounds them. But because high Andean peatlands may occur sometimes surrounded by forests, shrublands, or other ecosystems with similar NDVI values (especially in lower latitudes), differentiating vegetation classes is a challenge resulting in some studies combining this index with other indices in their classification algorithms. Other applied indices detect the water content (Normalized Difference of Water Index - NDWI, Land Surface Water Index - LSWI), correct the soil brightness (Tasseled Cap Transformation - TCT), or enhance other vegetation characteristics (Normalized Difference Infrared Index - NDII, TCT) (Jensen 2009). The studies regarding peatlands and bofedales that combined two or more indices

had either a modified methodological approach (Aponte-Saravia, Ospina-Noreña 2019, Garcia, E., Otto 2015, Garcia, J. L., Willems 2015, Jara, Delegido et al. 2019, Zeballos, Soruco et al. 2014), (Garcia, E., Otto 2015, Jara, Delegido et al. 2019, Otto, M., Scherer et al. 2011, Rojo, Arzamendia et al. 2019) or altered change analysis objectives (Garcia, E., Otto 2015).

In addition to the processing imagery, data about the landscape that comes from other sources different to satellite imagery (known as ancillary information) is helpful to improve the classification results (Ozesmi, Bauer 2002). From topographic maps, digital elevation models (DEM), or ecosystem distribution maps, the ancillary information helps researchers to narrow down the areas where peatlands can potentially occur. For example, large peatlands occur mostly on flat low-steeped areas along the bottom of glacier valleys or riverbanks (Squeo, Warner et al. 2006). Therefore, elevation above sea level or steep slope angles, derived from Digital Elevation Models (DEM) may help masking out areas where peatlands are not likely to occur (Hribljan, John A., Suarez et al. 2017, García, E., Lleellish 2012, Fonseca, Godoy et al. 2012).

Peatland mapping and inventory

Since the beginning of this century, mapping and inventorying bofedales has been a common application of the remote sensing tools (Prieto, Alzérreca et al. 2001). In the Andes, these inventories were performed at national, regional, and local scales, like natural protected areas, or certain micro basins. To date, a total inventory of peatlands has been done only in Chile and Argentina (Izquierdo, Foguet et al. 2015, Tapia Molina 2014, Direccion General de Aguas de Chile 2022), whereas Peru is currently preparing their own

national inventories (Tovar Narváez 2018). The absence of spatial distribution information in large portions of the Andean Cordilleras responds to the lack of standardized methods of classification and the complexity of the wetlands, peatlands, bofedales, and the orographic complexity of the environments wherein they are found. Therefore, there remains uncertainty in how many or how much area do the bofedales cover across the Andean Cordilleras.

On the other hand, the current inventories and studies done at smaller scales have thrown some light to understand the drivers that determine the distribution of wetlands. The factors that determine the size and concentration of bofedales are related to the altitude, latitude, the meteorological conditions, the proximity to glaciers, and the topography of the basins that contain them. For example, in the Chilean Altiplano, which mostly comprises the Dry Puna ecoregion, Chávez et al. (Chávez, Christie et al. 2019) found that most bofedales occur either at latitudes between 17° and 19° S, in the range of 4,000 and 4,500 m a.s.l., and in areas with slopes lower than 5%. In contrast, in the Argentine Dry and Central Puna, the bofedales average elevation is slightly above 4000 m asl, with more than half of the total area occurring between 3500 and 4500 m asl, and the majority occurring in the North-Eastern portion (part of the Central Puna ecoregion) (Izquierdo, Foguet et al. 2015). In Bolivia, the regional scale study done by Prieto et al. (Prieto, Alzérreca et al. 2001) indicate that the dominance of certain species within the bofedal varies with altitude, and water chemistry.

In the Cordillera Blanca in Peru, located in the northern part of the Central Puna, (Chimner, Bourgeau-Chavez et al. 2019) found a larger concentration of bofedales, in part because

the authors considered smaller peatlands, but also because this region holds the largest portion of tropical glaciers in the world, which provides a relatively stable source of water to the wetlands (Bury, Mark et al. 2013, Veettil, Bijeesh K., Kamp 2017). Despite this difference, bofedales in the Cordillera Blanca have a similar altitudinal range than in the Chilean Puna (between 3950 and 4650 m asl). Chimner et al. (2019) also identified that meadows dominate the bottom of the large U-shaped glacier valleys, whereas peatlands are more common at higher altitudes, which concords with Prieto et al. (2001).

Regarding the size, the distribution of size of peatlands does not have a Gauss distribution. Smaller peatlands are much more frequent than larger ones and while a few peatlands can be very large (i.e. > 100 km^2), the average size lies around 90,000 m^2 (Chávez, Christie et al. 2019, Izquierdo, Foguet et al. 2015) (Table 2).

Table 2. Summary of regional inventories of peatlands in the Central Andes.

Author	Year	Region	Number	Average size [m^2]	Total surface area [km^2]
Chavez et al.	2019	Chilean Altiplano	5665	90,074	510.27
Chimner et al	2019	Huascarán National Park	ND	ND	384.44
INRENA	2002	Peru	ND	ND	5,493.60
Izquierdo et al.	2015	Argentine Puna	10,428	90,552	944.28
Prieto et al.	2001	Bolivian Altiplano	1586	645,275	1,023.41

ND = No data

Southern Tropical Andes

The Southern Tropical Andes extend from 14° to 28° S in latitude across the borders of Peru, Bolivia, Chile and Argentina (Jomelli, Favier et al. 2009, Morrone 2002, Veettil, Bijeesh K., Kamp 2017) (Figure 3). This region is limited by series of individual stratigraphic volcanoes on the West, and serrated ranges of mountains, from extrusion

rocks, on the wetter Eastern ranges. In the center, a vast endorheic plateau, called the Altiplano, contains the largest and highest lakes and salt flats in the continent (e.g., Lake Titicaca, Lake Poopo, Uyuni salt flat), along with several conical hills and ephemeral lakes (Lamb 2004).

In this region, bofedales occur above 3,800 m a.s.l. (Maldonado Fonkén 2014), which falls within the phytogeographical provinces of the Puna (below 4,000 m a.s.l.), and the Altoandino (above 4,000 m a.s.l.) (Cabrera, Willink 1973) (Figure 7A). These provinces belong to the Andean-Patagonic Domain of the Neotropical Region of the World (Cabrera, Willink 1973) and occupy the highest portions of the Central Andes from 10° S to the North (around Cajamarca, Peru), to around 32°S (in San Juan, Argentina) (Matteucci, Morello et al. 2012). At these elevations, the vegetation is adapted to cold temperatures and a strong seasonality of precipitation, which may be snow during some times of the year, or even round-year in the areas that are above the snowline level (~4,800 m a.s.l.). The plant forms that comprise the Puna and the Altoandino provinces include grasslands, shrublands, low forests, and meadows (Cabrera, Willink 1973). However, large portions of this territory are also covered by croplands, bare soil, rocks, salt flats, high altitude lakes, or glaciated mountains. Along their large altitudinal and latitudinal gradient, there is a strong heterogeneity in the floristic structure and composition, conditioned at a large scale by the climatic characteristics, and at a smaller scale by local topographic, microclimatic, ecological, or even anthropogenic factors (Beck, S. G., García et al. 2015).

Because of the cold climate and clear dry seasons, the vegetation of the Puna comprises low shrubs, tussock grasslands, or cushion or rug-shaped humid meadows. The plants of

the Puna have developed different morphologic strategies to respond to the water stress, cold temperatures, and strong sun radiation, like having small, hard, or needle-shaped leafs, abundant resinous secretions, dense cover of trichomes, or deep and strong root systems (Cabrera, Willink 1973, Korner 2003).

The Puna and the Altoandino phytogeographical provinces are usually considered together as a single ecogeographical region (ecoregion), called also Puna (Griffith, Omernik et al. 1998, Olson, Dinerstein et al. 2001, Rivas-Martínez, Navarro et al. 2011). From different perspectives, several authors describe different extensions and subdivisions of the Puna ecoregion (López, Zambrana-Torrelio 2006). For example, while Rivas-Martinez et al. (Rivas-Martínez, Navarro et al. 2011) subdivides the Puna latitudinally into two provinces: Mesophytic Puna to the wetter North, and the Xerophytic Puna to the drier South (Figure 7B). Olson et al. (Olson, Dinerstein et al. 2001) considers a longitudinal gradient as well, with three subregions, the Central Andean Wet Puna, the Central Andean Puna, and the Central Andean Dry Puna. For them, the Central Puna has two separated portions, one in Peru to the Northwest, and one in the Eastern hills of the Bolivian and Argentinian Andes to the Southeastern side of the Southern Tropics (Figure 7).

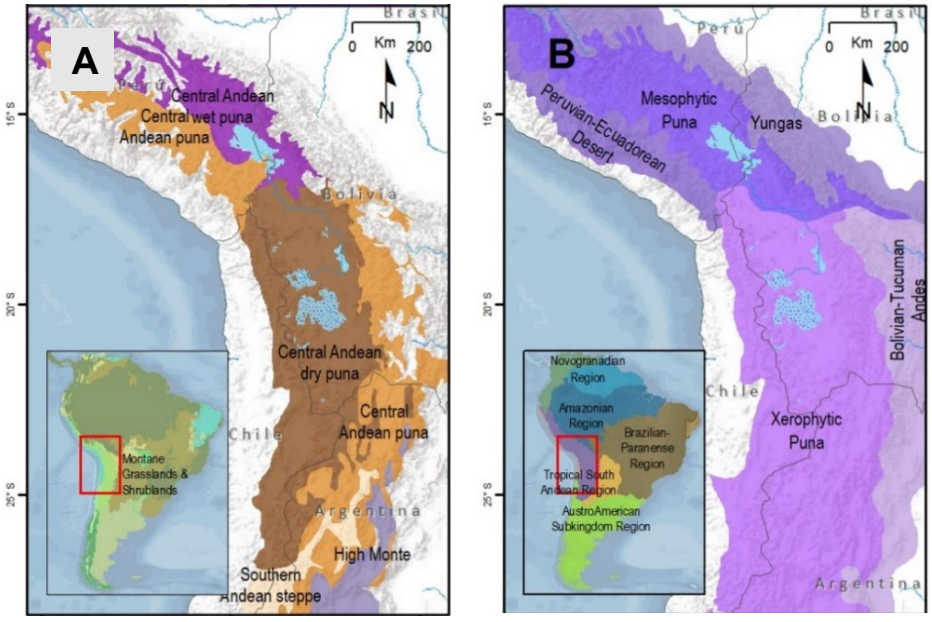

Figure 7. Ecoregion Maps of the Southern Tropical Andes. A) Based on Olson et al. (2001). B) Based on Rivas-Martinez et al. (2011).

Despite these differences, the occurrence of certain bofedales species, such as *Oxychloe andina, Distichia muscoides,* (Figure 4B and C), or *Patosia clandestina*, is transversal to all Puna subregions because of the bofedales' azonality (explained at the beginning of the Background section). However, it is possible that the water stress conditions result in a lower frequency and total area of bofedales in the subregions that have drier conditions.

In any case, some common climatic aspects of this region are their wet summers (80% of precipitation occurs between October and March) and dry winters (Jomelli et al., 2009; Rabatel et al., 2013). While the temperature in this region maintains small changes throughout the year (~2° C), the daily frost-thaw variations range to 15° C from day to night, as is common in the tropical mountains (Korner 2003). The rainfall seasonality responds to the South American monsoon (SAM) dynamics but may vary periodically by

effect of the El Niño Southern Oscillation (ENSO) (Garreaud, René, Vuille et al. 2003). The effects of the El Niño and La Niña phenomena are in some years so strong that cause severe droughts or flooding events, which are associated with major transformations in the vegetation distribution that may have occurred over the last 200 k. y. (thousands of years) (Bush, Hanselman et al. 2010).

As mentioned above, there is a strong latitudinal precipitation gradient. The annual precipitation decreases from 800 mm, in the northeast region at the limit with the Amazon basin, to less than 150 mm, in the southwest region, which lies along the Atacama Desert (Chávez et al., 2019).

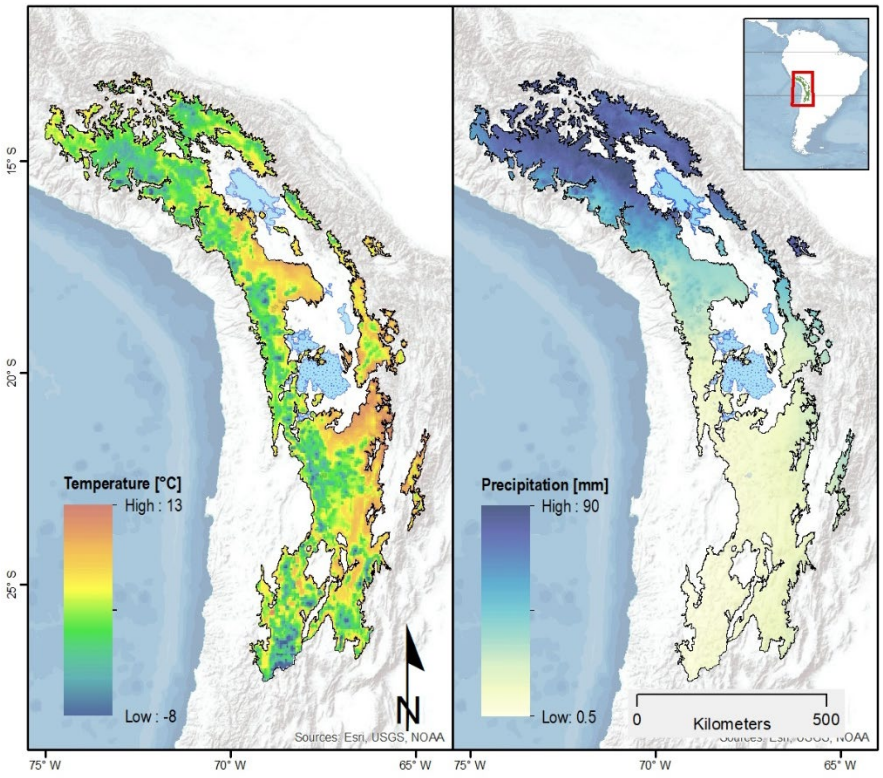

Figure 8. Average temperature and precipitation of the Southern tropical Andes. Source: Terraclimate dataset (1958 – 2020).

Considering the strong latitudinal gradient of precipitation in the Southern tropics (Figure 8), I combined the ecoregion and biogeographic maps from Olson (Olson, Dinerstein et al. 2001) and Rivas-Martinez (Rivas-Martínez, Navarro et al. 2011) to classify the Puna into three subregions: Humid Puna, Subhumid Puna, and Dry Puna (Figure 9).

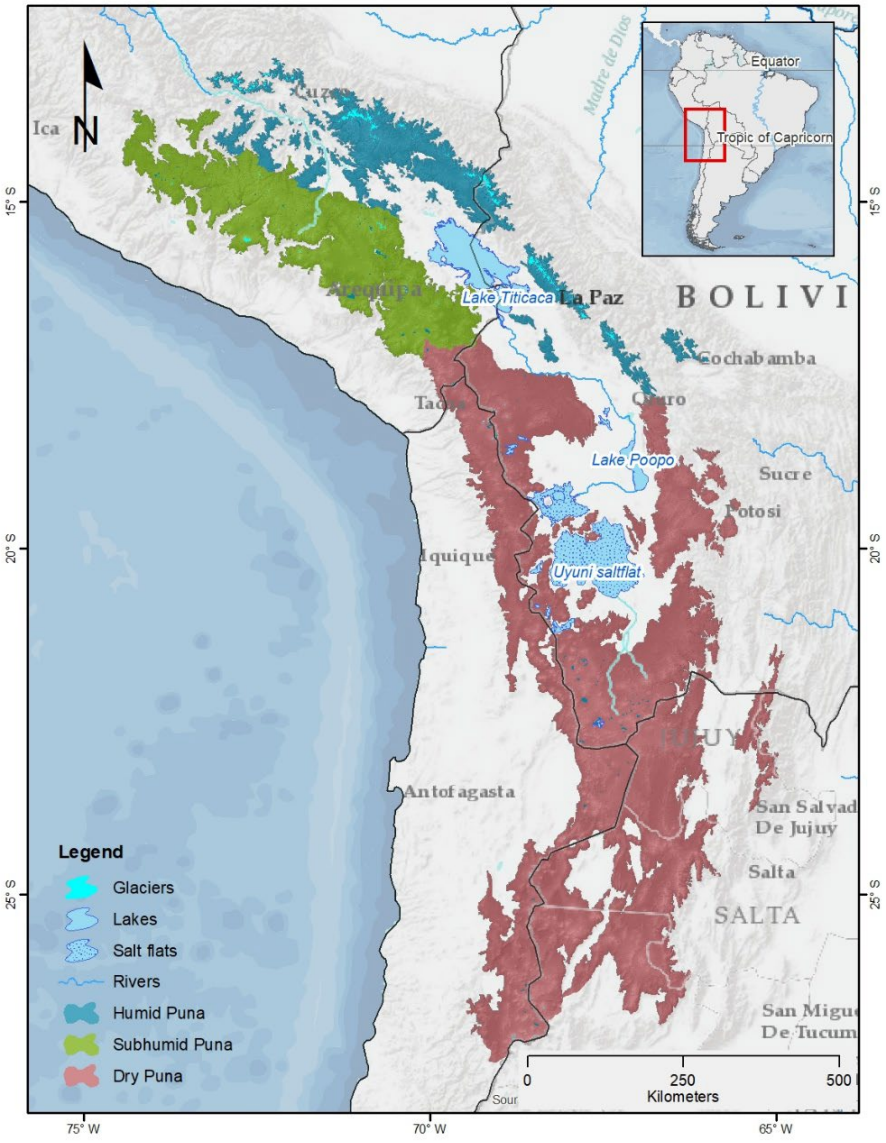

Figure 9. Puna sub-ecoregions of the Southern tropics considered for this study.

The Dry Puna considered in this study refers to the subregion delimited to the North on latitude 17°S, to the South in latitude 27°S (limiting with the South Andean Steppe) (Olson, Dinerstein et al. 2001) and a lower limit of 3800 m a.s.l. (Beck, Stephan, Domic et al. 2010). This region matches Rivas-Martinez' Xerophytic Puna (Figure 7B) and it has homogenously very low precipitation values, with only four humid months per year (Figure 9). The Humid Puna in this study is the area that other authors refer as Central Andean Wet Puna (Olson, Dinerstein et al. 2001). Climatically, it is the most humid and has three to four months of accumulated precipitation above 100 mm (hyper humid months) (Figure 10).

The Subhumid Puna (4000 m a.s.l.) is the region that Olson et al. (2001) refer as Central Andean Puna, in its northern portion (Garcia, E., Otto 2015). This subregion has four to eight dry months each year. Although the humid Puna doesn't have dry months, during June, July and August very low precipitation values are recorded (Figure 10). In summary, the three subregions have a strong precipitation seasonality.

Historically, pastoralist communities have inhabited this ecoregion for millennia (Baied, Wheeler 1993) and have managed the bofedales for the grazing of their livestock (Katia Villarroel, Pacheco Mollinedo et al. 2014, Meneses, Rosa, Ortuño et al. 2015, Yager, Valdivia et al. 2019). Thus, many wetlands have coexisted thanks to the presence and active management of water by pastoralist communities. However, activities related to mining, tourism, land cover change, or population reduction have changed the land use of these regions in the present. Consequently, the bofedales in many regions are showing degradation and deterioration (Squeo, Warner et al. 2006).

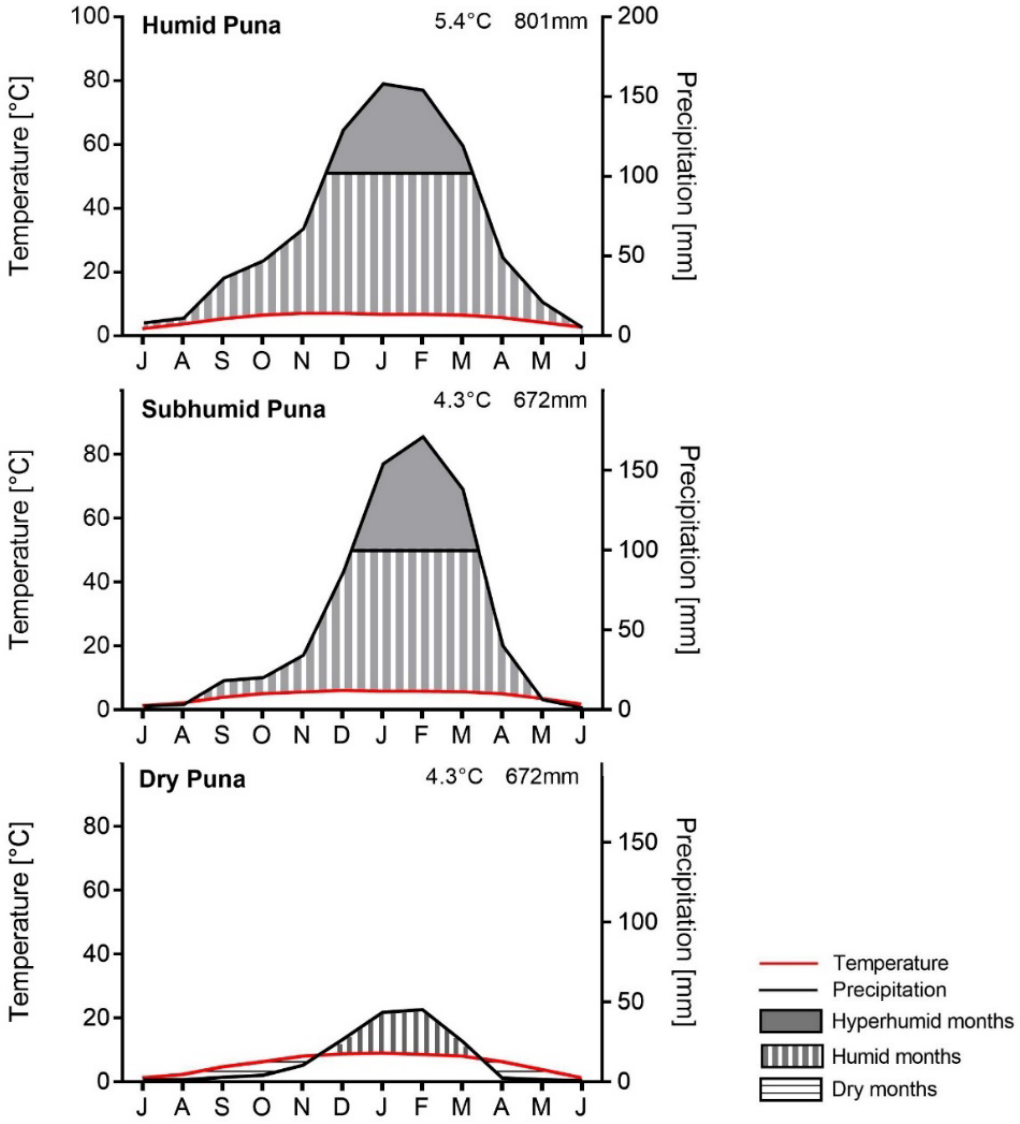

Figure 10. Climate diagrams of the Puna sub-ecoregions in the Southern Tropics. Source: TerraClimate.

Methods and data

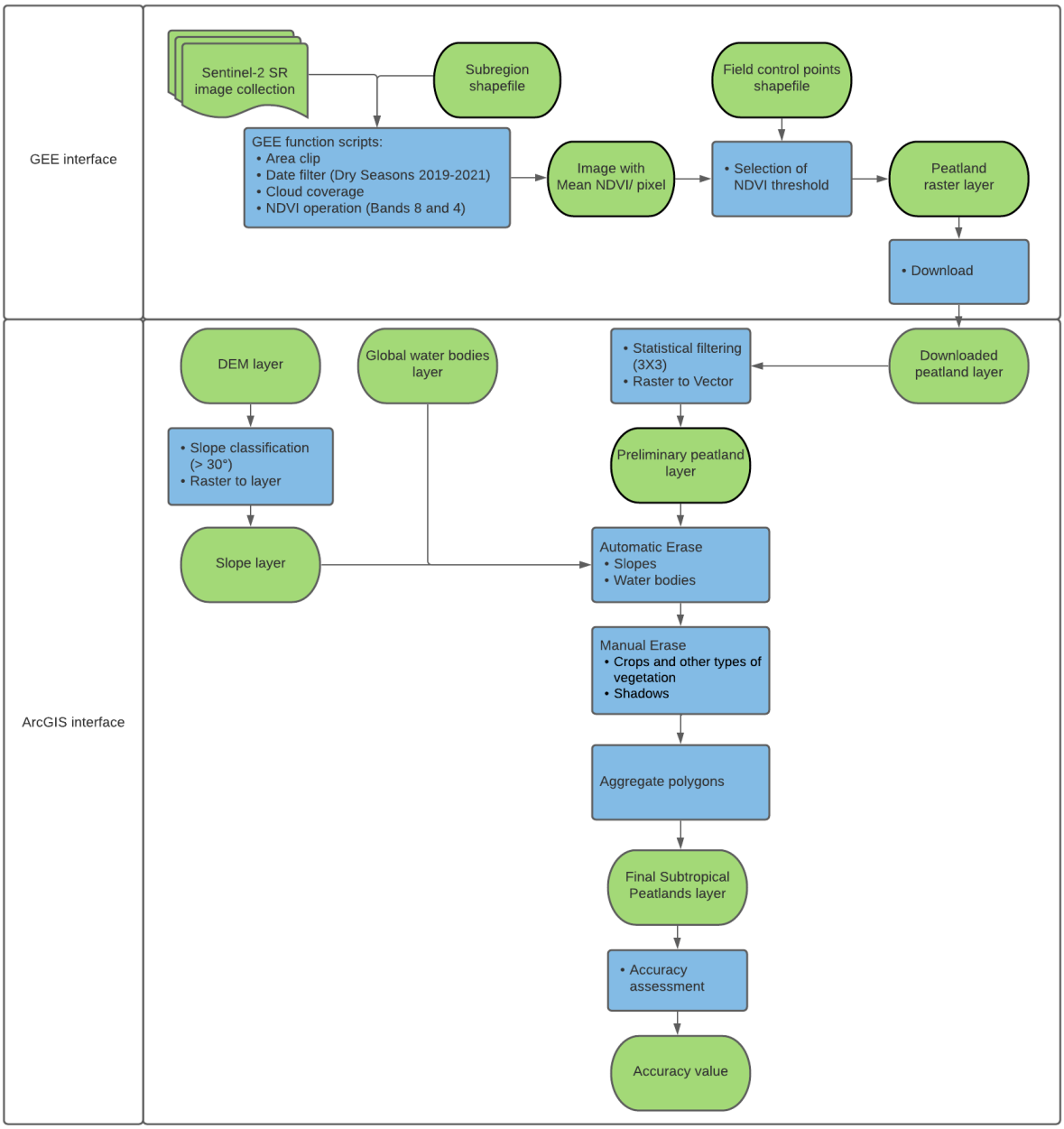

Figure 11. Flowchart of the peatland mapping process.

Datasets

The elevation layers, land cover imagery, ecological region layers and hydrographic basin layers were obtained from various sources (see Table 3). The Digital Elevation Model (DEM) was used to refine the ecoregion layers and to obtain zonal statistics for each polygon. The land cover imagery was used to generate the NDVI values and the hydrographic basin layers were used to determine the micro basins that comprised the bofedales.

Table 3. Summary of used datasets.

Category	Data set	Type	Scale	Time range or Date	Source/Author
Digital Elevation Model	ASTER	Raster	1:3,000,000	2011	Earth Engine Data Catalog
Land cover imagery	Sentinel MSI -2A/2B Surface reflectance level	Raster	1:30,000	09/01/2019 – 08/31/2021	Earth Engine Data Catalog
Hydrographic Basins	Peru Pfafstetter Level 4	Vector	1:100,000	2017	(CENEPRED 2022)
	Bolivia Pfafstetter Level 4	Vector	1:100,000	2010	(VRHR, UICN 2010)
	Argentina	Vector		2015	(Izquierdo, Foguet et al. 2015)
	Chile	Vector		2014	(Tapia Molina 2014)

Digital Elevation Model

I used the 30 m-grid raster layer derived from the Global 30 m Elevation Model archives of the Google Earth Engine database (Figure 12). This layer was used for the elaboration of elevation contours, delineation of hydrological basins, and the refinement of lower-scale ecological regions' polygons.

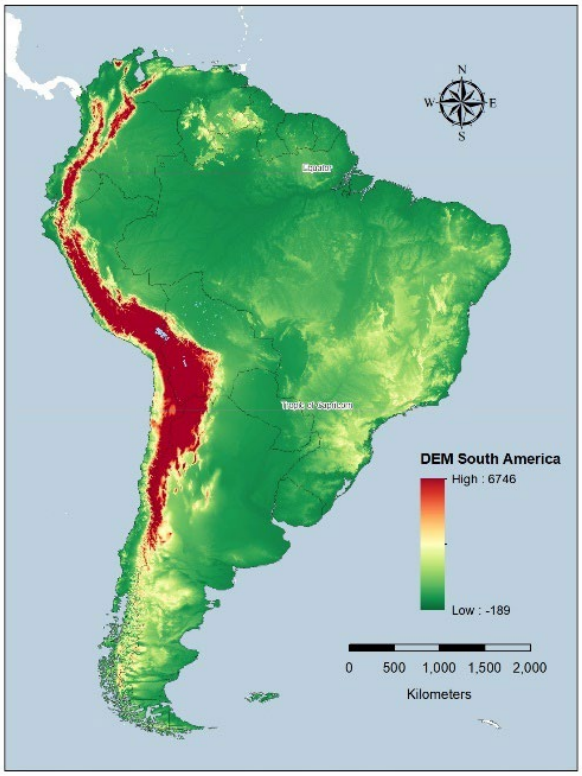

Figure 12. Digital Elevation Model of South America. NASADEM Merged DEM Global 1 arc second V001.

Land cover imagery

I used the Sentinel MSI -2A/2B Surface reflectance level image collection, a multi-spectral, multi-scale raster dataset oriented to observe and monitor the vegetation, soil and water cover of the Earth. Sentinel-2 Multi-Spectral Instrument (MSI) measures the Earth's reflected surface in 13 bands from Visible and Near-Infrared (VNIR) to Short Wave Infrared (SWIR) spectral wavelengths (Table 4). First Sentinel-2 sensor was launched in 2015 and second in 2017. The two satellites have the same sun-synchronous orbit separated by 180 degrees. The mean orbital altitude is 786 km, and the orbit inclination is 98.62° and the Mean Local Solar Time (MLST) at the descending node is 10:30 (am). Because each

satellite has a 10-day frequency, every image tile is covered at least every five days (SUHET 2015). Sentinel-2's Surface Level (L2) product includes Bottom Of Atmosphere (BOA) reflectance values in cartographic geometry and is available for public use from March 2017 to the present on the ESA's online platform (SciHub), as well as in other cloud-based dataset catalogs such as Google Earth Engine (GEE) (Gorelick, Hancher et al. 2017).

Table 4. Spectral bands for the SENTINEL-2 sensors (S2A & S2B).

Band Number	S2A		S2B		Spatial resolution (m)
	Central wavelength (nm)	Bandwidth (nm)	Central wavelength (nm)	Bandwidth (nm)	
1	442.7	21	442.3	21	60
2	492.4	66	492.1	66	10
3	559.8	36	559	36	10
4	664.6	31	665	31	10
5	704.1	15	703.8	16	20
6	740.5	15	739.1	15	20
7	782.8	20	779.7	20	20
8	832.8	106	833	106	10
8a	864.7	21	864	22	20
9	945.1	20	943.2	21	60
10	1373.5	31	1376.9	30	60
11	1613.7	91	1610.4	94	20
12	2202.4	175	2185.7	185	20

Source: (SUHET 2015)

The Subtropical Puna is comprised of 99 tiles of the Sentinel-2 grid (Figure 13). This study analyzed all cloud-free images from the two entire hydrological years from September 1st, 2019 to August 31st, 2021. In total, 7227 scenes were considered in the analysis (Bermúdez 2017)

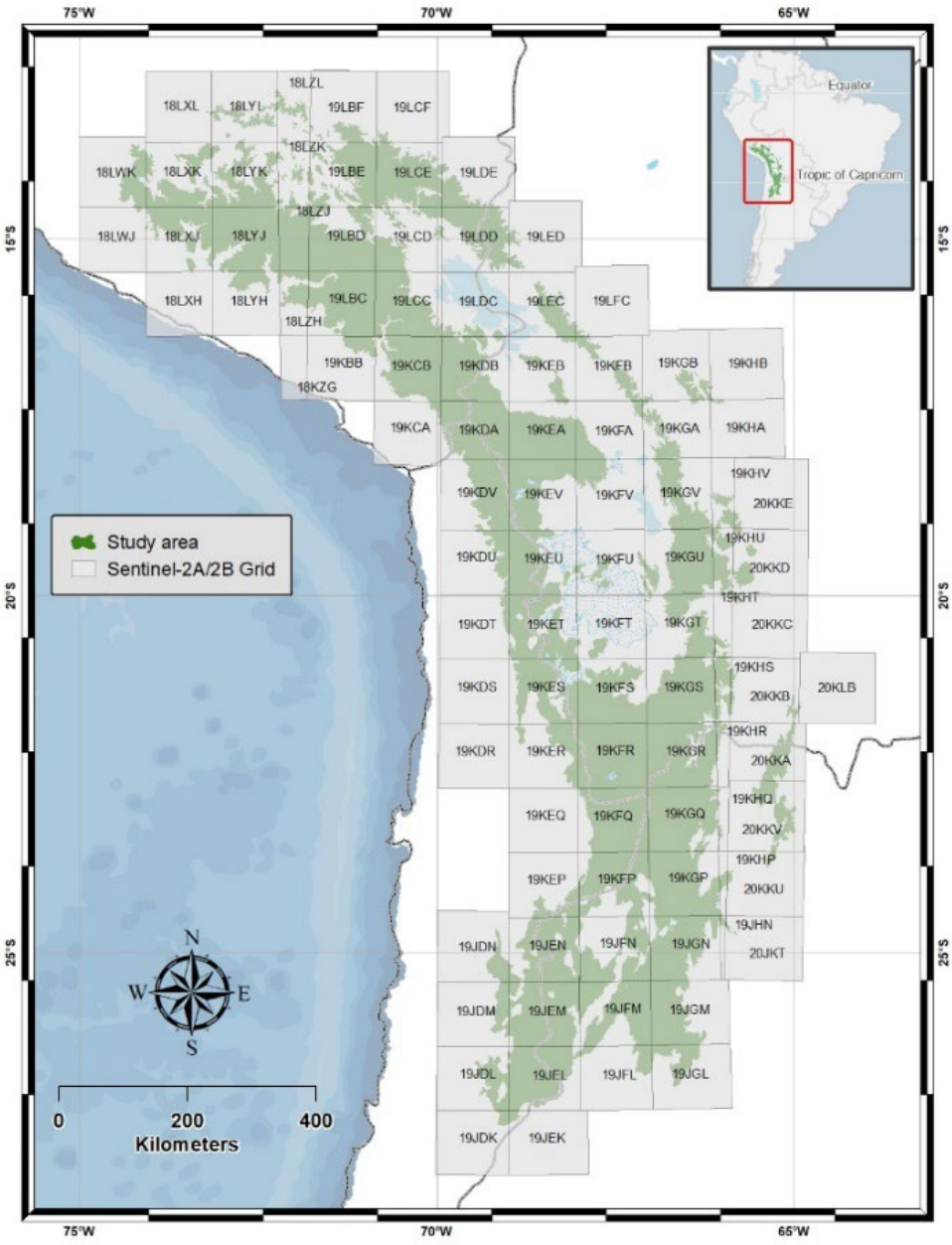

Figure 13. Sentinel-2 grid tiles comprising the study area.

Hydrological Basins

Each country has an official hydrological basins classification with codes to identify each basin (Figure 14). Once I obtained the peatland units from the image classifications, I used

the same basin codes for the peatland inventory. The national basins classifications of Peru (CENEPRED 2022) and Bolivia have adapted versions of the Pfafstetter method (VRHR, UICN 2010). I used the Level 5 in both cases. For Chile, I used the National Basin Inventory (Tapia Molina 2014), and for Argentina, I used the same microbasins used by Izquierdo et al. (2015).

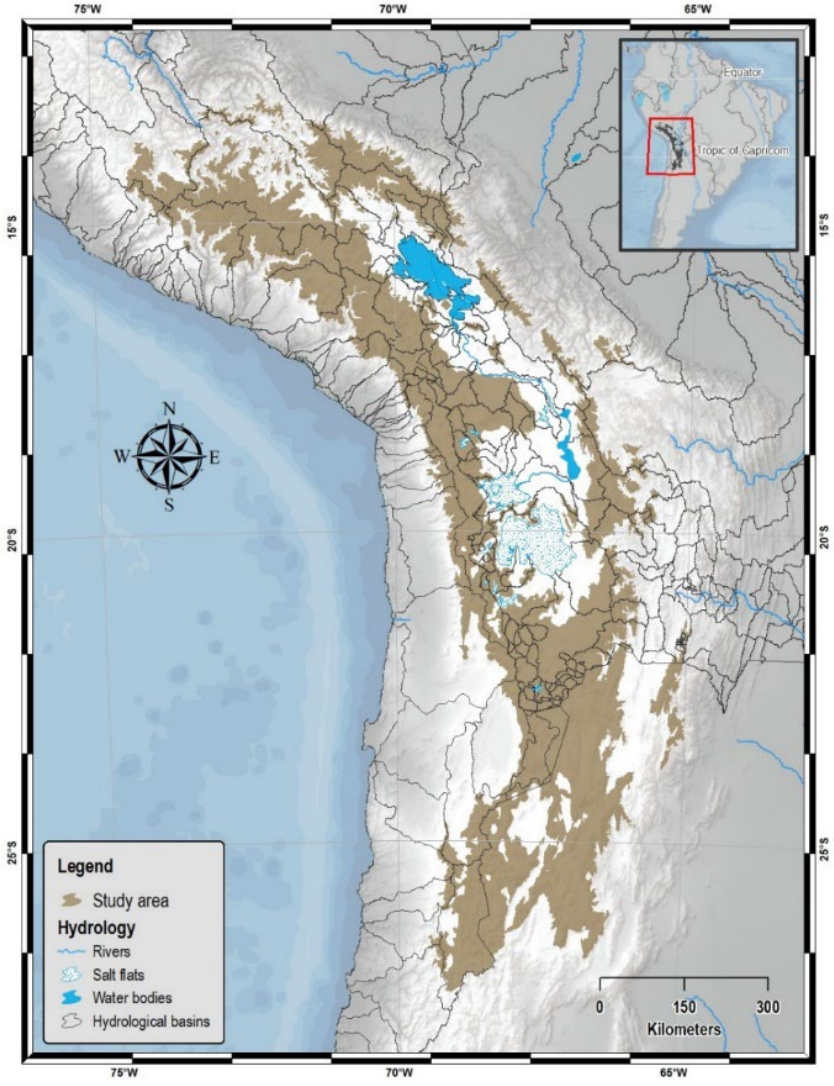

Figure 14. Hydrological basins of Argentina, Bolivia, Chile, and Peru.

Field data

To cover the entire study area with field control points, I compiled a database from different sources such as fieldtrips, literature, botanical archives, or datasets shared by other collaborators (Table 5). These points are important for adjusting the NDVI threshold in each region.

Table 5. Field control points datasets.

Data set	Number of peatlands	Period
Fieldtrips	352	2017 - 2021
Other collaborators	177	2012 - 2021
Literature	235	1999 - 2019
Botanical archives	18	1982 - 2008

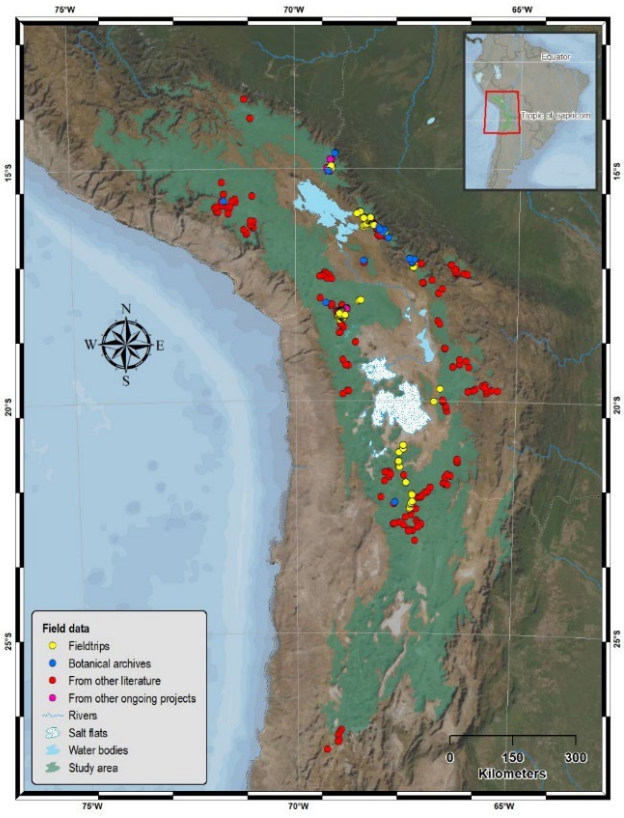

Figure 15. Field data points.

All fieldtrips were performed during the dry seasons and considered different characteristics for the inventory (see Table 6).

Table 6. Characteristics recorded for each site.

GPS code	#
Date	Day-Month-Year
Category	Bofedal / Zonal vegetation
Dominant species or landform	Species name

Delineation of bofedales

I applied the NDVI index to delineate the bofedales. NDVI highlights the photosynthetic activity of the vegetation from other objects and is a common index in the identification of wetlands worldwide (Ozesmi, Bauer 2002, Kandus, Minotti et al. 2018). Because in the drier Puna ecoregion bofedales are usually oases of vegetation, it is relatively easy to identify them in the landscape using this technique (Garcia, E., Otto 2015).

Google Earth Engine Algorithm

I run the NDVI algorithm on the Sentinel-2 surface-level image collections using a code in JavaScript language on the GEE interface. This code was based on the multiple functions available in the GEE platform (Amani, Ghorbanian et al. 2020) and included cloud filtering and spatial and temporal filters as presented in the script (Appendix A).

Threshold determination

To determine the boundaries of the peatland units, I used the field control points from recent literature and fieldwork (Figure 15) to test the most approximate NDVI threshold for each subregion. This process was done by visually comparing the control points with the calculated NDVI image from Sentinel-2 on the GEE map interface and adjusting the

threshold values that better approximate to the control points. An example of this process can be found in Figure 16.

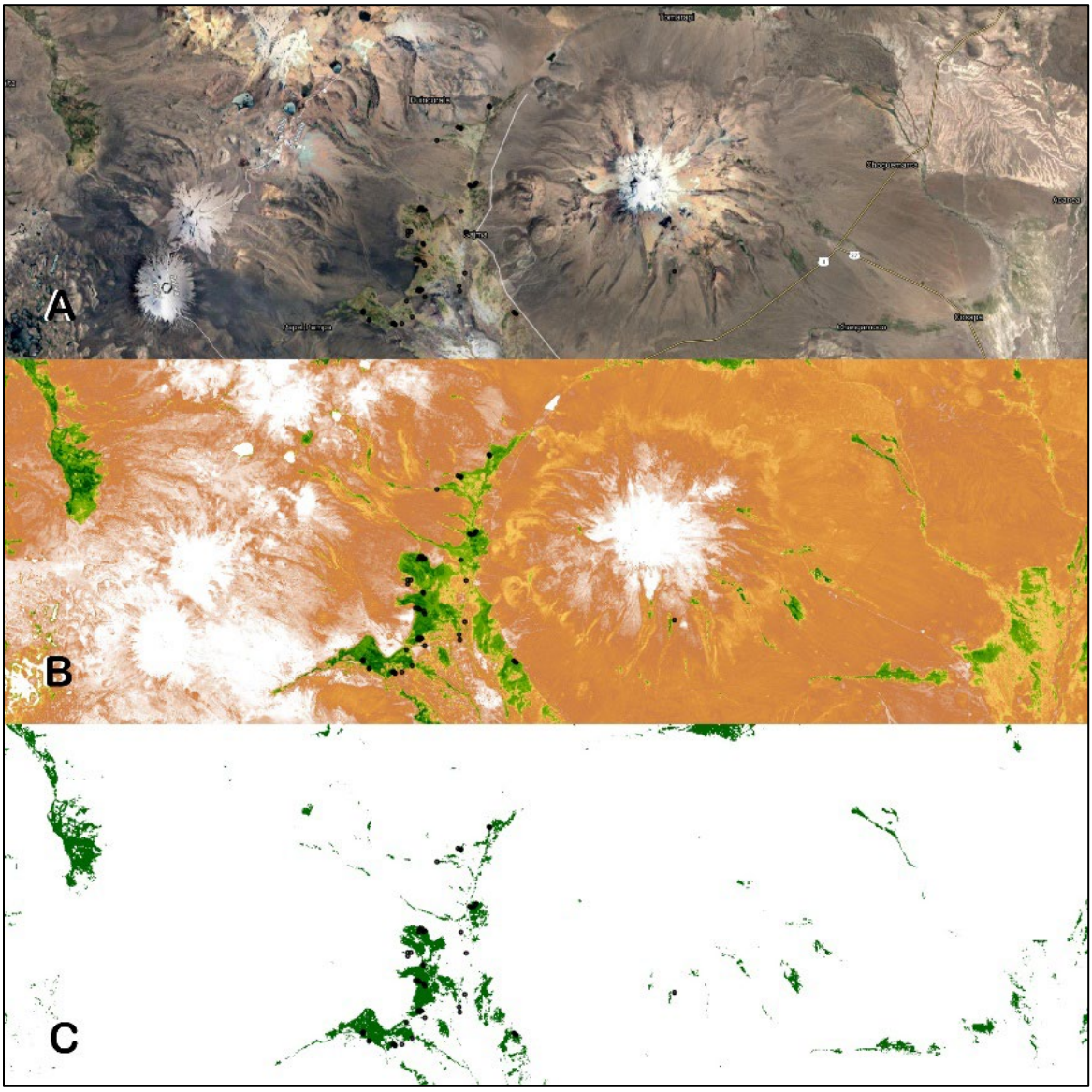

Figure 16. Example of selection of NDVI threshold values to determine the peatlands boundaries in the map section of the GEE interface. A) Satellite view, B) NDVI image,

C) Selected shapefile layer from a threshold of 0.4. Black dots are the field control points.

Peatland mapping

The downloaded layer was cleaned following different processes in ArcMap 10.8.1 (ESRI). First, the image was converted into a raster file to perform the Majority Filter tool at a 3x3 pixels. This helped eliminating small areas that usually are patches of non-peatland vegetation. Also, shadows, crops, steep slopes, other types of vegetation, and water bodies, were erased by applying automatic and manual analysis done in quadrants at a visual scale of 1:100,000 as shown in Figure 17.

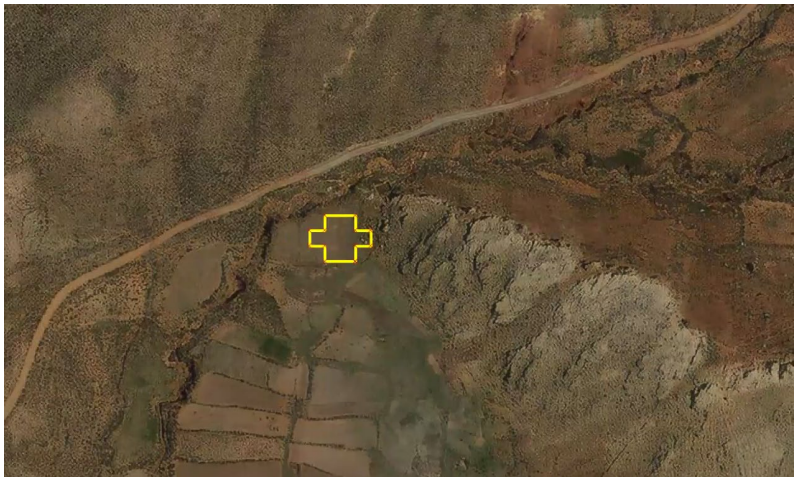

Figure 17. Example of deleted crop area initially classified as peatland with the NDVI analysis.

Results

In total, 153,900 bofedal units were identified with a total surface area of 6,753 km^2. The Humid Puna (2,714.0 km^2 in 63,304 units) and the Subhumid Puna (3,198.8 km^2 in 62,021 units) have largest total area of bofedales (Figure 18). The Dry Puna (837.8 km^2) has also less amount of bofedal units (28,016). Although the largest bofedal was 126.23 Km^2, the

median value in the three subregions oscillates between 5,000 and 7,000 m^2. The skewed distribution of bofedales can be observed in Figure 19.

.

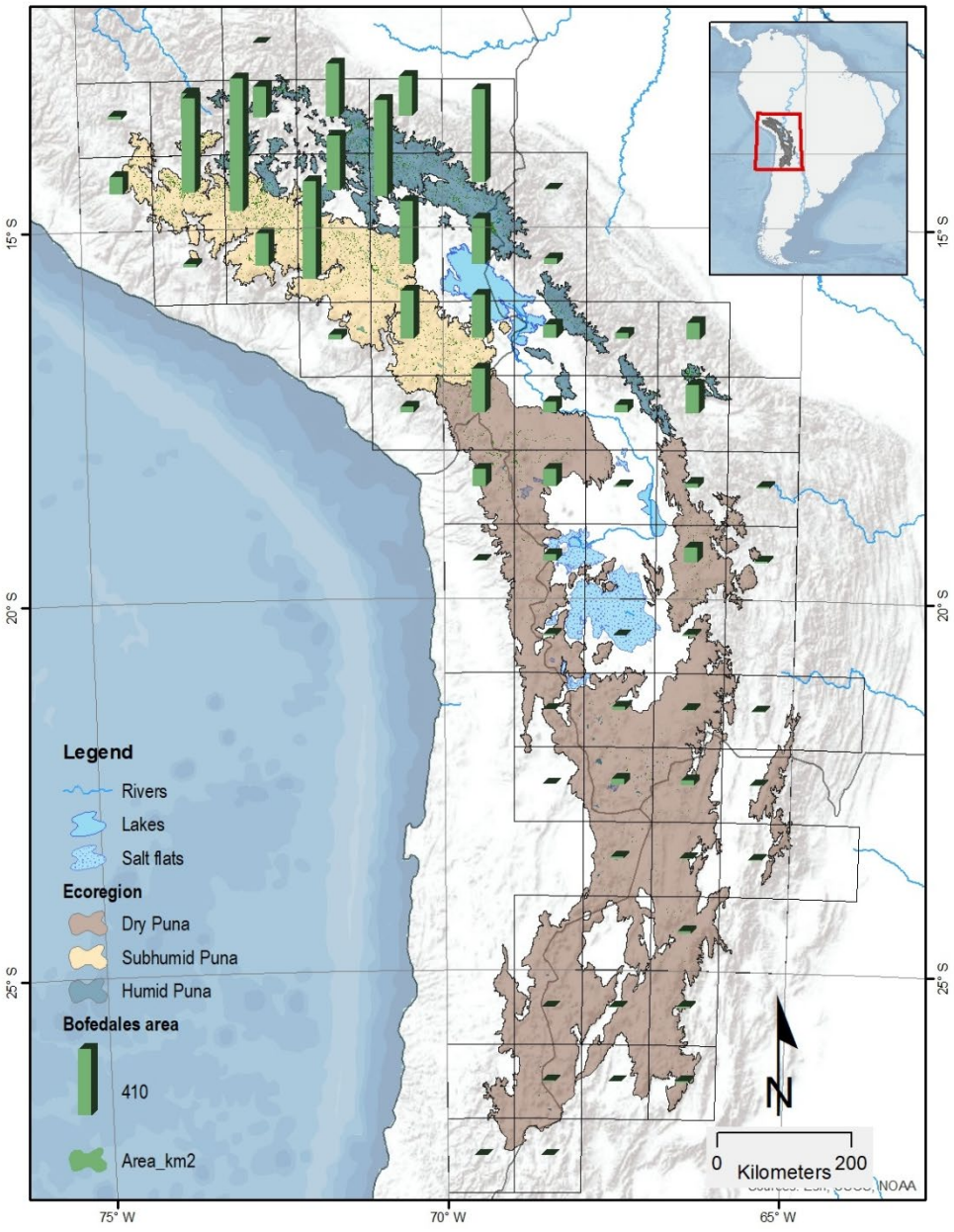

Figure 18. Total bofedal Area per 1° grid square in the Southern tropical Andes.

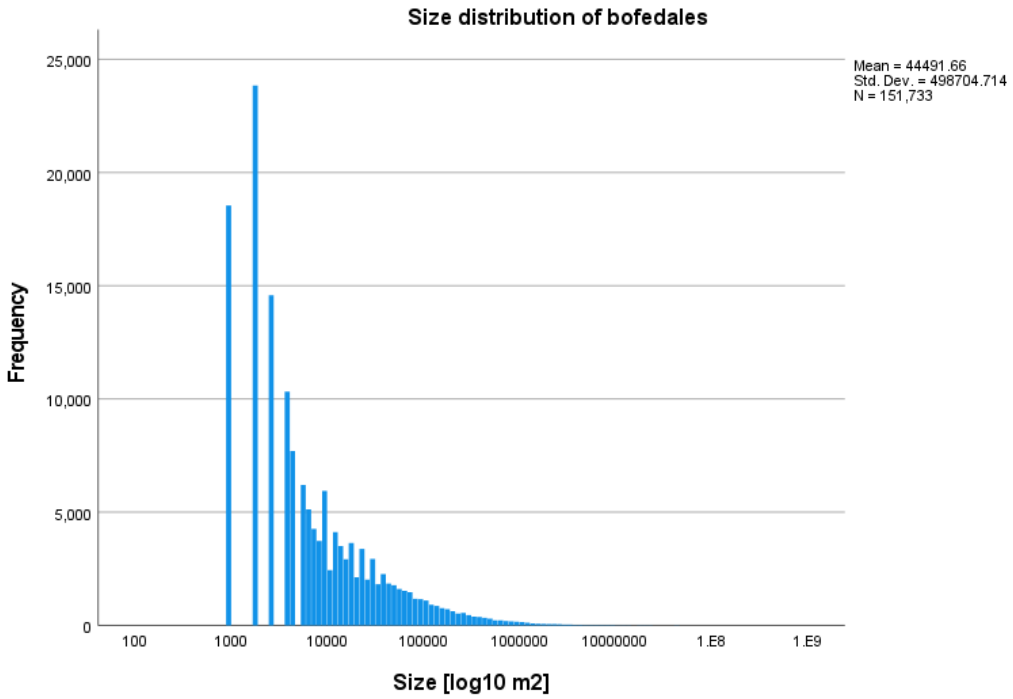

Figure 19. Size distribution of bofedales.

The inventory of bofedales was organized in three groups: administrative data, hydrological data, and topographical data. The full data table is in the digital appendix and will be available for the public. In the following section I summarize the most important aspects.

Administrative data

Most bofedales occur in Peru, followed by Bolivia, Chile, and Argentina (Table 6). Out of the 536 municipalities (called *Distritos* in Peru, *Municipios* in Argentina and Bolivia, and

Comunas in Chile) found in the study area, 492 have at least one bofedal unit. The municipalities with the largest bofedal areas are located in Peru and Bolivia (Figure 20).

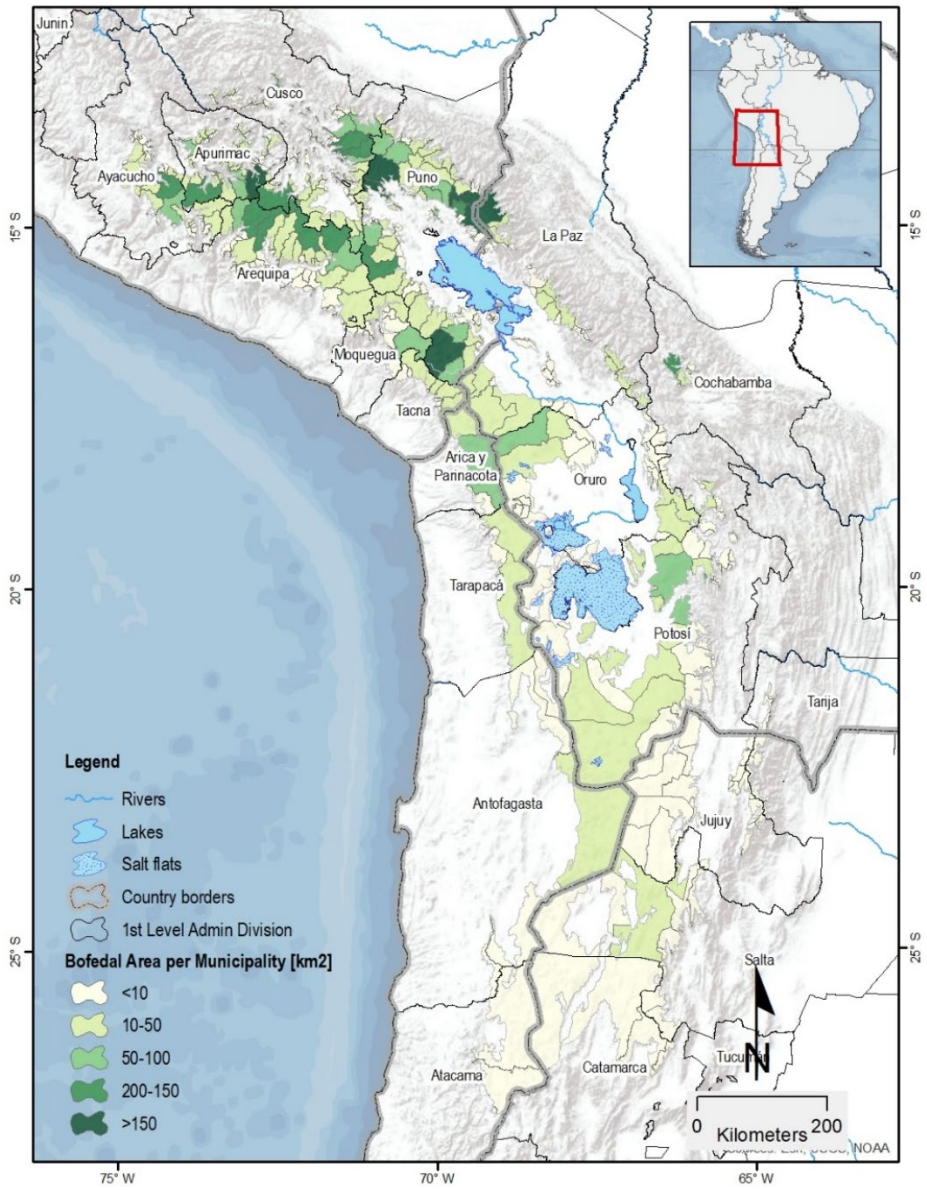

Figure 20. Area of bofedales per municipality.

The five municipalities with the largest amount of bofedales have, each one, more area of bofedales than the sum of all bofedales in Chile or Argentina. The Bolivian municipality

of Pelechuco, at the North of Lake Titicaca, has 268.5 km^2 of bofedales. The next eight municipalities with more bofedales belong to Peru, from Cojata (226.7 km^2) to Cotaruse (139.4 km^2). The Chilean municipality with most bofedales' area is Putre, to the North of the country (77.4 km^2), and in Argentina is San Antonio de Los Cobres (10.1 km^2). In Peru, the Department with more bofedales is Puno; in Bolivia is La Paz; the Chilean region with more bofedales is Arica and Parinacota and in Argentina is the Province of Salta.

Table 7. Number and surface area of bofedales per country.

Country	Municipalities with bofedales	Bofedal units	Bofedal area [km^2]
Argentina	37	9,435	84
Bolivia	116	28,985	1,068
Chile	14	3,215	163
Peru	325	112,265	5,438
Total	**492**	**153,900**	**6,753**

Hydrological data

The bofedales of the Southern tropics are distributed among four macro basins (Table 8). Although is not the largest basin in the study area, the bofedales on the Amazon macro basin are more numerous and cover more area than the bofedales of the other macro basins. Considering the density of bofedales per micro basin area, the micro basins from the Amazon basin, and from the North of the Altiplano basin have the largest values (Figure 21).

Table 8. Number and size of bofedales per macro basin

Basin	Number	Area [km^2]
Altiplano	46,766	2,315
Amazon	72,326	3,055
La Plata	8,151	108
Pacific Ocean	26,657	1,275
Total	**153,900**	**6,753**

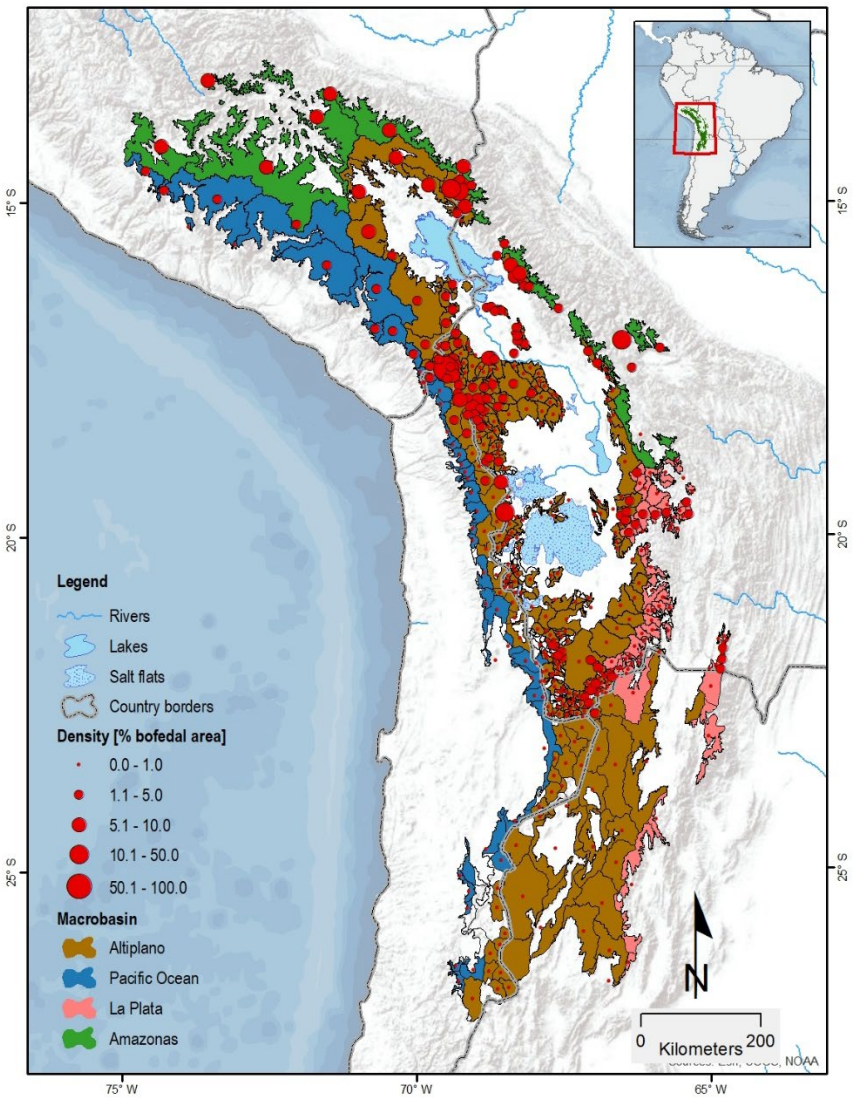

Figure 21. Area of bofedales per hydrological micro basin.

Topographical data

The zonal statistics of the bofedales provided data about elevation, slope angle, and orientation for each bofedal. The median elevation of bofedales is 4,397 m a.s.l. Fifty percent of the bofedales occur between 4,231 m and 4,583 m a.s.l. The largest bofedal (126 km^2) is above 4,400 m a.s.l. (Figure 22)

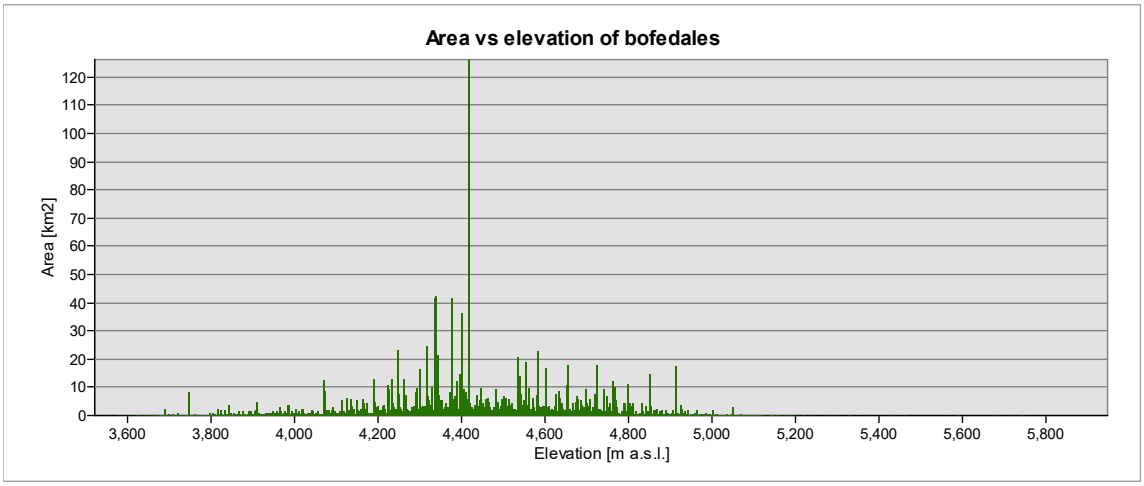

Figure 22. Size distribution of bofedales vs Elevation a.s.l.

The average slope angle of the bofedales is 9.6°. Except for the outliers, most bofedales occur in slopes with less than 25° (Figure 23).

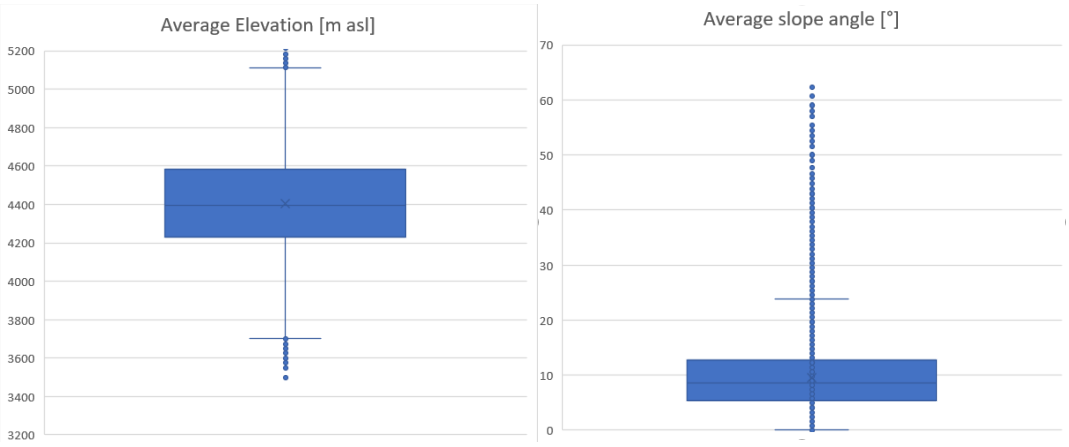

Figure 23. Distribution of bofedales based on the elevation and slope angles.

Discussion

This is the first inventory and map of the bofedales of the Southern tropical Andes. The availability of the Sentinel-2 imagery on the Google Earth Engine platform allowed this

map and inventory to be the most updated (years 2019 to 2021) and complete in the region. Similar studies only took into account one or a few points in time to determine the spatial distribution of peatlands (Chávez, Christie et al. 2019, Izquierdo, Foguet et al. 2015). With Sentinel-2's frequency of five days, a study area comprising 99 tiles, in two entire hydrological years, I analyzed the average NDVI values of over 14,000 scenes or ~1.4 trillion pixels. The NDVI allowed to identify bofedales because they are typically surrounded by grasslands and other landscape formations that don't have an intense photosynthetical activity (Chávez, Christie et al. 2019). Different types of bofedales, like peatlands, vegas, or other wet meadows are very hard to classify through this method. Therefore, this study considers all these different types under the term of *bofedales*.

Because of the large size and heterogeneity of the study area, I divided it into three ecoregions based on the existent biogeographical classifications of the Andes. The Humid Puna on the North has more precipitation across the year and almost doesn't have dry months. Because this region is more humid, the lowest elevation of this area was considered at 4,200 m a.s.l. In this region, it is possible to find bofedales below this level, but most authors also use the 4,200 m as the lower limit (Garcia, E., Otto 2015, Otto, M., Scherer et al. 2011, Otto, Marco, Gibbons 2017). On the other hand, bofedales on the Dry Puna can occur at even lower elevations (Beck, Stephan, Domic et al. 2010). For this reason the lowest limit for the study area in the Dry Puna was defined at 3,800 m a.s.l..

I also organized the study area into each country's political administrative divisions, and official hydrological basin codification. This linked information made it possible to assign to each bofedal various codes to make them easier to identify and manage.

Prior research in the same region was performed on Chilean and Argentinian bofedales in areas that correspond to what I consider the Dry Puna. Chávez et al. (2019) identified 5,665 bofedales covering 510 km^2 in Chile, including a 20 Km buffer zone. For a similar area, I identified 5,297 bofedales covering less area (313 km^2). Two reasons may explain this difference: I used a higher lower level (3,800 m a.s.l.) than Chávez (3,700 m a.s.l.) and the Sentinel-2 sensor that I used has a finer spatial resolution (10 m vs 30 m/pixel). That being said, the patterns found by Chavez regarding the clusters of bofedales between the latitudes 17° - 19° S and 22° - 24° S were also detected in this study.

In the case of the map of high Andean peatlands of Argentina (Izquierdo et al. 2015), there are important discordances because I used different study areas. Izquierdo et al. considered a lower level of 3,200 m a.s.l. and down to 30° S in latitude. This may explain why they identified 944.3 km^2 in 10,428 polygons, while I detected 78.4 km^2 in 8,183 for the Argentinian Southern tropics (down to 27 °S).

For the case of Peru, according to MINAM or INRENA (in (Maldonado Fonkén 2014), the entire country has between 917 to 5,494 km^2 of bofedales. The latter value is closer to our results since I identified 5,438.0 km^2 only in the Southern part of the country. In this study, Bolivia is the only country that can consider this inventory as a national inventory as well. The only previous inventory of bofedales of Bolivia was published in 2001 (Prieto, Alzérreca et al. 2001). That study affirmed that Bolivia has 1,023 km^2 of bofedales, which is similar to our result (1,068 km^2).

The Northern portions of the Puna, Humid and Subhumid, has around 10 times more peatlands than the Dry Puna, which is a surprising difference. Considering the important

role that bofedales have on the regulation of the downstream hydrology (Squeo, Warner et al. 2006) and on the sustaining of the ecological and social ecological dynamics (Yager, Valdivia et al. 2019), it is possible that the Dry Puna region might be more exposed to climate change impacts due to its smaller amount of bofedales. Although peatlands are azonal ecosystems, higher precipitation values, and the presence of more glaciers and high-altitude lakes in the North might reflect on the number of bofedales. Given that the size of glaciers in the study area sums up to 1,500 km^2, our results indicate that bofedales are at least four times larger in surface area than glaciers. This result helps understand the importance of bofedales to the ecosystem and to the hydrology. The fact that their distribution is very extensive, I suggest that bofedales might be for some areas (especially in those where there are no glaciers) the most important water reservoirs. The case of the starvation of hundreds of camelids in Sajama National Park in 2015 and 2016 due to the desiccation of bofedales indicates that their conservation and monitoring is critical for the survival of the indigenous, traditional, and agropastoral communities.

Conclusion

This study provided the first topographical, hydrological, and political administrative inventory of the bofedales of the Southern tropical Andes. It was done analyzing Sentinel-2 imagery from the dry months (June to September) from 2019 to 2021. A total of 6,753 km^2 of bofedales in 153,900 polygons. Most bofedales occur in the North, but their presence in the Altiplano and in desertic areas of the Dry Puna implies that they have a role as oases of vegetation.

Chapter 2. Classification of bofedales using supervised machine learning

Introduction

Bofedales are a unique group of low-lying peat-forming vegetation communities that grow in areas with permanent saturation of water, often surrounded by arid grasslands (Squeo, Warner et al. 2006). These wetland ecosystems occupy glacier valleys, floodplains, and slopes between 3,500 m and 5100 m a.s.l. along the entire Andes, from Venezuela to the Patagonia (Squeo, Warner et al. 2006, Ruthsatz 2012, Izquierdo, Foguet et al. 2016, Maldonado Fonkén 2014). Bofedales have a critical role in the social, ecological and hydrological systems because they provide habitat and food for both domesticated and wild animals, as well as being regulators of the hydrological cycles in the high Andes (Squeo, Warner et al. 2006, Yager, Prieto et al. 2021, Yager, Valdivia et al. 2019). In addition, bofedales provide multiple services to the ecosystem and society. For example, they have the highest rate of carbon sequestration among peatlands (Hribljan, J. A., Cooper et al. 2015, Cooper, Kaczynski et al. 2015, Moreau, Le Toan 2003), they filter the water coming from mining pollution (Domic, Meneses et al. 2019), and they represent abstract sacred entities intimately linked with the life and traditions of the pastoralist communities that depend on them for their subsistence (Meneses et al. in preparation).

The main genera of plants that comprise bofedales form peat cushions and carpets in complex mosaics; are well adapted to water saturated soil conditions; and dominant species belong to the Juncaceous family (*i.e. Distichia*, *Oxychloe*, and *Patosia*) (Ruthsatz 2012). Associated with these species is possible to find other types of grasses and herbs which are more resilient to dry soil conditions; and commonly belong to the Cyperaceous (*e.g*. *Zameioscirpus*, *Phylloscirpus*), Plantaginaceous (e.g. *Plantago tubulosa*), and Graminae (*e.g*. *Poa spp*., *Deyeuxia spp*.) families (Ruthsatz 2012). Although the latter species are more common in the margins of the bofedales, they often are found intermixed within the mosaics of the cushions of *Distichia*, *Oxychloe*, and *Patosia* (Ruthsatz 2012). The way in which the biological species are distributed within an ecosystem is called ecological community structure. The community structure in each bofedal unit varies depending on a number of factors related to the geographical location, climate, environmental pressures, or water availability. This means that the occurrence, and distribution of species may be different in each bofedal depending on the water chemistry, the availability of water, air temperature, hydraulic infrastructure, hydroclimatic conditions, the plant-animal interactions (i.e. grazing, cattle trampling, seed dispersion, manure fertilization, etc.), and the particular ecological successions occurring in each bofedal (Ruthsatz 2012). In some cases, the peat forming plants are dominant in the landscape, but in other cases the dominance belongs to the non-peat forming plants, typical of wet meadows (or *vegas*). Other vegetation communities also occur intermixed with the bofedales. For example, communities of halophytic (flexible to saline environments) vegetation, waterbodies with aquatic plants, islands of grasslands and other types of upland vegetation. It is also common

to find areas covered by sand or rocks, some areas are covered in animal manure, and areas where there is only dead vegetation (Domic, Meneses et al. 2019).

This phytosociological heterogeneity has a strong impact on the ecohydrological role of the bofedales (Yager, Prieto et al. 2021). For example, healthy peatlands of *Distichia*, which forms more compacted cushions than *Oxychloe*, occur in soils with lower salinity and have the ability to contain larger and more numerous pools in the bofedal mosaics (Oyague, Cooper 2020). Furthermore, both Juncaceous species have thicker soils with larger percentages of organic matter, porosity, and hydraulic conductivity, than the other species from the cyperaceous and graminoid families (Oyague, Cooper 2020). Therefore, the bofedal units with healthy and dominant populations of *Distichia*, and *Oxychloe* regulate better the groundwater flow, have larger carbon sequestration rates, and an overall higher biomass productivity (Izquierdo, Foguet et al. 2016, Ruthsatz 2012). However, the ecological community structures not only vary from site to site but also are in permanent change (Ruthsatz 2012, Loza Herrera, Meneses et al. 2015). It has been reported the advancement of ecotone species over the bofedal cushions as drying conditions grow, and vice versa, the peat forming species advance over the ecotone species if there is sufficient water (Ruthsatz 2012). Pastoralist communities know this very well and, when possible, actively create the conditions for the advancing of peat forming bofedales by constructing canals, building wells, reintroducing bofedal plants, or managing pastures (Yager, Valdivia et al. 2019). Unfortunately, bofedales are degrading in most areas due to climate change and anthropogenic activities (Maldonado Fonkén 2014, Oyague, Cooper 2020, Yager, Valdivia et al. 2019) and is expected that the bofedales' community structures will be

changing as well (Loza Herrera, Meneses et al. 2015). Bofedales heterogeneity also respond to other factors such as soil and water chemistry (Loza Herrera, Meneses et al. 2015, Ruthsatz 2012), grazing dynamics (Cochi-Machaca, Condori et al. 2018), climate change, global warming, and glacier retreat (Loza Herrera, Meneses et al. 2015, Zimmer, Meneses et al. 2018), variations in the pasture management (Yager, Valdivia et al. 2019), among others. However, when using remote sensing tools for the identification of bofedales, only few studies have addressed their structure complexity and considered their strong heterogeneity (Yager et al. 2019). This omission was due in part to the limited accessibility of bofedales, but also to the restricted availability of high resolution sensors and imagery (Kandus, Minotti et al. 2018). Since the cloud-based computing platform Google Earth Engine (GEE) became available (Gorelick, Hancher et al. 2017), more researchers have started to use GEE's computing power and multi-peta byte imagery accessibility to classify the landscape. For example, Phan et al. (Phan, Kuch et al. 2020) applied the Random Forest classification on the GEE platform to classify large regions and demonstrated that this process could be done relatively easy and fast.

In any case, botanical assessments in the field are a key tool to understand the phytosociological dynamics of the bofedales and to accurately classify the satellite imagery with supervised classification methods. The botanical assessments may consider different scales of analyses, from 1 m grid interpretations, (micro scale), to 'bird's eye' interpretations of the landscape.

Meeting these challenges and opportunities, I combined 1) the use of the 10 m of spatial resolution imagery from Sentinel-2 sensors (available since 2015), 2) machine learning

techniques for satellite image classification on the Google Earth Engine cloud-based platform, and 3) thorough field botanical observations, to elaborate a comprehensive map that considered the different types of bofedales that potentially occur in the Bolivian Altiplano. With these activities, I planned to identify the occurrence of different classes of bofedales within the wetland polygons in three regions of the Bolivian Altiplano, under an exploratory approach, applying mixed methods of botanical assessment and machine learning techniques to classify satellite imagery.

Study regions

Based on the bofedal polygons, elaborated in the previous chapter, I chose three regions in the Bolivian Altiplano to categorize the bofedales into seven different classes. Each class represents different types of bofedales considering different association of species. The three regions were selected across a latitudinal gradient of the Bolivian Altiplano: Cordillera Real, the Sajama National Park, and the Sud Lipez Sector (Figure 24).

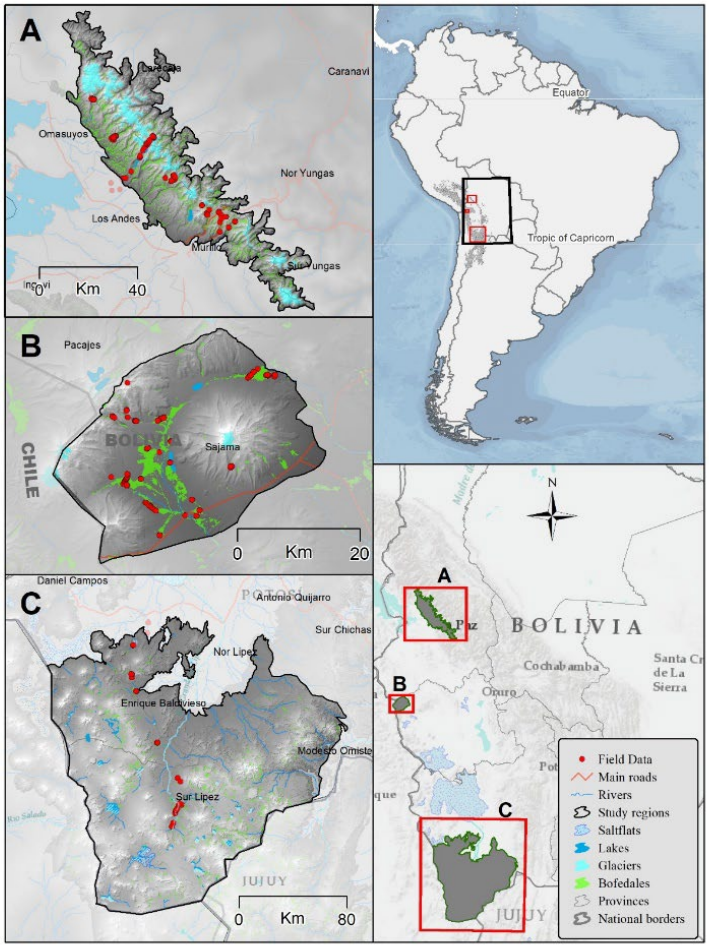

Figure 24. Study regions showing the field control points. A) Cordillera Real. B) Sajama National Park. C) Sud Lipez sector.

Cordillera Real

The Cordillera Real (Figure 24A) is a mountain range of plutonic rock origin that forms part of the Oriental (Eastern) range of the Bolivian Andes. It is located in the Department of La Paz across the watershed of the Amazon and the Lake Titicaca basins. It holds 11% of all tropical glaciers in the planet, and 55% of the total glaciers in Bolivia (Jordan 1991). Considering a lower elevation limit of 4,200 m a.s.l., the mountain range extends from

Latitudes 15°45’ to 16°45’S, and Longitudes 67°30’ to 68°30’ along a NW – SE direction along 180 km that separates the Altiplanic basin from the Amazon basin (Soruco, Vincent et al. 2009). Along the mountain range, several peaks rise above 6,000 m a.s.l., including Nevado Illampu, Ancohuma, Chiaraco, Chachacomani, Huayna Potosí, and Illimani.

Climatically, the Cordillera Real has a distinct dry season that starts in April and ends in September (Andrade, Moreno et al. 2018). The humidity is brought annually by the Intertropical Convergence Zone, and in smaller scale by convection systems from the Lake Titicaca. Also, in some years some humidity is brought by polar fronts from the Antarctic during winters (Jordan 2015). The precipitations occur mostly from November through April and is simultaneous with an increase in the temperature. Although the annual variations or air temperature (± 5°C) are smaller than the daily variations (± 15°C), the cold temperatures during the dry winters usually cause the vegetation to slow their growth (Korner 2003). The Cordillera Real belongs to the Humid Puna ecoregion and contains 3,518 bofedales (3.8% of the area).

The Cordillera Real is one of the most studied regions regarding bofedales in Bolivia. Since 1997 (Meneses, Rosa I. 1997), a number of studies were done in this region considering spatial distribution (Prieto, Alzérreca et al. 2001, Zeballos, Soruco et al. 2014), floristic composition (Meneses, Rosa, Ortuño et al. 2015, Ruthsatz 2012, Meneses, Rosa Iselas, Stephan et al. 2015), carbon sequestration and biomass productivity (Moreau, Le Toan 2003, Hribljan, J. A., Cooper et al. 2015, Cooper, Sueltenfuss et al. 2019), climate change impacts (Zimmer, Meneses et al. 2018, Loza Herrera, Meneses et al. 2015, Dangles, Rabatel et al. 2017), macroinvertebrate diversity (Quenta, Molina-Rodriguez et al. 2016,

Gonzales, Quenta et al. 2014, Quenta Herrera, Jacobsen et al. 2018), bird diversity (Cardenas, Naoki et al. 2022), herbivory and grazing dynamics (Cochi-Machaca, Condori et al. 2018), and environmental risks (Meneses, Rosa I. 1997).

Sajama National Park

Sajama National Park (PNS) (Figure 23B) is the first protected area of Bolivia, stablished in 1939, and was created for the protection of its unique alpine forests and ecosystems. The PNS is in the Sajama Province of the Department of Oruro and limits to the North with the Department of La Paz, to the West to the Lauca National Park in Chile. The park is in the Western Central Bolivian Altiplano between latitudes 17º56' and 18º17' S and 68º38' - 69º08' W. Its extension is around 1000 km^2 on high plateau that has an average elevation of 4,200 m a.s.l. In the center of the park lays the highest peak in Bolivia (the Sajama Volcano, 6,542 m a.s.l.) (Beck, Stephan, Domic et al. 2010). There are multiple alpine ecosystems, like bofedales, the *queñuales* (endemic trees of the high Andes), shrublands, geysers, and grasslands, that are habitat for hundreds of endangered plant and animal species (Beck, Stephan, Domic et al. 2010).

Geomorphologically, the PNS belongs to the Western Cordillera that has a volcanic origin (Beck, Stephan, Domic et al. 2010). Besides the Sajama Volcano, the also extinct volcanoes Parinacota (6,295 m a.s.l.) and Pomerape (6282 m a.s.l.), at the western edge of the Park, contain glaciers and are source for the sandy sediments that dominate the soils of the plateau. The depth of the glacier layer in the Sajama volcano ranges from 121 to 177 m (Thompson, Davis et al. 1998) and is an important source of fresh surface and groundwater for the area. The plateau has a bedrock of ignimbrite rock. Hydrographically,

the PNS belongs to the Altiplano endorheic basin. Streams from the glacier valleys drain into the Sajama and Tomarapi rivers and eventually outflow through the Lauca river into the Coipasa Lake to the South of the Department of Oruro (Beck, Stephan, Domic et al. 2010). The climate is characterized by a strong daily freeze-thaw cycle, and a clear humid summer and dry winter seasonality. The average annual temperature is 4.6 °C and the average annual precipitation rate is 321 mm (Beck et al. 2010). The Sajama National Park belongs to the Dry Puna ecoregion and contains 675 bofedales (7.3% of the area).

Lipez district

This biogeographical district, also known as the Lipez Region (Figure 24C), belongs to the Central Altiplanic Sector. It is located to the south of the Bolivian Altiplano between latitudes 20°58' and 22°59'S, and longitudes 66°12' and 68°11'W with an extension of 26,530 km^2. It limits to the West and South with Chile, and to the East to Argentina, and to the North with Uyuni Biogeographic District (Navarro, G., Maldonado 2011). The Lipez region is part of the provinces Nor Lipez, Enrique Baldivieso, and Sud Lipez of the Department of Potosí.

Climatically, has an average temperature between 5.0 and 7.7 °C and has an annual precipitation that varies from 59.6 to 200 mm/yr. Geomorphologically, it is comprised by a vast plateau of ignimbrite rocks, of an average elevation of 4,000 to 5,000 m a.s.l., with scattered stratovolcanoes, volcanic domes, and a few sedimentary rock outcrops, that rise from the plateau (Alzérreca, Prieto et al. 2001).

The vegetation is xerophytic, and is characterized by arid grasslands, shrublands, some scattered forests of *Polylepis,* and bofedales. The Lipez District belongs to the Dry Puna ecoregion and contains 2,452 bofedales (0.3 % of the area).

Materials and methods

Image database and collection

The Sentinel-2 A and B Satellite imagery was analyzed to classify the landcover within the wetland areas. The imagery was acquired from the Google Earth Engine platform matching the time range of the field vegetation surveys.

Table 9. Specifications of the Sentinel MSI (Multi Spectral Instrument)-2A/2B used in the study. All bands were available at a surface reflectance level.

Bands	Wavelength [nm]	Resolution [m]
B1 (aerosols)	443.9 (S2A) 442.3 (S2B)	60
B2 (blue)	496.6 (S2A) 492.1 (S2B)	10
B3 (green)	560 (S2A) 559 (S2B)	10
B4 (red)	664.5 (S2A) 665 (S2B)	10
B5 (red edge)	703.9 (S2A) 703.8 (S2B)	20
B6 (red edge)	740.2 (S2A) 739.1 (S2B)	20
B7 (red edge)	782.5 (S2A) 779.7 (S2B)	20
B8 (NIR)	835.1 (S2A) 833 (S2B)	10
B8a (red edge)	864.8 (S2A) 864 (S2B)	20
B9 (water vapor)	945 (S2A) 943.2 (S2B)	60
B11 (SWIR1)	1613.7 (S2A) 1610.4 (S2B)	20

Bofedal classes

Bofedales may be classified by different typologies and depending on the region or scope of study, different authors specify or generalize these variants (Yager, Prieto et al. 2021, Maldonado Fonkén 2014). Under a broad sense (*sensu latu*), bofedales are understood as any wetland system in the high Andes dominated by low, peat-forming, cushion-shaped, vascular plants (Yager, Prieto et al. 2021). Terms that are often associated with bofedales include *vega*, *cienaga*, *turbera*, wet meadow, cushion mire, Andean peatbog, Andean peatland, high altitude wetland of the Andes, highland marsh, *hok'o*, *oqho*, *oconal* (the last three in local indigenous languages) (White-Nockleby, Prieto et al. 2021). The different classes of bofedales may be defined by the predominant associations of plant species that occur in complex mosaics one next to other (Yager, Prieto et al. 2021, Maldonado Fonkén 2014). Due to the diverse typology of bofedales applied across the social and natural sciences, many studies that apply remote sensing techniques for their mapping use a broad generalized term because, among other reasons, the spatial and radiometric resolutions of their analysis usually would not distinguish one class of bofedal from another, depending on how bofedales are defined. In this study, I used the plant associations to discern the following types of bofedales: dense bofedal, mixed bofedal, dry bofedal, zonal vegetation, and water bodies, as described in the following sections. Among these classes, mixed bofedal and dry bofedal are the most difficult to distinguish from a spectral approach and possibly would be a source of error. These categories are important because each one represents a different ecohydrological role. Unless the specific class of bofedal is

mentioned (*i.e*. dense, mixed, or dry), the term bofedal from now on will refer to the broad sense (*sensu latu*) only.

Dense bofedal

This class includes cushion-shaped plants as the dominant species (*Distichia muscoides, Oxychloe andina*) which may or may not occur together (Ruthsatz 2012, Squeo, Warner et al. 2006). These species form peat and are indicators of humid environments, groundwater, natural springs, small ponds, and streams (Figure 25). Associated to these species it is possible to find, in smaller total cover percentages, other vascular plants that don't form peat and that are adapted to both humid or dry soil conditions, such as *Phylloscyrpus desertícola, Zameioscyrpus muticus, Werneria spathulata, Werneria heteroloba, Werneria pygmaea, Cuatrecasassiella argentina, Deyeuxia spicigera* and *Luzula racemosa* (Beck, Stephan, Domic et al. 2010, Domic, Meneses et al. 2019). When the site is close to surface water it is also possible to find the following species: *Cotula mexicana, Lachemilla diplophylla*, *Lilaeopsis macloviana*, *Ranunculus uniflorus*, *Deyeuxia chrysantha*, *Limosella aquatica, Myriophyllum quitense* (Beck, Stephan, Domic et al. 2010, Maldonado, Navarro et al. 2014). This class is analogous, but not restricted, to the categories "healthy bofedal" (Yager et al. 2019), or *Distichia* peatland (Maldonado Fonkén 2014).

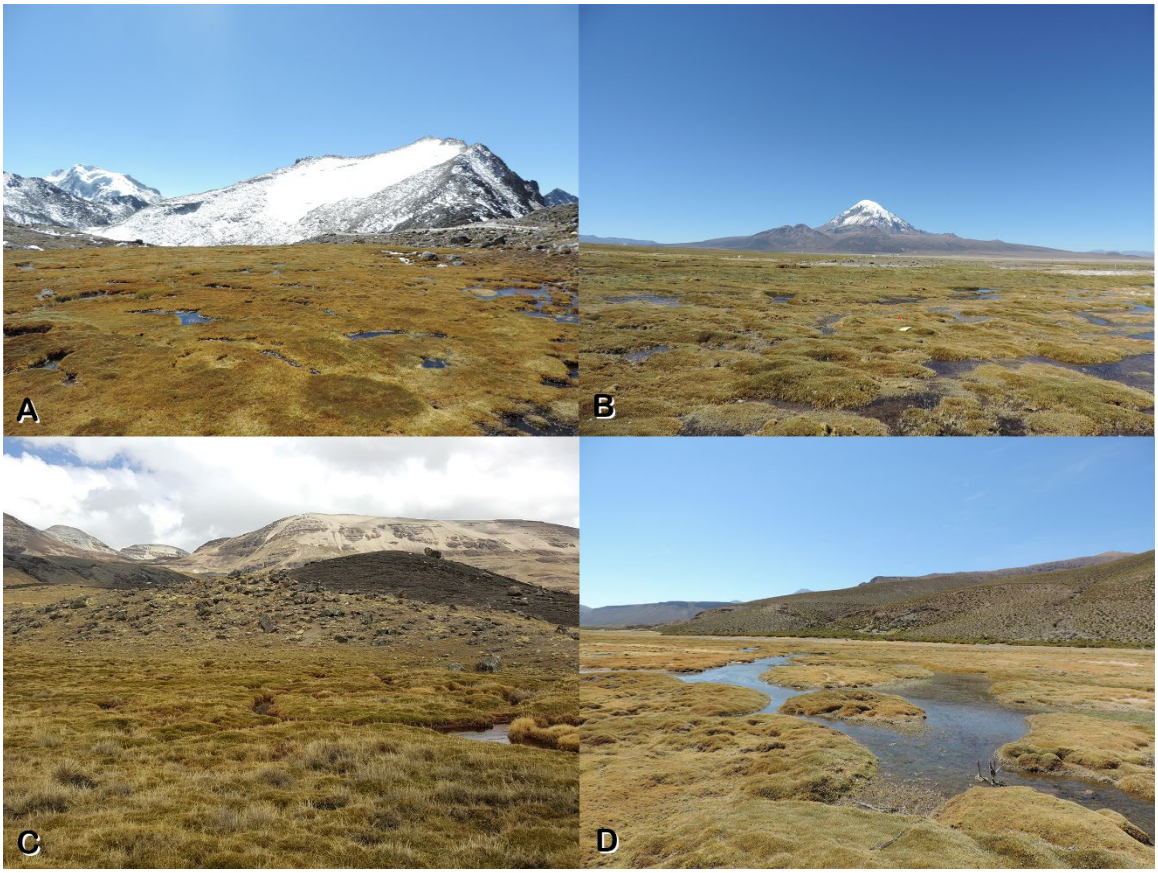

Figure 25. Examples of dense bofedales. A) Bofedal dominated by Distichia muscoides and D. filamentosa (Wila Llojeta valley, Cordillera Real). B) Bofedal dominated by Oxychloe andina (Sajama National Park). C) Bofedal dominated by O. andina showing some invasion from Zameioscirpus sp. and Deyeuxia chrisanta (Charquini valley, Cordillera Real). D) Bofedal dominated by Oxychloe andina (Villa Alota, Sud Lipez).

Mixed bofedal/ Mixed vegetation

This class indicates a drying transition from dense to dry bofedales (Figure 26). The invasive species that start dominating the landscape, called secondary species, are adapted to both dry and humid soil conditions, such as *Zameioscirpus muticus*, *Eleocharis melanocephala,* and *Juncus stipulatus.* Although healthy bofedal species are still present (*Oxychloe sp.* or *Distichia sp.*), they are no longer dominant and are replaced by non-peat forming plants, like *Festuca rigescens, Plantago tubulosa*, *Phylloscirpus sp.*, *Deyeuxia*

curvula, and *Deyeuxia vicunarum.* This class is analogous, but not restricted, to the categories "dry bofedal/mixed pastures" (Yager et al. 2019), or Peaty meadow (Maldonado Fonkén 2014).

Figure 26. Examples of mixed vegetation associations referred as mixed bofedal class. A) Mixed bofedal of O. andina, Festuca rigescens, Deyeuxia spicigera, and Deyeuxia chrisanta (La Cumbre, Cordillera Real). B) Mixed bofedal of O. andina and Festuca rigescens (Illampu valley, Cordillera Real). C) Mixed bofedal of drying individuals of O. andina invaded by tusocks of Festuca sp. (Sajama National Park). D) Mixed bofedal of O. andina, Zameioscirpus muticus, Festuca rigescens, and Phylloscirpus sp. (Eduardo Avaroa Natural Reserve, Sud Lipez).

Dry bofedal and mixed pastures

This class comprises both bofedales that are drying out and also other humid meadows that have mixed vegetation associations, including low grasslands, and local vegetation classes

like *vegas, qullpares,* or *porqe*. In general, all plants that comprise this complex class require less amount of water, that are adapted to high saline environments, or that indicate advanced degradation process of a dense bofedal (Figure 27). In the case of *vegas* or *porqe* dominated meadows, the dominant species may include *Plantago tubulosa, Poa gymnantha*, *Eleocharis melanocephala*, *Hypochaeris taraxacoides, Festuca rigescens, Lachemilla pinnata*, *Deyeuxia vicunarum, Deyeuxia chrysantha*, *Deyeuxia rigescens, Phylloscirpus deserticola*, *Lachemilla pinnata*, and *Carex sp*. In the case of a *qullpar* class (salt flat humid meadow), the dominant species are *Sarcocornia sp., Distichlis humilis*, or *Frankenia sp.* Since this class also includes former dense bofedal sites that underwent prolonged droughts or other types of stress, like overgrazing, it is possible to find some smaller patches of *Oxychloe andina* or *Distichia sp.* in poor health and degrading conditions. This class is analogous, but not restricted, to the categories "dry bofedal/mixed pastures" (Yager et al. 2019), or stream grassland (Maldonado Fonkén 2014).

Figure 27. Examples of dry bofedales and mixed pastures. A) Vega wetland dominated by Plantago tubulosa and Phylloscirpus sp. (Ichu Quta valley, Cordillera Real) B) Dry bofedal of Deyeuxia spicigera growing over dying individual of Distichia filamentosa (Ichu Quta valley, Cordillera Real). C) Low pastures of species adapted to saline environments (also known as qollpares) Sarcocornia pulvinata, Frankenia sp., and Distichlis humilis (Villa Alota, Sud Lipez). D) Porqe wetland dominated by Deyeuxia curvula (Sajama National Park).

Zonal vegetation

This class refers to the vegetation that are often external to bofedales, like forests, shrublands, grasslands, or dry pastures (Beck, Stephan, Domic et al. 2010), but may occur sometimes as patches inside a bofedal. "Zonal" vegetation is called so because their occurrence responds completely to the climate characteristics of the ecoregion (Sieben 2019), as opposed to bofedales that, being "azonal," depend on local hydroclimatic factors.

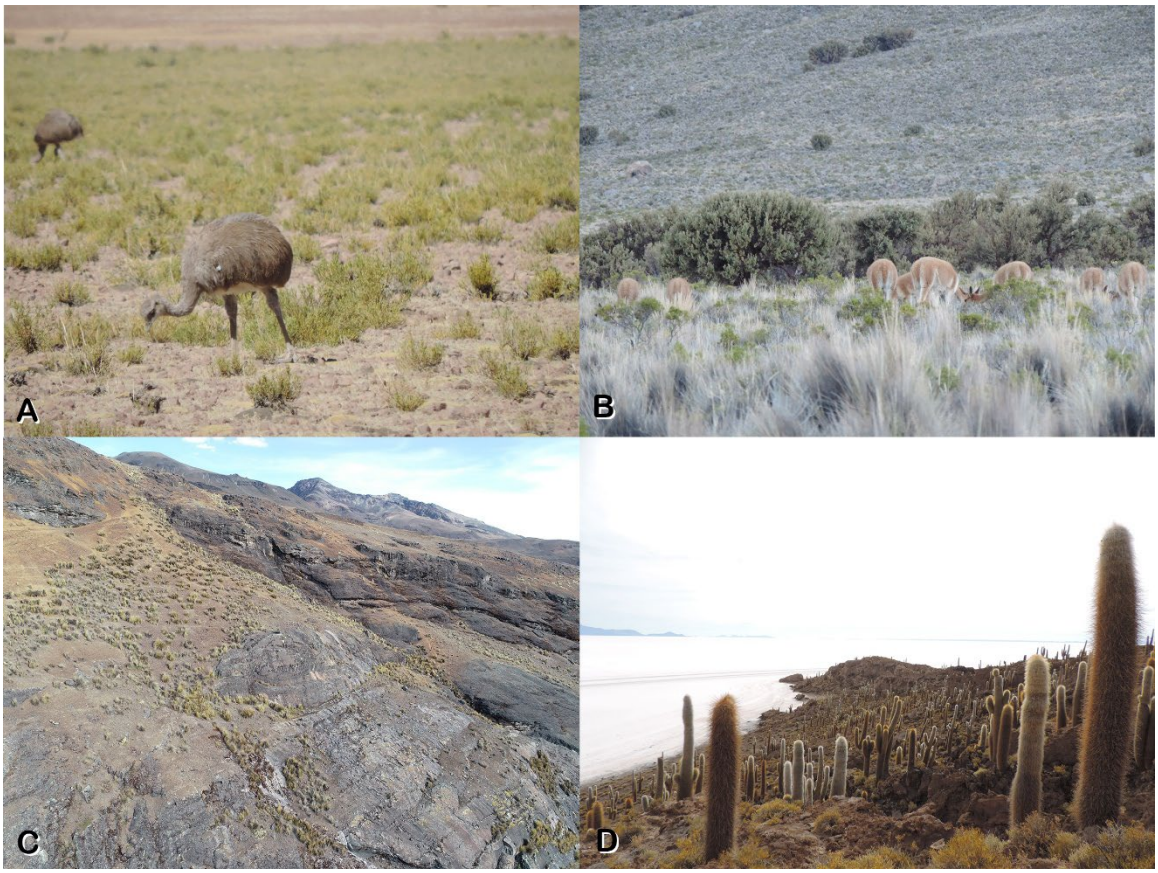

Figure 28. Examples of zonal vegetation found in the Bolivian Altiplano. A) Parastrephia sp. shrublands grazed by two individuals of suri (Pterocnemia pennata) (Sud Lipez). B) A herd of vicugnas (Vicugna vicugna) grazing on tussocks and shrubs of Festuca orthophylla and Parastrephia sp. In the background, some patches of queñua trees (Polylepis tarapacana) are visible (Sajama National Park). C) tussock grasslands of Stipa ichu on a rocky slope (Hampaturi valley, Cordillera Real). D) A cactus patch or Echinopsis atacamensis in the Incahuasi island in the Uyuni Saltflat.

Water body

This class corresponds to water features found in association with bofedales, which include streams, rivers, or large ponds, that often become the largest feature in certain points of a bofedal (Figure 29). This class comprises those areas where the water is the dominant feature. The water may include aquatic plants like *Elodea potamogeton, Myriophyllum quitense, Stuckenia pectinata, Ranunculus trichophyllus, Lemna gibba,* or *Azolla*

filiculoides. Also, it is possible to find certain algae groups like chlorophytes (green algae), rhodophytes (red algae), or cyanophytes (blue-green algae) (Beck, Stephan, Domic et al. 2010).

Figure 29. Examples of water bodies found near bofedales. A) pond with green algae and aquatic plants like Myriophyllum quitense (Ichu Quta valley, Cordillera Real). B) Pond in the Lagunas community (Sajama National Park). C) Pond with some floating individuals of Azolla filiculoides (Chachacomani valley, Cordillera Real). D) Shallow stream at the edge of some cushions of Oxychloe andina (Quetena, Sud Lipez).

Field data

Vegetation assessments of the bofedal were conducted during the dry seasons of 2018, 2019, and 2021 when there is less cloud coverage. I tried to match as close as possible the orbit of Sentinel-2 satellites in space with the surveying times and dates, so that it was

possible to associate the field data with the imagery scenes from the satellite sensors. A total of 241 points were surveyed, considering a scale of 10 m x 10 m, and annotating the following information from each site: Waypoint number, location name, GPS point, land cover description, observations date, latitude, longitude, elevation. The land cover classes (Table 10) were established as percentage of cover of the prevalent vegetation types. The information was accompanied with ground photographs (detailed and panoramic), and, when possible, imagery from an Unmanned Aerial Vehicle (Phantom 4 Advanced from the company DJI).

In addition to the data from the field surveys, I used landcover data (197 points) from past and ongoing projects of other collaborators (Yager, Valdivia et al. 2019, Meneses et al. in preparation), in order to add more training points to the image classifications. New field data was obtained following similar vegetation sampling and phytosociological methodology.

Table 10. Summary of landcover classes considered to classify bofedales.

#	Class	Land cover
1	Dense bofedal	Dominance of *Oxychloe*, *Distichia.*
2	Mixed bofedal/Mixed vegetation	Drying presence of *Oxychloe*, *Distichia.*
3	Dry bofedal/Mixed pastures	Absence of *Oxychloe*, *Distichia.*
4	Zonal vegetation	Shrublands, Grasslands, Forests, Dry meadows
5	Water body	Streams, ponds, swamps

Image classification

I applied the random forest classification to classify the bofedal classes from Sentinel-2 imagery. Random forest classification is based on the combination of decision tree predictors where each tree depends on values of random vectors sampled independently and with the same distribution for all trees in the forest (Breiman 2001). The classification

was performed on the Google Earth Engine (GEE) platform using a code written in the JavaScript programming language and results in a raster image. The code for random forest is based on the Statistical Machine Intelligence and Learning Engine (SMILE) classifier from the JAVA library, which is available in the GEE platform (Hasan, AL-Hameedawi et al. 2022). I applied filters for masking of clouds, selection of time periods, and selection of region of interest. Further code details are described in Appendix A. For the accuracy assessment I randomly selected 20% of the training points to run a validation error matrix. This contingency table was prepared in the same classification script code (Appendix A).

Results

In all three study regions, the assumption that bofedales (*sensu latu*) occur in mosaics of different classes of bofedales and vegetation forms was confirmed. The structure of these mosaics was very intricated and was inherently associated to the scale of analysis, which in this case was 10 m x 10 m of minimum size object. The dominant classes in the bofedales varied depending on the geographical and ecohydrological factors. In some cases, these factors involved overgrazing processes, droughts, physical removal and extraction, among some others. Following, I describe the major findings in each region of analysis.

Field data

In general, most control points were dense bofedales (186), followed by mixed bofedales (122), and dry bofedales (84). Zonal vegetation and water bodies combined 46 points (Table 11).

Table 11. Summary of field control points assessed in this study.

#	Class	Land cover	Number of points
1	Dense bofedal	Dominance of *Oxychloe*, *Distichia*	**186**
2	Mixed bofedal/Mixed vegetation	Drying presence of *Oxychloe*, *Distichia*	**122**
3	Dry bofedal/mixed pastures	Absence of *Oxychloe*, *Distichia*	**84**
4	Zonal vegetation	Shrublands, Grasslands, Forests, Dry meadows	**28**
5	Water body	Streams, ponds, swamps	**18**

Complete table of the field control points are shown in the Appendix B.

Classification results in the Cordillera Real

In terms of total size, dense bofedales were the most common class (42%). Mixed bofedales follow in total size (32%) but are the most numerous (see Table 12 and Figure 30). On average, dense bofedales were twice as large as mixed bofedales or zonal vegetation classes. Dry bofedales and water bodies, when present, were on average the smaller classes and also are the less numerous in the region. The accuracy of the classification was 0.96 using 67 randomly selected points (See Table 13).

Table 12. Summary of the classification of bofedales in the Cordillera Real.

#	Class	Land cover	Count	Area [m^2]	[%]	Average [m^2]
1	Dense bofedal	Dominance of *Oxychloe*, *Distichia*	26,505	55,311,847	42.1	2,087
2	Mixed bofedal/Mixed vegetation	Drying presence of *Oxychloe*, *Distichia*	39,272	42,385,126	32.2	1,079
3	Dry bofedal/Mixed pastures	Absence of *Oxychloe*, *Distichia*	15,047	7,685,076	5.8	511
4	Zonal vegetation	Shrublands, Grasslands, Forests, Dry meadows	25,725	25,064,676	19.1	974
5	Water body	Streams, ponds, swamps	2,280	1,020,783	0.8	448
	TOTAL		**108,829**	**131,467,508**	**100**	**1,208**

Table 13. Confusion matrix of the classification algorithm in the Cordillera Real (20% of the control points).

	Predicted Class				
Actual Class	1	2	3	4	5
1	30	0	0	0	0
2	3	18	0	0	0
3	0	0	6	0	0
4	0	0	0	8	0
5	0	0	0	0	2

Validation overall accuracy: 0.96

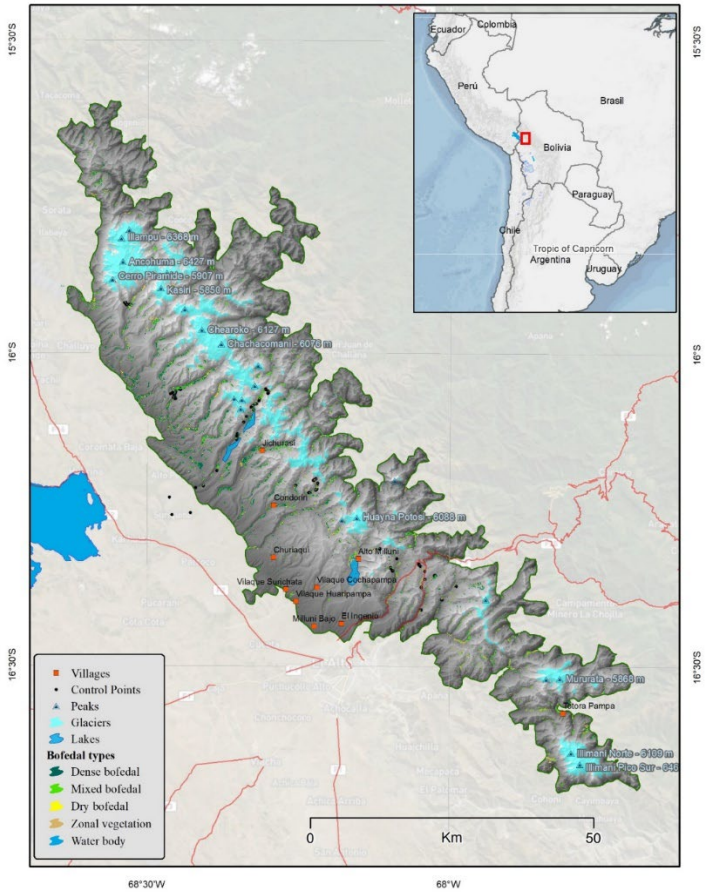

Figure 30. Map of bofedal types in the Cordillera Real.

Among dense bofedales, the most common dominant species were *Oxychloe andina* and *Distichia muscoides*. On the other hand, the genera that were present in the transition to mixed and dry bofedales were *Plantago, Deyeuxia, Festuca, Phylloscirpus, Carex,*

Werneria, Eleocharis, and *Juncus*. The dominant species that comprised the areas of zonal vegetation belonged to the genera *Festuca* and *Stipa*. In the case of water bodies, the prevalent species were *Myriophyllum quitense*, *Lachemilla pinnata, Liliopsis macrocephala, Ranunculus sp., Azolla filiculoides*, and the algae *Chara*. Figure 31 shows the location of certain control points in reference to a mosaic of aerial pictures taken from the UAV and to the resulting classification.

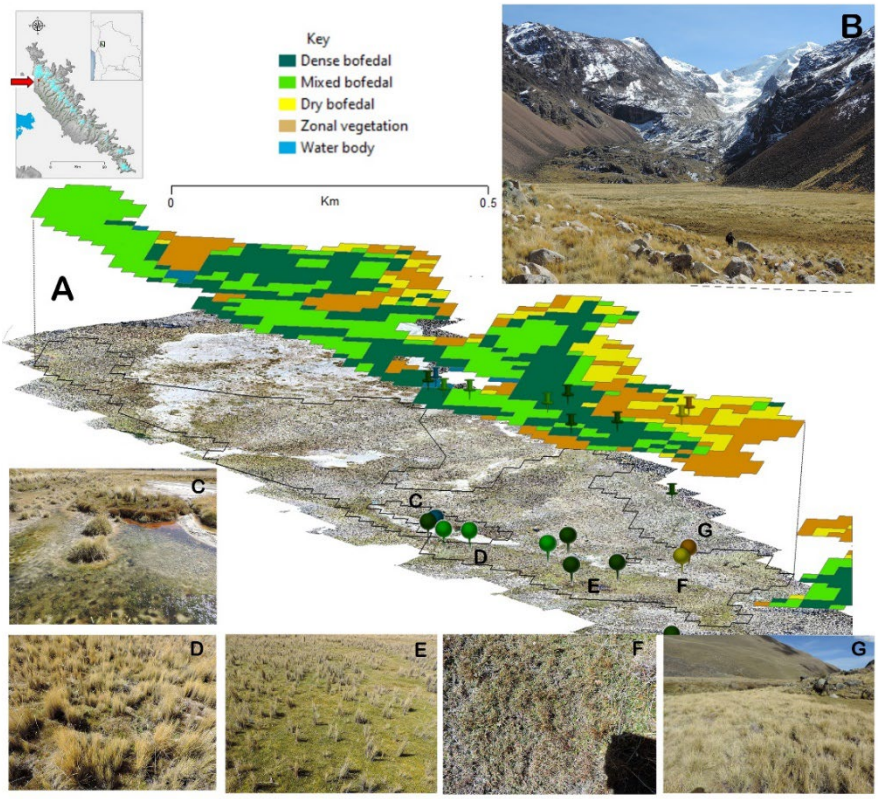

Figure 31. Example of the outcome of the classification of different bofedal classes in the Ancohuma valley (Cordillera Real). A) Classification and mosaic of aerial pictures showing the locations of the field assessment points. B) Panoramic picture of the valley. C) Waterbody with Myriophyllum and Oxychloe andina on the sides. D) Mixed bofedal of Festuca sp and Oxychloe andina. E) Dense bofedal of Oxychloe andina. F) Dry bofedal of Phylloscirpus deserticola. G) Zonal vegetation of tussock grasses of Stipa ichu.

In the areas where desiccation seemed to be the cause of succession from dense to dry bofedales, the indicator species were *Carex sp., Aciachne pulvinata, and Deyeuxia spicigera.* A cover of organic matter from dead individuals of *Oxychloe* was observed (Figure 32A). On the other hand, areas with evidence of overgrazing (fecal material from camelids) showed a larger presence of *Deyeuxia rigescens* (Figure 32B). I found evidence of other animals grazing in the bofedal. For example, donkeys removed individuals of *Oxychloe* to reach other plants.

Figure 32C shows the dead extracted leafs of *Oxychloe* lying on the ground. In some bofedales, I found abandoned *estancias* (houses of pastoralists used to spend the night), which is evidence of prior management. When no management techniques or active presence of pastoralist activities were occurring, I observed associations of mixed bofedales of *Oxychloe* with *Festuca* and *Deyeuxia* (Figure 32D).

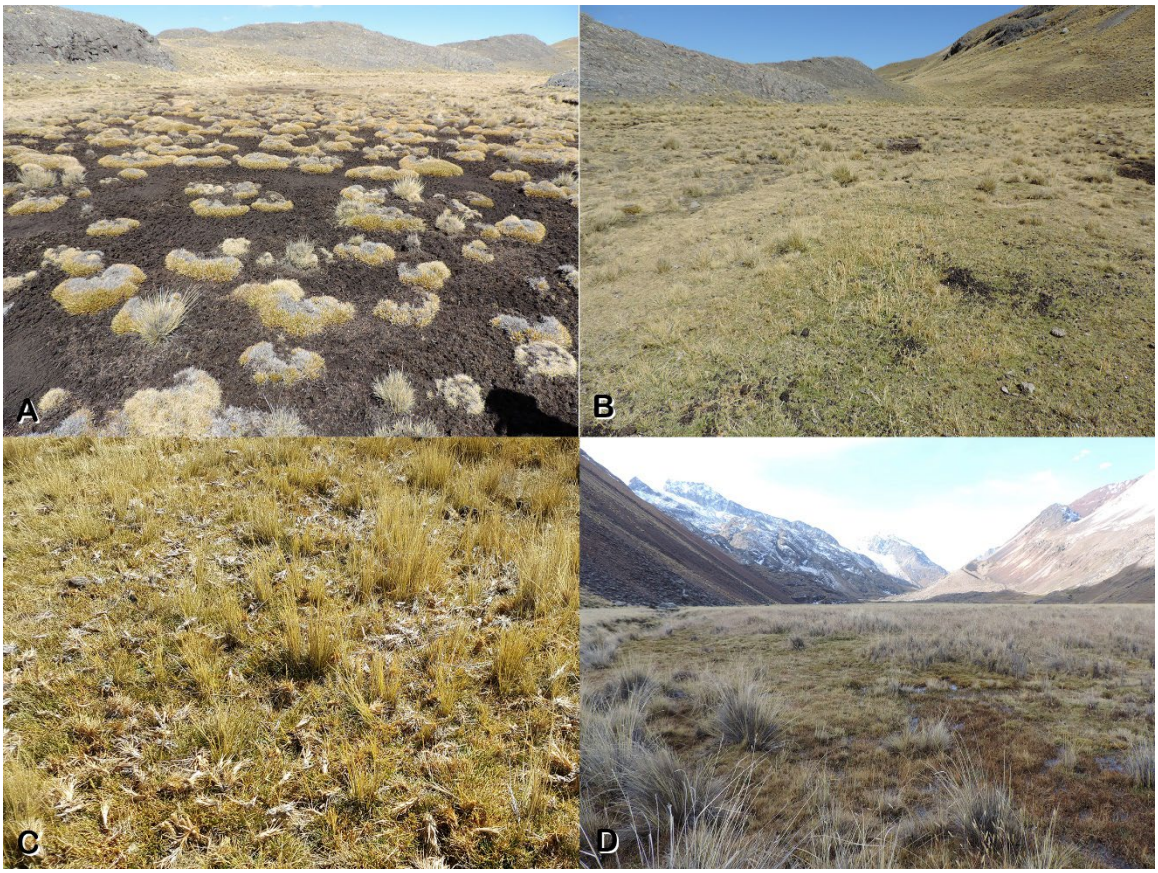

Figure 32. Different types of succession processes found in the bofedales of Cordillera Real. A) Desiccation of a dense bofedal. Dead individuals of Oxychloe *turn into soil organic matter. B) Overgrazing process on a dense bofedal.* Deyeuxia rigescens *appears close to the fecal rests of camelids. C) Donkeys extract the leafs of* Oxychloe *to reach other plants. D) Without the presence of camelids or any management technique,* Festuca sp*. invades a patch of* Oxychloe*, turning it to a mixed bofedal.*

Classification results in the Sajama National Park

In Sajama National Park dense bofedales and mixed bofedales were the dominant classes of bofedales in the area (32% and 40% of the total) (See Table 14 and Figure 33). On average, dense bofedales were similar in size as mixed bofedales and both classes were at least twice as large as the zonal vegetation. Dry bofedales occupied a larger area than in the Cordillera Real (18%) and although on average they were smaller than 1000 m^2 they

were the most frequent class with more than dense and mixed bofedales combined. Water bodies were the smallest class with only 198 m^2 of size. The accuracy of the classification was 0.95 using 60 points randomly selected (See Table 15).

Table 14. Summary of the classification of bofedales in the Sajama National Park.

#	Class	Land cover	Count	Area [m^2]	[%]	Average [m^2]
1	Dense bofedal	Dominance of *Oxychloe*, *Distichia*	5,924	22,212,991	32.0	3750
2	Mixed bofedal/ Mixed pastures	Drying presence of *Oxychloe*, *Distichia*	8,055	27,825,630	40.1	3454
3	Dry bofedal/ Mixed pastures	Absence of *Oxychloe*, *Distichia*	14,511	12,699,685	18.3	875
4	Zonal vegetation	Shrublands, Grasslands, Forests, Dry meadows	3,941	6,434,552	9.3	1633
5	Water body	Streams, ponds, swamps	743	147,407	0.2	198
	TOTAL		**33,174**	**69,320,265**	**100.0**	**2090**

Table 15. Confusion matrix of the classification algorithm in the Sajama National Park (20% of the control points)

	Predicted Class				
Actual Class	1	2	3	4	5
1	32	0	0	0	0
2	2	8	0	0	0
3	0	0	14	0	0
4	0	0	1	1	0
5	0	0	0	0	2

Validation overall accuracy: 0.95

Among dense bofedales, the most common dominant species were *Oxychloe andina* and *Distichia muscoides,* associated mostly with *Phylloscirpus deserticola, Zameioscirpus muticus, Werneria sp.* and *Deyeuxia curvula*. In some cases, the dominant species of dense bofedales was *D. curvula*. Many of the species that comprise dry bofedales and mixed bofedales found in the Cordillera Real, also were present in Sajama, like *Plantago tubulosa, Eleocharis melanocephala, Festuca rigescens,* and *Lachemilla pinnata*. However, the dominant species that comprised the areas of zonal vegetation were *Festuca ortophylla* and *Parastrephia sp.* . In the case of water bodies, the prevalent aquatic species

were *Myriophyllum quitense, Ranunculus trichophyllus,* and *Cotula mexicana*. In humid and soil saturated environments the species found were *Lachemilla diplophylla* and *Lachemilla* pinnata. On the edge of some waterbodies, it was possible to find *Deyeuxia chrysantha*. Many dry bofedales were in soils with high concentrations of salt and minerals that acquired a white color when the evapotranspiration rates were high. The species found in these environments were *Sarcocornia pulvinata, Distichlis humilis,* and *Cuatrecasasiella argentina*.

The distribution of bofedal classes also varied between communities. In Caripe, where there are more saline soils but also important water irrigation projects there was an even distribution of the different classes of bofedales. In Manasaya, the dry bofedales occupied a larger area, whereas in the Sajama and Lagunas communities the mixed bofedales were the larger class. The bofedales in Papel Pampa were mostly dense bofedales (Figure 33).

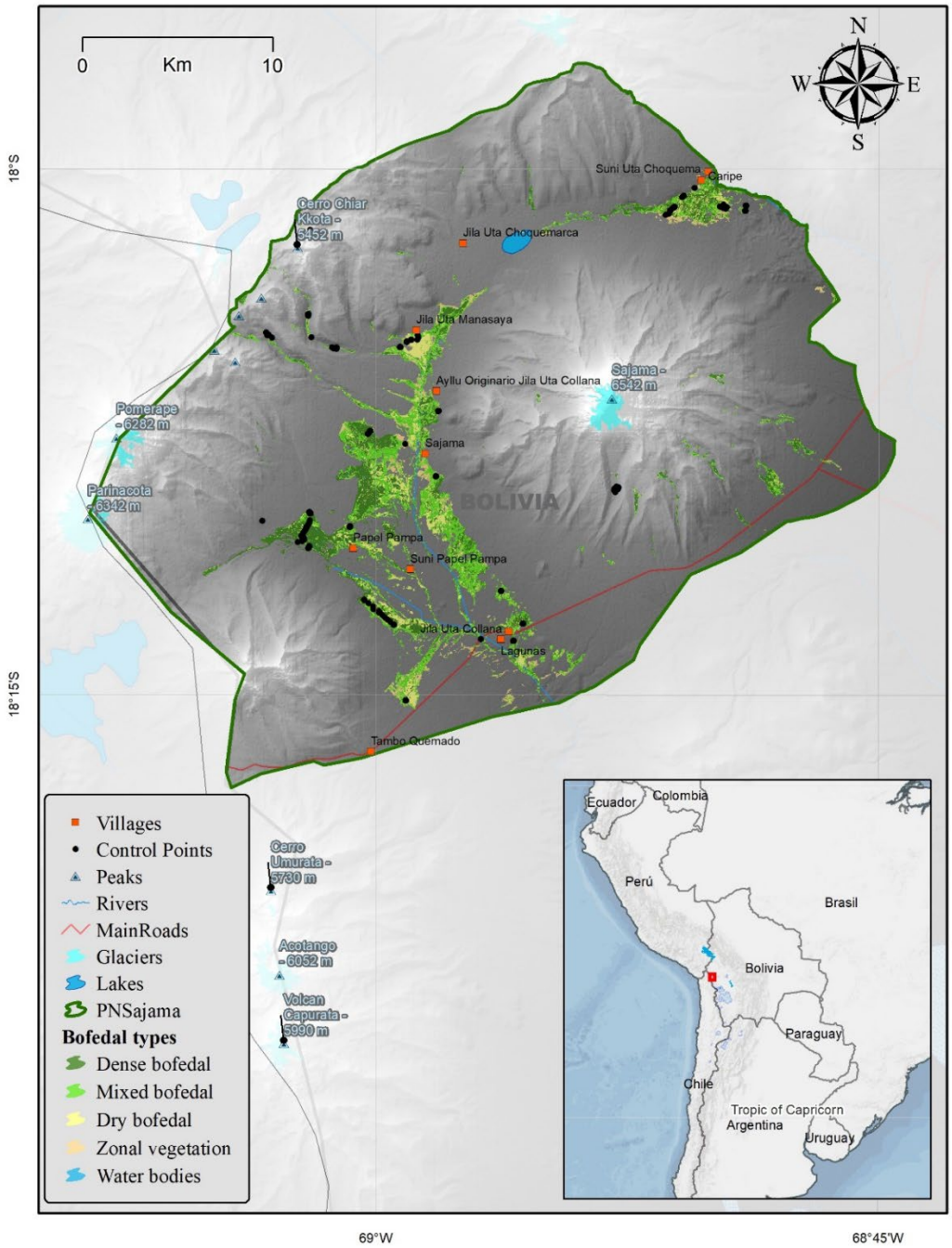

Figure 33. Map of bofedal types in the Sajama National Park.

One of the most heterogenous bofedal *sensu latu* was the one in the Caripe community, to the northern region of the national park. Figure 34 shows the complexity of the bofedal

structure. Dense bofedales were few and scattered and large areas of dry and mixed bofedales were identified. Despite the active irrigation of the area, many sectors were dry or covered in salt.

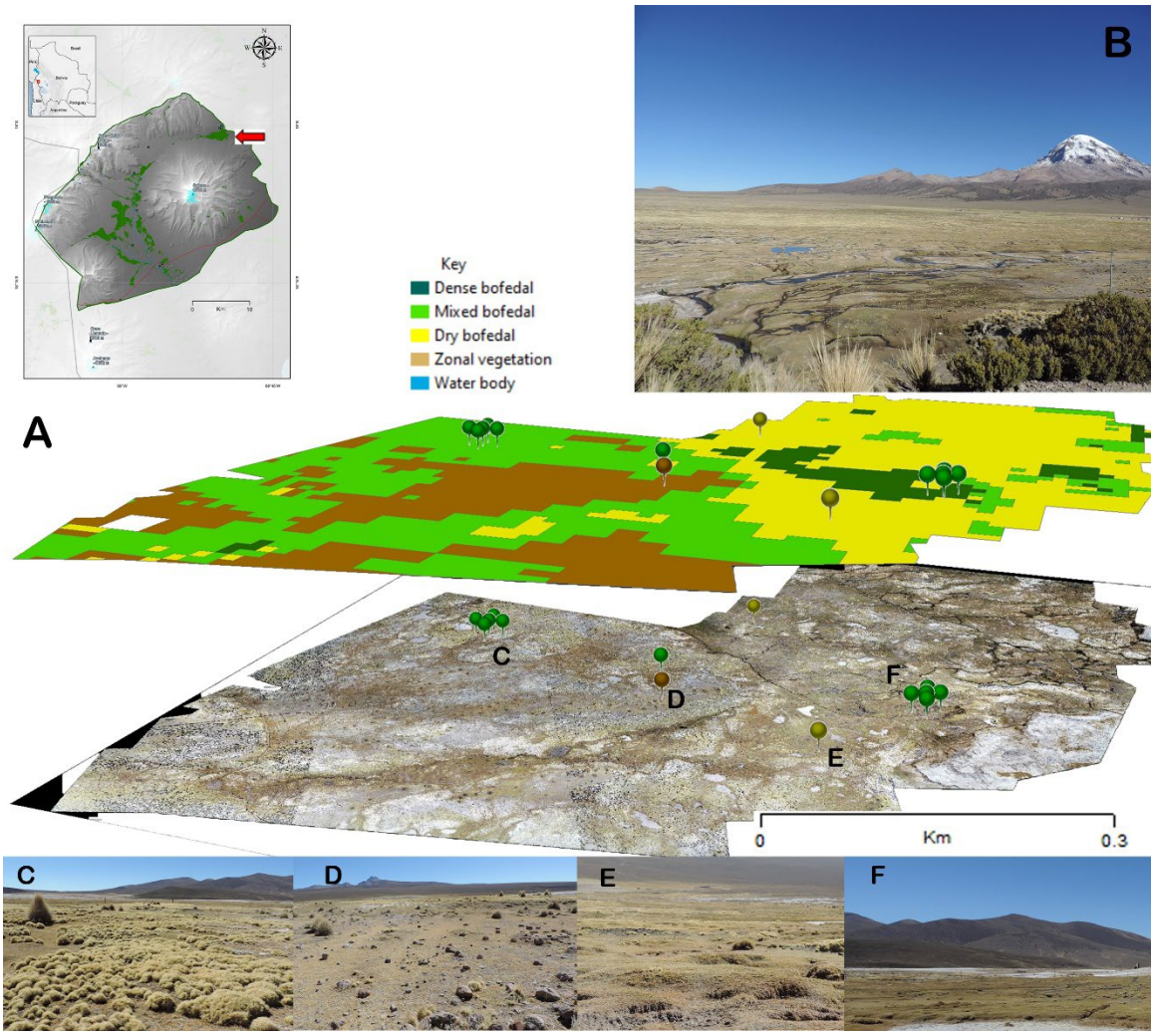

Figure 34. Example of the outcome of the classification of different bofedal classes in a bofedal sensu latu of the Caripe community (Sajama National Park). A) Classification and mosaic of aerial pictures showing the locations of the field assessment points. B) Panoramic picture of the study sector. C) Mixed bofedal of Deyeuxia curvula. D) Zonal vegetation of Festuca orthophylla and low grasses of Distichlis sp. E) Dry bofedal of Phylloscirpus deserticola. F) Mixed bofedal of Phylloscirpus deserticola and a few patches of Oxychloe andina.

Classification results in the Lípez district

In the Lipez district dry bofedales were the dominant class in the area (82% of the total), followed by mixed bofedales (6.7%) and zonal vegetation (6.4%) (See Table 16 and Figure 35). Dense bofedales were the smallest type (less than 1%) and the less numerous as well (452 polygons). As shown in Figure 35, bofedales in Lipez occupy the riverbeds and therefore don't occupy large extensions. However, dry bofedales were the largest type of polygons in all three studied regions (7,000 m^2). Water bodies, which occupied a 4.4% of the bofedales area were on average the second largest feature with 2,740 m^2. The rest of the classes had an average size smaller than 1000 m^2. The accuracy of the classification was 0.97 using 31 randomly selected points (Table 17).

Table 16. Summary of the classification of bofedales in the Lipez district.

#	Class	Land cover	Count	Area [m^2]	[%]	Average [m^2]
1	Dense bofedal	Dominance of *Oxychloe*	452	228,713	0.3	506
2	Mixed bofedal/ Mixed pastures	Drying presence of *Oxychloe*	9,402	4,934,290	6.7	525
3	Dry bofedal/ Mixed pastures	Absence of *Oxychloe*	8,763	60,464,362	82.2	6,900
4	Zonal vegetation	Shrublands, Grasslands, Forests, Dry meadows	7,559	4,671,381	6.4	618
5	Water body	Streams, ponds, swamps	1,186	3,249,840	4.4	2,740
	TOTAL		**27,362**	**73,548,586**	**100.0**	**2,688**

Table 17. Confusion matrix of the classification algorithm in the Lipez District (20% of the control points).

	Predicted Class				
Actual Class	1	2	3	4	5
1	3	0	0	0	0
2	0	3	1	0	0
3	0	0	17	0	0
4	0	0	1	3	0
5	0	0	0	0	4

Validation overall accuracy: 0.97

Among dense bofedales, the most common dominant species was *Oxychloe andina*, usually associated with *Zameioscirpus muticus, Phylloscirpus atacamensis,* and *Deyeuxia curvula*. Dry and mixed bofedales were dominated by *Deyeuxia curvula, Phylloscirpus atacamensis, Zameioscirpus muticus, Baccharis acaulis*, *Arenaria sp*., *Werneria sp*., and *Carex sp.* In this region, like in Sajama, the saline environments (*qullpares*) were common among the dry bofedales class. The species that were common in the *qullpares* were *Sarcocornia*, *Frankenia*, *Distichlis humilis, Plantago tubulosa, Carex sp.,* and the orhid *Mirosmodes*. The dominant species that comprised the areas of zonal vegetation were shrublands of *Parastrephia sp.* In the case of water bodies, the prevalent species were *Eleocharis melanocephala*, and *Myriophyllum quitense*.

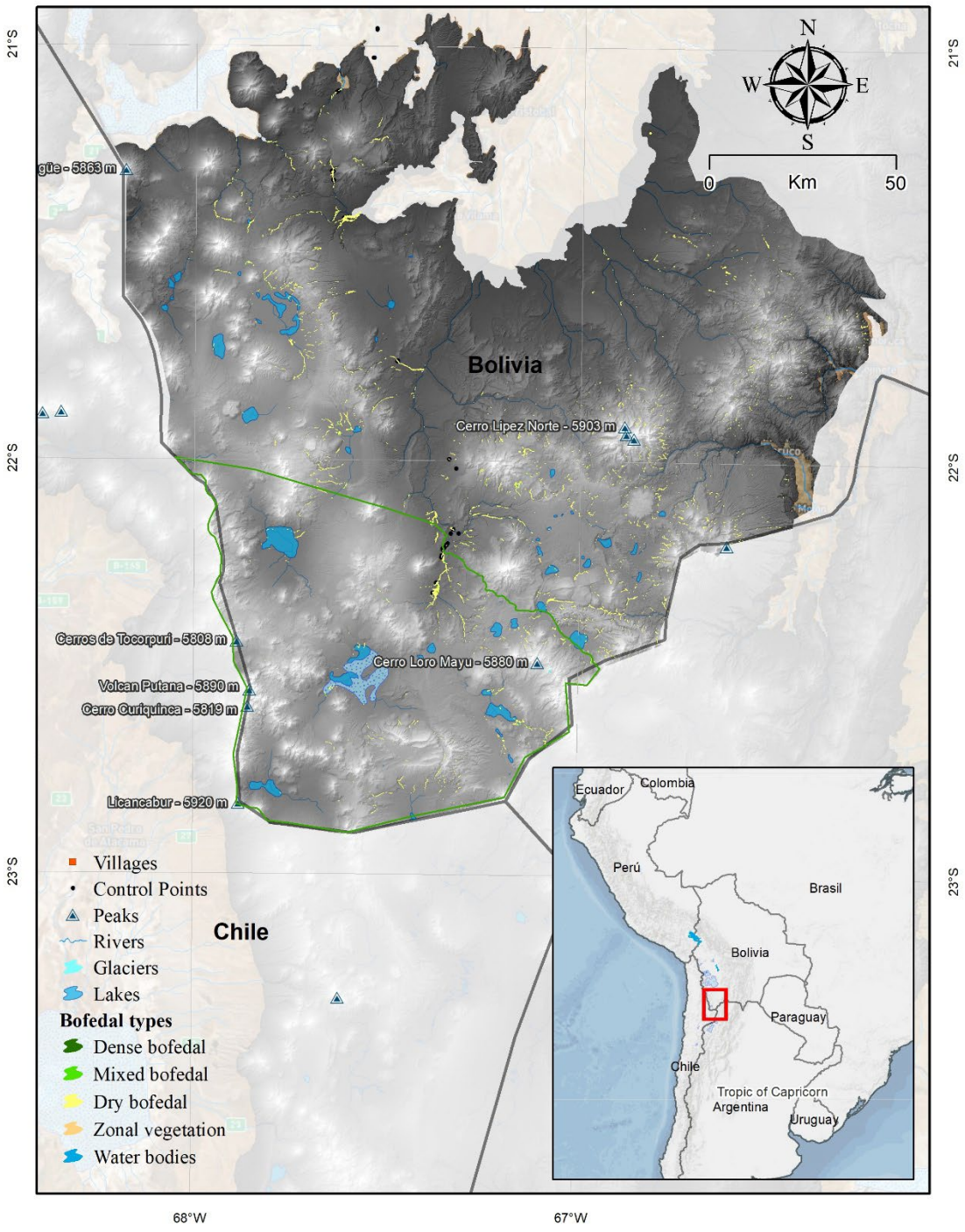

Figure 35. Map of bofedal types in the Lipez District.

Bofedales in Lipez were in all cases mosaics dominated by a matrix of dry bofedales with small patches of mixed and dense bofedales. Figure 36 shows this structure of bofedal. Mixed bofedales were few and scattered within a matrix of dry and shallow bofedales. Many sectors were dry or covered in salt.

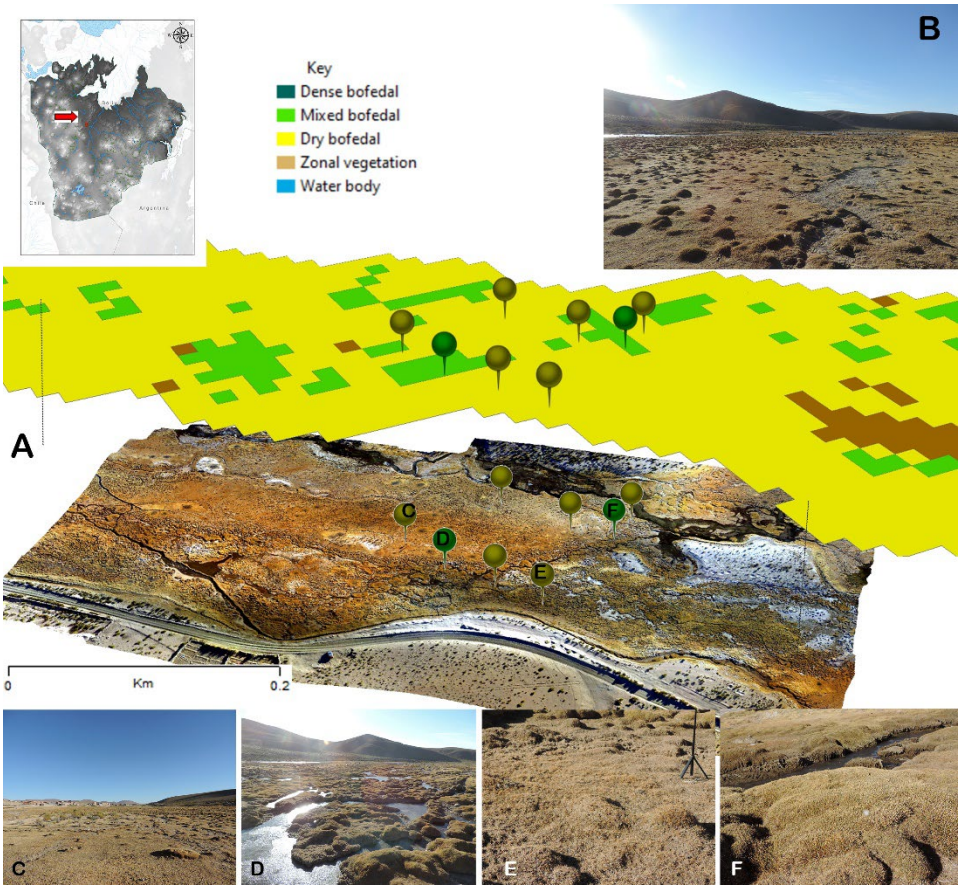

Figure 36. Example of the outcome of the classification of different bofedal classes in a bofedal (sensu latu) of the Villamar community (Lipez biogeographic district). A) Classification and mosaic of aerial pictures showing the locations of the field assessment points. B) Panoramic view of the sector. C) Dry bofedal of Phylloscirpus deserticola. D) Mixed bofedal of cushions of Oxychloe andina and Zameioscirpus muticus. E) Dry bofedal of Phylloscirpus deserticola and Carex sp. F) Mixed bofedal of Oxychloe andina and Zameioscirpus muticus.

Discussion

Bofedales are not homogeneous ecosystems and instead form complex mosaics of diverse associations of plant species (Ruthsatz 2012, Meneses et al., 2021). Our results showed that this heterogeneity could be identified with remote sensing tools that otherwise have only been studied with botanical field assessments. I found that the use of *Distichia muscoides* and *Oxychloe andina* is important for the definition of dense bofedales because not only these species form peat and have larger rates of carbon sequestration (Cooper, Kaczynski et al. 2015) but also because they play a role in the survival of other species associated to them (Loza et al. 2015). On the other hand, future studies should consider the further classification of bofedales dominated by *Distichia* from those dominated by *Oxychloe* since it has been observed that Distichia is more sensitive to drought conditions and occupies mostly the center of the wetland units (Loza et al. 2015).

Classification of bofedales has been done considering other parameters than plant species associations. In their analysis of grazing pressure and water presence on bofedales, Cochi-Machaca et al. (2018) considered two types of bofedales, mesic and hydromorphic. However, they were not able to identify significant differences between these two types regarding number of species, water presence, or dominance. Nonetheless, they obtained through a botanical composition analysis three clusters of bofedales regarding their floristic composition. This is consistent with the relevance of classifying the vegetation based on the floristic composition to analyze bofedales. Ruthsatz (2012) identified several microenvironments within the bofedales mosaics based on the floristic composition and species association and some of those can be compared to the bofedal classes of the present

study. For example, what she mentions as ‘compact and continuous layers of peat forming cushion plants’ fall within the class of dense bofedales because it comprises the species *Patosia clandestina, Distichia muscoides, D. filamentosa, Oxychloe andina,* or *Zameioscirpus atacamensis.* Other similarities were also found between the categories grass and aquatic vegetation, with zonal vegetation and waterbodies classes that I employed in this study. However, not all types of microenvironments identified in this latter study were exactly analogous with the classes I used. The class ‘dry bofedales’ and ‘mixed bofedales’ may include several microenvironments identified by Ruthsatz like ‘continuous flat growing cushion layers of cyperaceous plants’, ‘low herbs of seasonally humid environments’, ‘isolated plants that benefit from the cushion plants’, ‘associated species to the ecotone cushions’, and ‘halophytic plants.’ The reason for this classification resides on the scale of analysis. Many of these plants are very small (~1 cm^2), occur interstitially in the cushion matrices, and would not be able to be recognized by satellite sensors that have a minimum pixel size of 10 m.

Despite the potential error between the location of the field surveys and the classified pixel, the model showed very high accuracy, which means that the random forest classification is a fit method to classify bofedales in the Bolivian Altiplano.

In addition to the identification of the structure of bofedal classes inside the wetland units, it was evident that this structure varied among the three analyzed regions. The predominant class varied from dense bofedal, to mixed bofedal, to dry bofedal as the southern latitude increased. These results showed that the mapping of bofedales may provide more depth in interpretations of the ecological and environmental dynamics when considering

subcategories. For example, the absence of *Distichia muscoides* in Lipez, or the presence of *Distichia filamentosa* only in Cordillera Real, are signs of the variations between regions that is consistent with variability found in this study's classification results. Also, *D. filamentosa* is very rare, only found in very high altitudes, and is considered a threatened species. Being much more dry, the Lipez sector has more bofedales dominated by *Zameioscirpus muticus* and *Z. atacamensis*, which forms only a shallow layer of peat. Ruthsatz (2012), who also found this characteristic, associated it with the prevalence of halophytic environments in the South. Among the plants that dominate the peripheral dry bofedales, in Lipez *Distichlis humilis* was more common, whereas in Sajama the most common species was *Plantago tubulosa*. There were also some similarities between these two regions. For example, a common association of *Sarcocornia* and *Plantago* was found between the dry bofedales of Sajama National Park and the Lipez sector.

The Cordillera Real region has more input of water sources thanks to the presence of glaciers and because it receives higher annual rates of precipitation (Andrade, Moreno et al. 2018)but also is more exposed to the impacts of the retreat of ice cover (Zimmer, Meneses et al. 2018). Future research, monitoring the change of the structure of bofedales and Andean wetlands, would put more light on our understanding of the impacts of glacier retreat and global warming upon high altitude wetland ecosystems.

It has been observed in all regions that dry bofedales also are classified in areas where dense bofedales or mixed bofedales are starting to deteriorate or desiccate. However, the succession may be different from site to site depending on the presence of groundwater,

and the salinity level of the soil. In the case of saline environments, the transition to dry bofedales occur with the increase of *Distichlis* and *Sarcocornia*.

Conclusion

Bofedales are complex and heterogenous mosaics of associations of plant species adapted to permanent or temporal water saturation. Depending on the species that comprise these associations, bofedales may form peat and have different ecohydrological functions. From a combined botanical and remote sensing points of view, I differentiated five classes: dense bofedales, mixed bofedales, dry bofedales, zonal vegetation, and water bodies. Through extensive botanical assessments and the application of a classification algorithm on the Google Earth Engine platform, the spatial distribution of these associations classes was determined in three regions on the Bolivian Altiplano. The northern region, the Cordillera Real, had larger coverage of dense bofedales (42.1% of the total bofedal area) than the central and southern regions (32% and 0.3%). In the central region, the Sajama National Park, mixed bofedales/ mixed pastures were the predominant association (40.1%), whereas in the Lipez sector (the southernmost region of the Bolivian Altiplano) dry bofedales were the predominant association within the bofedales extension (82.2%). Dense bofedales in the Cordillera Real and in the Sajama National Park were dominated by *Oxychloe andina*, *Distichia muscoides*, or a combination of both species. In some sectors of Cordillera Real *Distichia filamentosa* was also part of dense bofedales. *Patosia clandestina,* another dense bofedal species, was not found in the botanical assessments because its distribution is outside of the study regions. Dense and mixed bofedales of Lipez sector were dominated

by *Zameioscirpus muticus* and formed shallow cushions. Some sectors of the dry bofedales of Sajama and Lipez were highly saline and were occupied by *Distichlis* and *Sarcocornia.* Finally, bofedales that underwent desiccation processes due to droughts or land use changes (with visible signs of abandonment, construction activities, or peat extraction) showed larger presence of mixed and dry bofedales compared to that of dense bofedales. Dense bofedales in poor health conditions were classified as mixed or dry bofedales with the algorithm.

Chapter 3. Spatiotemporal patterns of bofedales in the Bolivian Altiplano

Introduction

Climate change is affecting every ecosystem on the planet, particularly in the high altitude regions of the tropics, where global warming is projected to increase by over 6 °C within the present century (Bradley, R. S., Vuille et al. 2006). In the tropical Andes, climate change manifests as the rise of the elevation of the snowline and the retreat of glaciers (Bradley, Raymond S., Keimig et al. 2009, Rabatel, Francou et al. 2013), the increment of extreme weather events (Thibeault, Seth et al. 2010), changes of species distribution (Anderson, E. P., Marengo et al. 2011), species migrations, increase of illnesses (Seimon, Seimon et al. 2017, Grabherr, Gottfried et al. 2000), and alterations of the hydrological cycle (Mark, French et al. 2017, Baraer, Mark et al. 2012, Mark 2008). One of the most important factors of climatic change in the tropical Andes is the El Niño Southern Oscillation (ENSO) phenomenon (Diaz, Hoerling et al. 2001). The anomalies of sea surface temperature and circulation in the different regions of the tropical Pacific Ocean, that characterize ENSO have been shown to have a direct relationship with variations in the weather patterns of many regions, including the Andes (Aguado, Burt 2015). These teleconnections have increased in strength since the 1980s (Diaz, Hoerling et al. 2001), and might have a critical positive feedback in the mechanisms that promoted drier and warmer

conditions in the Bolivian Altiplano over the last 370 thousand years (Bush, Hanselman et al. 2010) and will possibly play a role in the climatic changes of the present century.

Bofedales are one of the many ecosystems that are threatened by these impacts because they strongly depend on the availability of water (Squeo, Warner et al. 2006). Although there are other human activities that also threaten bofedales, (e.g. overgrazing, mining, peat extraction, flooding, or abandonment), climate change effects cuts across all other factors of degradation (Yager, Valdivia et al. 2019). Previous studies have shown that bofedales are sensitive to alterations in precipitation patterns, glacier and snow cover retreat, and ground water depletion (Anderson, T. G., Christie et al. 2021, Dangles, Rabatel et al. 2017, Garcia, E., Otto 2015). The observed responses of bofedales to these events include reductions in their number and extension (Dangles et al 2017), lags in the greening response (Anderson et al. 2021), and shifts in the floristic composition (Loza Herrera, Meneses et al. 2015). However, it is difficult to quantify the impact of climate change on bofedales because their intraannual variability patterns are not fully understood (Domic et al. 2019). To date, only a few studies have tried to understand the interactions between bofedales conditions and hydroclimatic variables. Initial studies showed a strong relation between precipitation patterns and the occurrence of bofedales in the Central Andes. In a multidecadal interannual analysis in Bolivia, Dangles et al. (2017) found that the number and size of bofedales correlate with the meteorological conditions, and with the presence of glacier coverage in the headwalls of high-altitude valleys. Their approach, based on satellite monitoring, was the first study to consider interannual variability on a multidecadal time range but didn't consider possible intra annual trends. Thus, the observed variability

in wetland productivity was explained only partially. Later, Chávez et al. (2019) and Anderson et al. (2021) performed a monthly analysis of Chilean peatlands over a similar period of time (over 30 years) and found that part of the variability of bofedales size is explained by the strong phenological seasonality. Their study confirmed that wetlands' productivity correlates with hydroclimatic variables, such as precipitation and snow cover. Furthermore, Squeo et al. (2006) identified that vegetation productivity in the Southern Andean Steppe is affected by the ENSO phenomena, showing that there might be multiple connections between the climate variability and sensitivity of bofedales.

Following these studies, the aim of this work is to examine the seasonal patterns of bofedales in Bolivia over the last two decades and examine 1) their response to meteorological variables, 2) their relationship with the ENSO dynamics, and 3) the interaction between ENSO dynamics and local meteorological variables. To achieve these objectives, I selected 11 bofedales from the wetlands delineated in chapter 1, considering a latitudinal transect and evaluated the Normalized Difference of Vegetation Index (NDVI) monthly values, used as a proxy of the biomass productivity and health conditions, to determine their seasonal and interannual patterns. I then evaluated the correlation between those temporal patterns with the temperature and precipitation, and with the Pacific Ocean Sea surface temperatures and anomalies. Finally, I evaluated the correlation between ENSO dynamics and the meteorological variables in order to examine the relationship between ENSO dynamics, meteorological events, and NDVI values.

Data and methods

Study Area

The Bolivian Altiplano is a high plateau that spans from 14° S to 23° S with an average elevation of 4,000 m a.s.l. (Lamb 2004). It is located between the Western and Eastern Cordilleras of the Andes and contains in the center ephemeral shallow lagoons, large endorheic lakes, extensive salt flats, and some conical hills (Lamb 2004). The Bolivian Altiplano is classified within the South American Central Puna ecoregion and comprises the Humid (to the North) and the Dry Puna (to the South) subregions. The vegetation classes include shrublands, grasslands, crops, and scattered wetlands. The climate is characterized by a year-round daily frost-thaw cycle with small monthly average temperature variations and a clearly defined dry and wet seasons (Figure 37). The North and Northwestern regions (Humid Puna) are closer to the Equator and lie along the Amazon Basin headwalls, whereas the southern regions (Dry Puna) occur closer to the Atacama Desert and to the subtropical high-pressure latitudes (beyond 20° S).

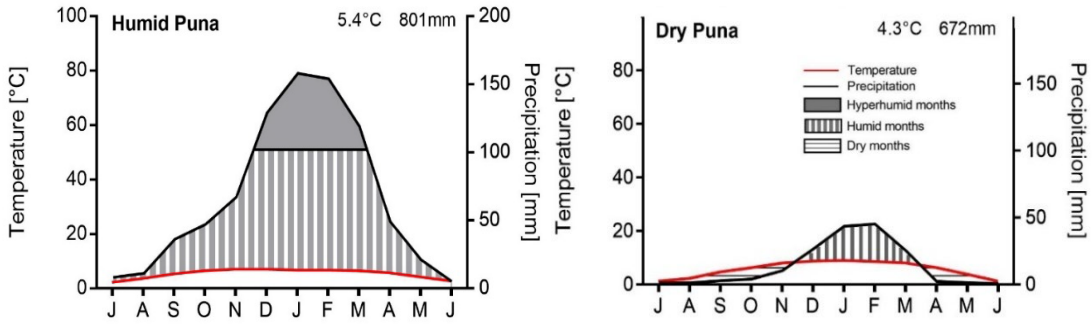

Figure 37. Climate diagrams of Northern and Southern Altiplano.

Selected sites

From the delineated bofedales obtained in chapter 1, I selected 11 bofedal polygons in the Bolivian Altiplano (Figure 38). The criteria to select these 11 bofedales was that they were latitudinally distributed along the Bolivian Altiplano, and that they had a size larger than 0.2 km^2 so that the spatial resolution of the MODIS imagery could capture their variability (MODIS pixel size was 250 m x 250 m). Field campaigns during the dry seasons of 2019 and 2021 were conducted to confirm in the field the presence of the bofedal and validate its characteristics. The location and characteristics of each bofedal are shown in Table 18.

Table 18. Physical characteristics of the selected bofedales.

Site	Name	Latitude [m]	Longitude [m]	Elevation [m a.s.l.]	Aspect	Size [km2]	Number of MODIS pixels
Humid Puna							
1	Apolobamba	14°59'45"	69°18'38"	4360	SW	104.00	2441
2	Cordillera Real	16°02'48"	68°25'26"	4438	SE	2.86	104
3	Tres Cruces	16°56'12"	67°25'40"	4534	S	0.21	12
Dry Puna							
4	Caripe	18°01"01"	68°50'30"	4193	NE	5.26	133
5	Manasaya	18°04'28"	68°58'01"	4296	SE	2.82	97
6	Sajama	18°08'34"	69°00'06"	4246	SE	9.62	230
7	Papel Pampa 1	18°10'29"	69°01'39"	4219	E	5.49	142
8	Papel Pampa 2	18°12'38"	68°59'35"	4178	NE	3.17	90
9	Villa Alota	21°25'01"	67°36'25"	3817	E	2.63	98
10	Quetena Chico	22°08'23"	67°22'38"	4116	E	1.16	56
11	Quetena Grande	22°18'52"	67°22'11"	4211	E	3.79	116

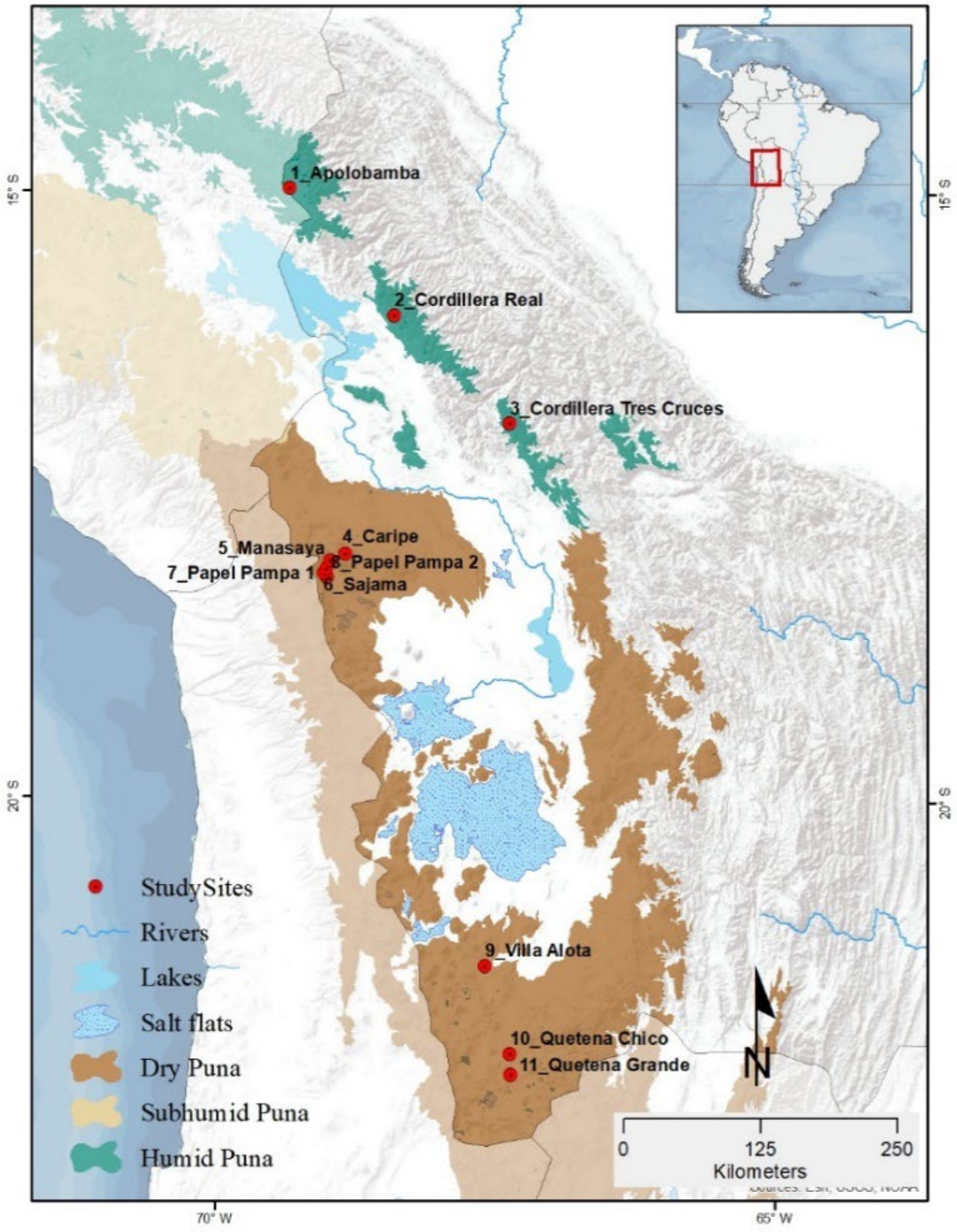

Figure 38. Geographic distribution of the selected sites.

Datasets and image collections

A summary of the datasets used in this chapter is in Table 19. I used the Image Time Series code on the Google Earth Engine platform to collect the data from the NDVI band of the Terra Moderate Resolution Imaging Spectroradiometer (MODIS) (250 m pixel) (Table 19) for each one of the selected bofedales, from February 2000 to December 2021. In the code, I averaged all pixel values of the polygons within each point in time. Because the frequency of the datasets is every 16 days, I chose the maximum value per month because it represented the highest vegetation values corresponding also to less influence of cloud coverage. Precipitation, minimum and maximum temperature values were obtained using the same Google Earth Engine code from the TerraClimate Monthly Climate and Climatic Water Balance for Global Terrestrial Surfaces dataset (Abatzoglou, Dobrowski et al. 2018). Average maximum and minimum temperature were calculated in a Microsoft Excel database to obtain a single monthly value per site/polygon. Once I obtained the monthly time series, I normalized the data and seasonally adjusted the values using a 12-month moving average and an estimated seasonal component in MATLAB in order to detect the annual trend. Lastly, I downloaded the Pacific Ocean Sea Surface Temperatures and sea surface temperature anomalies for regions 1+2, 3, 3.4, and 4, from the National Oceanic and Atmospheric Administration (NOAA) web data portal.

Table 19. Datasets of NDVI, temperature, precipitation, and Pacific Ocean Sea Surface Temperature.

Parameter	Dataset	Frequency	Resolution	Time range	Source/Author
NDVI	Terra Moderate Resolution Imaging Spectroradiometer (MODIS) Vegetation Indices (MOD13Q1) Version 6.1	16-Day	250m/pixel	2000/Feb – 2021/Dec	NASA's Land Processes Distributed Active Archive Center (LP DAAC)
Maximum and minimum temperature	TerraClimate: Monthly Climate and Climatic Water Balance for Global Terrestrial Surfaces	1 Month	4638.3 m/pixel	1958/Jan – 2020/Dec	(Abatzoglou, Dobrowski et al. 2018)
Precipitation accumulation	TerraClimate: Monthly Climate and Climatic Water Balance for Global Terrestrial Surfaces	1 Month	4638.3 m/pixel	1958/Jan – 2020/Dec	(Abatzoglou, Dobrowski et al. 2018)
El Niño/La Niña	Pacific Ocean Sea Surface Temperature and Anomalies	1 Month	Regions N1+2, N3, N3.4, N4	1979/Jan – 2021/Dec	NOAA (www.cpc.ncep.noaa.gov/data/indices/sstoi.indices)

The regions of sea surface temperatures considered in this study were Niño 1+2, Niño 3, Niño 3.4, and Niño 4 (Figure 39). These regions are important for monitoring both El Niño and La Niña developments.

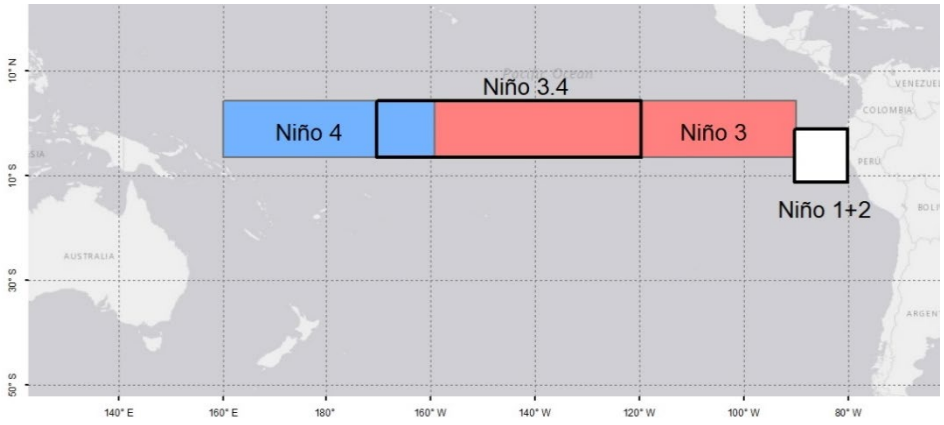

Figure 39. ENSO regions of the tropical Pacific Ocean.

NDVI climatology, and correlations

I compiled data from the NDVI values, temperature, and precipitation for the 11 sites to evaluate the intraannual variability among bofedales. Then, in MATLAB, I ran multiple correlation analyses between NDVI, and the average temperature, and precipitation to evaluate the lag response of bofedales to meteorological conditions. Finally, I ran independent cross-correlation analyses for precipitation and temperature with NDVI values to determine the lag response in months between these time series.

Multiple regression of ENSO dynamics

To evaluate the influence of the ENSO dynamics over NDVI variability, and over temperature and precipitation on each bofedal, I ran multiple linear correlation analyses in MATLAB using the following regression models (Table 20). Each regression model represents a function between the independent variables (right side of the equation), and the independent variable or response (left side of the equation).

Table 20. Models of multiple regression evaluated in MATLAB.

Model	Variables	Linear regression model:
1	sst vs NDVI	NDVI ≈ Intercept + x_1(sst R1+2) + x_2(sst R3) + x_3(sst R3.4) + x_4(sst R4)
2	sstA vs NDVId	NDVId ≈ Intercept + x_1(sstA R1+2) + x_2(sstA R3) + x_3(sstA R3.4) + x_4(sstA R4)
3	T P vs NDVI	NDVI ≈ Intercept + x_1(T) + x_2(P)
4	Td Pd vs NDVId	NDVId ≈ Intercept + x_1(Td) + x_2(Pd)
5	T P vs NDVId	NDVId ≈ Intercept + x_1(T) + x_2(P)
6	Td Pd vs NDVI	NDVI ≈ Intercept + x_1(Td) + x_2(Pd)
7	sst vs T	T ≈ Intercept + x_1(sst R1+2) + x_2(sst R3) + x_3(sst R3.4) + x_4(sst R4)
8	sst vs Td	Td ≈ Intercept + x_1(sst R1+2) + x_2(sst R3) + x_3(sst R3.4) + x_4(sst R4)
9	sstA vs T	T ≈ Intercept + x_1(sstA R1+2) + x_2(sstA R3) + x_3(sstA R3.4) + x_4(sstA R4)
10	sstA vs Td	Td ≈ Intercept + x_1(sstA R1+2) + x_2(sstA R3) + x_3(sstA R3.4) + x_4(sstA R4)
11	sst vs P	P ≈ Intercept + x_1(sst R1+2) + x_2(sst R3) + x_3(sst R3.4) + x_4(sst R4)
12	sst vs Pd	Pd ≈ Intercept + x_1(sst R1+2) + x_2(sst R3) + x_3(sst R3.4) + x_4(sst R4)
13	sstA vs P	P ≈ Intercept + x_1(sstA R1+2) + x_2(sstA R3) + x_3(sstA R3.4) + x_4(sstA R4)
14	sstA vs Pd	Pd ≈ Intercept + x_1(sstA R1+2) + x_2(sstA R3) + x_3(sstA R3.4) + x_4(sstA R4)

Where:

sst	Sea surface temperature
sstA	Sea surface temperature Anomaly
NDVI	Normalized NDVI
NDVId	Deseasonalized NDVI
T	Temperature
Td	Deseasonalized temperature
P	Precipitation
Pd	Deseasonalized precipitation
R	Region

Results

NDVI climatology and correlations

Complete time series datasets of the bofedales monthly NDVI and deseasonalized values are showed in Appendix B. Bofedales showed strong seasonality that is evident in the NDVI climatology (Figure 40). For all bofedales, the peak of vegetation productivity was between March and April, whereas the lowest values were between July and August. The bofedal in Cordillera Tres Cruces is the only one to have two peak values of NDVI along

the year (January, and March). In most sites, precipitation and average temperature peaks matched to be between January or February. Precipitation on the sites in the dry Puna (Figure 40, 4 to 11) had six to seven months with zero or almost zero values.

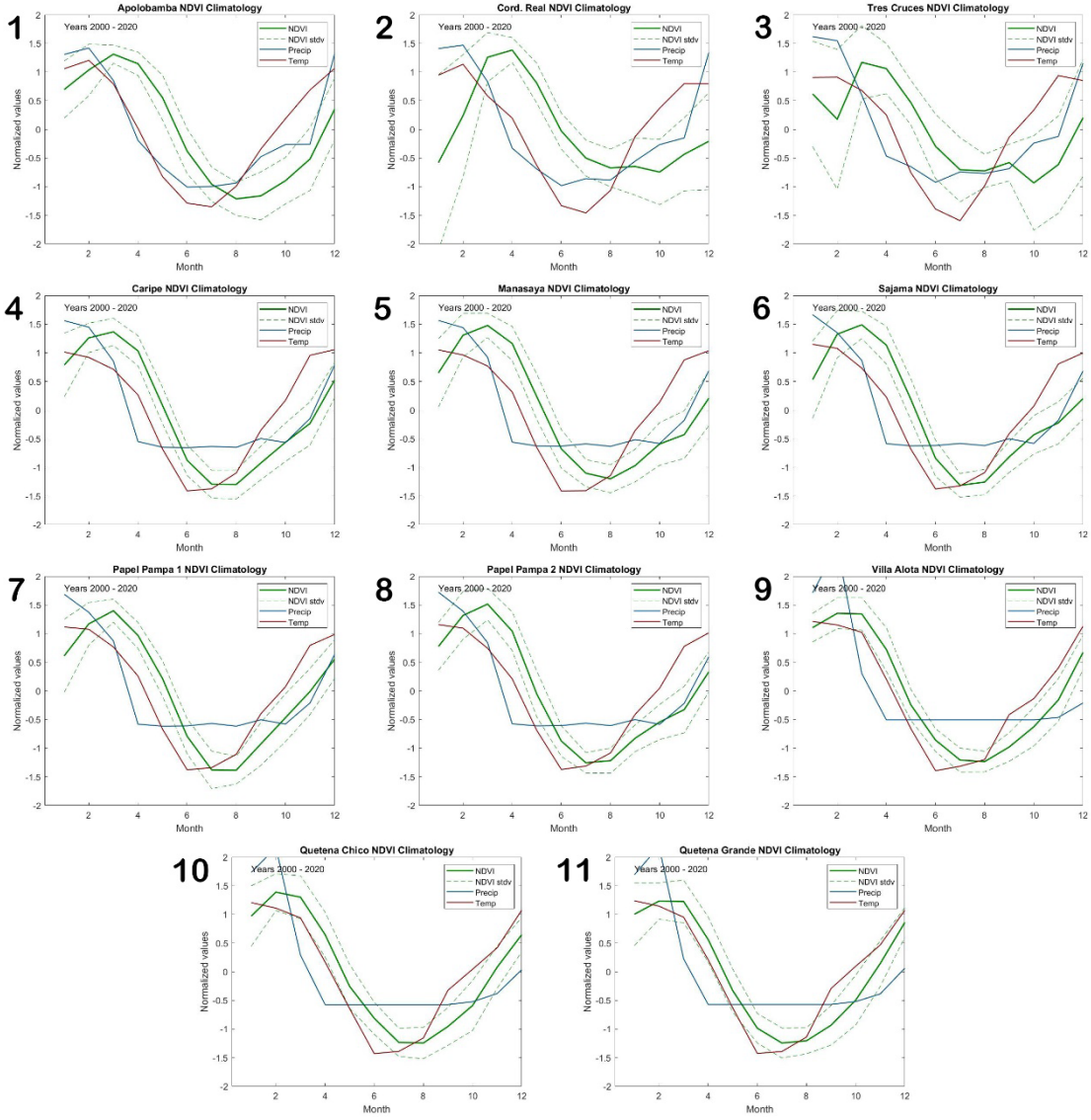

Figure 40. Climatology of NDVI, precipitation, and temperature for the 11 study sites. 1) Apolobamba, 2) Cordillera Real, 3) Cordillera Tres Cruces, 4) Caripe, 5) Manasaya, 6) Sajama, 7) Papel Pampa 1, 8) Papel Pampa 2, 9) Villa Alota, 10)Quetena Chico, 11) Quetena Grande.

Local average temperature and precipitation correlated positively with NDVI values in all bofedales (Table 21). When analyzing the relationship between deseasonalized values of NDVI and meteorological variables, only six bofedales showed some sort of correlation. In all of these cases, the β estimates were rather low ($\beta \leq 0.11$).

Extreme high or low values of precipitation did not result in major variations of the seasonality of NDVI (See Appendix C), which shows the influence of multiple factors on the NDVI seasonality.

Table 21. Results of β-Estimates for the multiple regression models between normalized and deseasonalized values of temperature and precipitation with NDVI. Only statistically (P<0.1) values are shown.

Model	NDVI ~ Intercept + x_1(T) + x_2(P)		NDVId ~ Intercept + x_1(Td) + x_2(Pd)	
Humid Puna	x1	x2	x1	x2
Apolobamba	0.23	0.36	NS	NS
Cordillera Real	0.15	NS	0.10	NS
Tres Cruces	0.16	0.19	NS	NS
Dry Puna	x1	x2	x1	x2
Caripe	0.58	0.25	0.09	NS
Manasaya	0.48	0.23	NS	NS
Sajama	0.57	0.15	NS	NS
Papel Pampa 1	0.66	0.13	NS	NS
Papel Pampa 2	0.55	0.26	NS	0.11
Villa Alota	0.75	0.18	0.05	0.10
Quetena Chico	0.68	0.22	0.04	0.10
Quetena Grande	0.75	0.15	0.06	NS

NS: Not significant results. NDVI: Normalized NDVI; NDVId: Deseasonalized NDVI; T: Temperature; Td: Deseasonalized temperature; P: Precipitation; Pd: Deseasonalized precipitation.

Regarding the cross-correlation, most bofedales showed a peak of correlation with temperature or precipitation after lags of one (Dry Puna) or two months (Humid Puna) (Table 22).

Table 22. Lag in the peak of correlation with NDVI [in months].

Site	vs Temperature	Pearson coefficient	vs Precipitation	Pearson coefficient
Apolobamba	2	0.85	2	0.77
Cordillera Real	2	0.56	2	0.65
Tres Cruces	2	0.56	2	0.54
Caripe	1	0.88	1	0.73
Manasaya	1	0.81	1	0.73
Sajama	1	0.83	1	0.73
Papel Pampa 1	1	0.88	1	0.65
Papel Pampa 2	1	0.86	1	0.76
Villa Alota	1	0.92	1	0.65
Quetena Chico	1	0.90	1	0.67
Quetena Grande	1	0.89	1	0.65

Multiple regression

The results of the models of multiple regression are shown in Appendix D. Statistically significant correlations were found between ENSO sea surface temperatures (SST) with both meteorological parameters (temperature and precipitation) and bofedales' NDVI. Furthermore, correlations with SST in the Pacific Ocean were different depending on the specific El Niño Region. For instance, NDVI correlated positively with the SST of El Niño Region 1+2 (10 sites out of 11), and Region 4 (7 out of 11 sites). However, bofedales' NDVI correlated negatively with Region 3 in all cases except on one single case (Cordillera Real site) which is represented with an * in Figure 41. In the case of NDVI deseasonalized values, the SST anomalies of Regions 3.4 and 4, also correlated positively in 6 of 11 sites. Almost all negative correlations between the NDVI values and the SST were found for Region 3 (7 sites). Region 3 SST anomalies also correlated negatively with the deseasonalized NDVI values of three sites.

The relationships between SST and temperature and precipitation and temperature were very similar to the relation between SST and with NDVI. Positive correlations were found

between temperature and precipitation and the SST/SSTA in Regions 1+2, and 4. And also like with NDVI values, Region 3 correlated negatively with temperature and precipitation values (either normalized and deseasonalized). Region 3.4, on the other hand, had mixed results. While it correlated positively with precipitation, it correlated negatively with the temperature (Figure 41).

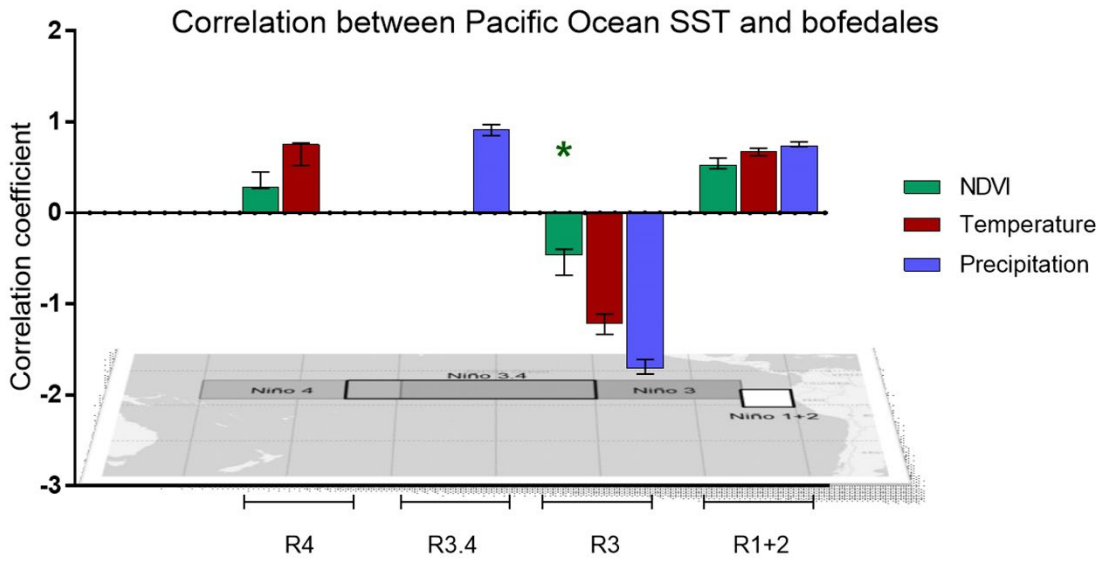

Figure 41. Correlation values between ENSO sst and NDVI, temperature, and precipitation. Only significant values were considered in the figure.

Discussion

NDVI climatology and correlations

This is the first time that bofedales in Bolivia are characterized by the spatiotemporal variability of their productivity at a monthly scale. This was possible due in part to the use of the multi Peta byte datasets of satellite imagery on the Google Earth Engine cloud-based platform. I used the NDVI product of the Terra Moderate Resolution Imaging

Spectroradiometer (MODIS) Vegetation Indices (MOD13Q1) Version 6.1 because it is the longest available time series dataset of satellite imagery (from 2000 to the present) that has no gaps. Although other available image collections, like Landsat TM 5, have finer spatial resolutions, they have a much lower temporal resolution, which results in having discontinuous sets of information. Other satellites or constellation of satellites with good temporal resolutions, like Landsat 8 and 9, or Sentinel 2-A/B, only have a few years of time series datasets. As these sensors continue to acquire data in the coming years, it would be possible in the near future to replicate this study with better spatial accuracy.

In any case, despite a lower spatial resolution (250 m pixel), the MOD13Q1 dataset was sufficient to detect a clear seasonality of large bofedales (> 0.2 Km^2). It is not the first time that NDVI is used as a tool to detect climatic and extreme weather events in the Altiplano. Canedo-Rosso et al. (2019) applied the NDVI product from the Global Inventory Monitoring and Modelling System (GIMMS) on field crops to detect the risk of droughts in the Bolivian Altiplano. In the present study, the NDVI seasonality of bofedales in Bolivia showed a sinusoidal oscillation where the highest productivity occurs between March and April, and the lowest productivity occurs in July and August (Figure 40). In their study in the Chilean Altiplano, Anderson et al. (2021) obtained similar fluctuations using Landsat imagery. Also, like other authors (Anderson, T. G., Christie et al. 2021, Dangles, Rabatel et al. 2017, Otto, M., Scherer et al. 2011), I identified statistically significant correlation between precipitation and temperature with NDVI. However, along the latitudinal gradient, I detected differences in the lag response of bofedales to precipitation. For example, bofedales from the northern Humid Puna had a peak of

productivity that extended up to two months following the peaks of temperature and precipitation, whereas in the southern Dry Puna, the lag between peaks was only of one month. Dangles et al. (2017), found that the bofedales in the Cordillera Real (Humid Puna) have a lag of three months in the response between the peak of precipitation and the wetlands' number and size. This small difference may be due to the different methodology and broader wetland definition that they used. On the other hand, the smaller lag of response in the Southern bofedales (one month) may be related to the fewer extant glaciers in the southern regions. Since glaciers contribute to the accumulation of solid precipitation and the regulation of hydrological cycles in the Andes (Baraer, Mark et al. 2012), it has been found that their presence have a positive effect on the productivity and size of bofedales (Polk, Young et al. 2017, Dangles, Rabatel et al. 2017, Anderson, T. G., Christie et al. 2021).

One other factor that may give some clues to understand the differences in the lag response between bofedales from Humid and Dry Puna, is the relation with the groundwater availability. For example, during the 2015/2016 drought, bofedales in Sajama and from the Southern Altiplano still showed relatively regular seasonality despite almost no precipitation occurred that year. The ground water table dynamics may explain this regularity as it has been proven that bofedales in some regions are recharged by groundwater sources (Cooper, Sueltenfuss et al. 2019). Further research is recommended to explore the interactions between groundwater, meteorology, and bofedales productivity in order to improve our understanding of the vulnerability of bofedales to climate change.

In addition, some sources of noise on the seasonality of bofedales come from multiple anthropogenic factors, which widespread across the Altiplano. These factors have a local origin and would require extensive work at multiple scales to be able to be quantified. Some factors may be negative to bofedales (*e.g.* overgrazing, grazing with non-native animals, mining, extraction, abandonment, or ecosystem destruction for the construction of roads or dams) (Maldonado Fonkén 2014, Yager, Valdivia et al. 2019), or positive (*e.g.* traditional management, rotation of animals, irrigation, cleaning of canals, fencing, construction of erosion control structures) (Yager, Valdivia et al. 2019, Mazzarino, Finn 2016, Hartman, Bookhagen et al. 2016). In any case, further studies are needed to establish the extent and intensity of anthropogenic factors and how they are juxtaposed with the hydroclimatic events.

Finally, the intraannual fluctuations found in this study were far larger than the interannual variability. The linear regression of the NDVI along the past 22 years showed little or no change at all. This is not necessarily coherent with the multiple reports on degradation of bofedales that go back to the 1980s (Squeo, Warner et al. 2006). Furthermore, other multitemporal analyses that applied remote sensing tools have disagreements regarding the long-term trends of bofedales health conditions, size, or productivity. For example, whereas some authors (Yager, Valdivia et al. 2019, Zorogastúa-Cruz 2012, Mazzarino, Finn 2016) indicate that bofedales are overall decreasing in extension. Other authors have found an overall increase in bofedales size or productivity (Pauca-Tanco, Ramos-Mamani et al. 2020, Dangles, Rabatel et al. 2017, Chávez, Christie et al. 2019). However, during focus groups with local stakeholders and participatory mapping in the Sajama National

Park in Bolivia, local perceptions of pastoralist communities indicates that bofedales are rapidly deteriorating due to a combination of climate factors related to extreme weather events and socio-ecological factors influencing access to irrigation (Yager, Valdivia et al. 2019). Perhaps the explanation lies on the large floristic heterogeneity of bofedales. As opposed to other objects that frequently are observed and studied with remote sensing tools, like glaciers or high-altitude lakes, bofedales are far more complex as features. While it is possible that the temporal increase of available water from melting glaciers be the reason why bofedales are showing to grow in some areas despite climate change, it must be considered as well that the floristic population structure is also shifting, as demonstrated by Loza et al. (Loza Herrera, Meneses et al. 2015). Therefore, it is important to not assume, in multitemporal analysis, that the bofedal units remain always the same object with the same species composition and structure. Within this line, Dangles et al. (2017) suggested that one of the reasons why they found a great variability in the wetland extension between dry and humid years was that maybe their method was including certain types of humid pastures only during some very humid years and not necessarily during the dry years. This showcases some of the challenges that remote sensing tools have when it comes to interpret the data from pixels and the importance of including ground control assessments in every remote sensing study.

Aside of trying to understand the overall interannual trends of bofedales, the positive correlations of bofedales' NDVI patterns with temperature and precipitation fluctuations demonstrates that these ecosystems are sensitive to changes in climatic and hydro meteorological conditions, as also noted by other authors (Dangles, Rabatel et al. 2017,

Anderson, T. G., Christie et al. 2021, Squeo, Warner et al. 2006, Polk, Young et al. 2017, Yager, Valdivia et al. 2019).

Multiple correlation between ENSO dynamics with bofedales' trends

I ran multiple correlation analyses of bofedales' NDVI, temperature, and precipitation with the Pacific Ocean SST of the four ENSO regions to detect some signals that may explain the patterns observed in the bofedales seasonality. I found statistically significant correlations, which were also consistent across the different ENSO Regions. For example, ENSO Region 1+2, and 4, positively correlated with NDVI and with temperature and precipitation. On the other hand, that same relation was inversely proportional for Region 3. Region 3.4 didn't show statistically significant correlations with NDVI but showed in some cases positive correlation with precipitation and negative correlation with temperature.

There are different reasons for which each region may correlate with the effects on the Bolivian Altiplano. To start, the seasonal warming of Region 1+2 directly responds to the beginning of summer and the seasonal fluctuations of the Earth. As the sun radiation zenithal position moves southward of the Equator, it warms the Pacific and Atlantic oceans and it also sets the beginning of the South American Monsoon System (Liebmann, Mechoso 2011). Anomalous warming of Region 1+2 is related to some extent to the early stages of the ENSO cycle and therefore is not the best indicator of its effects even during a strong El Niño year (Philander 1983). In summary, the cyclic increments in the SST of the Pacific Ocean usually occur during the beginning of the Austral summer, which may explain why the SST of Region 1+2 correlate positively with the NDVI values of bofedales.

The inversely proportional correlation between NDVI and the SST of Region 3 suggest that bofedales are more sensitive to the increase of SST in Region 3 than in Region 3.4. Although historically Region 3.4 is known to better correlate with El Niño, Region 3 also is used to identify El Niño (Trenberth 1997). The multiple correlation between SST and meteorological events in the Altiplano also showed that temperature, and especially precipitation values, strongly decrease when the SST rises in Region 3. Since the bofedales productivity has a strong correlation with precipitation, is possible that there exists a teleconnection of the SST of Region 3 with bofedales through the negative effects on precipitation. Additionally, Region 3 SST anomalies also correlated negatively with the deseasonalized NDVI values in at least three sites. These effects suggest that bofedales are bioindicators of El Niño dynamics.

On the other hand, the increase of SST and SSTA in Region 4 is usually an indication of normal years or La Niña years. In the Bolivian Altiplano, La Niña is associated with atypical humid winters (Garreaud, R. D. 2009). Our results showed increase of SST in this region correlates with higher NDVI values. However, future research should consider lag effects.

In summary, NDVI patterns of bofedales in the Bolivian Altiplano correlated with SST in the Pacific Ocean. Further research is needed to explore the mechanisms that connect ENSO events with the bofedales productivity. My results corroborate Squeo et al. (2006), who mentioned that the biomass production of bofedales respond to the water availability and length of the growing season that depend on the ENSO dynamics. In the case of the bofedales of the Central Andes, El Niño dynamics reduce the precipitation accumulation

during the humid season, causing droughts (Cai, McPhaden et al. 2020). The studied bofedales showed this effect having lower values of NDVI when the SST in the region 3 of the Pacific Ocean was anomalously high.

Conclusion

Bofedales of the Bolivian Altiplano have a clear seasonality of their vegetation productivity. The patterns of the NDVI climatology showed statistically significant correlation with temperature and precipitation with a peak of correlation between one and two months of lag. The timeseries also correlated with the SST of the ENSO regions, which suggests that bofedales are important bioindicators of the ENSO events. Remarkably, events associated with less precipitation and drought correlated better with Region 3 than Region 3.4. The positive correlation between bofedales NDVI and SST in Region 4 suggests also that they are sensitive to La Niña events. Further research is needed to explore the mechanisms that condition the effects of ENSO events on the bofedales productivity. This is the first time that ENSO events are found to have a direct relationship with bofedales productivity applying remote sensing tools. As living systems, bofedales are accurate bioindicators of the potential impacts of the ENSO events on the high-altitude ecosystems and biodiversity.

Bibliography

ABATZOGLOU, J.T., DOBROWSKI, S.Z., PARKS, S.A. and HEGEWISCH, K.C., 2018. TerraClimate, a high-resolution global dataset of monthly climate and climatic water balance from 1958–2015. *Scientific data,* **5**(1), pp. 1-12.

AGUADO, E. and BURT, J., 2015. *UNDERSTANDING WEATHER AND CLIMATE, OLP WITH ETEXT, GLOBAL EDITION.* PEARSON EDUCATION LIMITED.

ALZÉRRECA, H., PRIETO, G., LAURA, J., LUNA, D. and LAGUNA, S., 2001. Características y distribución de los bofedales en el ámbito boliviano. *Informe Final.Subcontrato,* **21**.

AMANI, M., GHORBANIAN, A., AHMADI, S.A., KAKOOEI, M., MOGHIMI, A., MIRMAZLOUMI, S.M., MOGHADDAM, S.H.A., MAHDAVI, S., GHAHREMANLOO, M. and PARSIAN, S., 2020. Google earth engine cloud computing platform for remote sensing big data applications: A comprehensive review. *IEEE Journal of Selected Topics in Applied Earth Observations and Remote Sensing,* **13**, pp. 5326-5350.

ANDERSON, E.P., MARENGO, J., VILLALBA, R., HALLOY, S., YOUNG, B., CORDERO, D., GAST, F., JAIMES, E. and RUIZ, D., 2011. Consequences of climate change for ecosystems and ecosystem services in the tropical Andes. *Climate change and biodiversity in the tropical Andes,* **1**, pp. 1-18.

ANDERSON, T.G., CHRISTIE, D.A., CHÁVEZ, R.O., OLEA, M. and ANCHUKAITIS, K.J., 2021. Spatiotemporal peatland productivity and climate relationships across the western South American Altiplano. *Journal of Geophysical Research: Biogeosciences,* .

ANDRADE, M.F., MORENO, I., CALLE, J.M., TICONA, L., BLACUTT, L., LAVADO-CASIMIRO, W., SABINO, E., HUERTA, A., AYBAR, C. and HUNZIKER, S., 2018. Atlas-Clima y eventos extremos del Altiplano Central perú-boliviano.

APONTE-SARAVIA, J. and OSPINA-NOREÑA, J.E., 2019. Evaluando el desempeño de índices espectrales para identificar humedales alto andinos. *Revista de Teledetección,* (53), pp. 59-72.

ARAYA-LÓPEZ, R.A., LOPATIN, J., FASSNACHT, F.E. and HERNÁNDEZ, H.J., 2018. Monitoring Andean high altitude wetlands in central Chile with seasonal optical data: A comparison between Worldview-2 and Sentinel-2 imagery. *ISPRS journal of photogrammetry and remote sensing,* **145**, pp. 213-224.

BAIED, C.A. and WHEELER, J.C., 1993. Evolution of high Andean puna ecosystems: environment, climate, and culture change over the last 12,000 years in the Central Andes. *Mountain Research and Development,* , pp. 145-156.

BALDASSINI, P., VOLANTE, J.N., CALIFANO, M.L. and PARUELO, J., 2012. Caracterización regional de la estructura y de la productividad de la vegetación de la Puna mediante el uso de imágenes MODIS.

BARAER, M., MARK, B.G., MCKENZIE, J.M., CONDOM, T., BURY, J., HUH, K., PORTOCARRERO, C., GÓMEZ, J. and RATHAY, S., 2012. Glacier recession and water resources in Peru's Cordillera Blanca. *Journal of Glaciology,* **58**(207), pp. 134-150.

BECK, S.G., GARCÍA, E., THOMPSON, N., MENESES, R.I., ZENTENO, F., LÓPEZ, R.P. and FUENTES, A., 2015. Paisajes, eco-regiones y vegetación. *Historia natural de un valle en los Andes: La Paz, Bolivia,* , pp. 130-137.

BECK, S., DOMIC, A., GARCÍA, C., MENESES, R.I., YAGER, K. and HALLOY, S., 2010. *El Parque Nacional Sajama y sus Plantas. Departamento de Oruro, Bolivia.* La Paz: Herbario Nacional de Bolivia.

BERMÚDEZ, L.M., 2017. *Pachamama kawsan: hacia una ecología andina.* Pontificia Universidad Católica del Perú, Instituto de Ciencias de la ….

BHANDARI, A.K., KUMAR, A. and SINGH, G.K., 2012. Feature extraction using Normalized Difference Vegetation Index (NDVI): A case study of Jabalpur city. *Procedia technology,* **6**, pp. 612-621.

BRADLEY, R.S., VUILLE, M., DIAZ, H.F. and VERGARA, W., 2006. Climate change. Threats to water supplies in the tropical Andes. *Science (New York, N.Y.),* **312**(5781), pp. 1755-1756.

BRADLEY, R.S., KEIMIG, F.T., DIAZ, H.F. and HARDY, D.R., 2009. Recent changes in freezing level heights in the Tropics with implications for the deglacierization of high mountain regions. *Geophysical Research Letters,* **36**(17),.

BREIMAN, L., 2001. Random forests. *Machine Learning,* **45**(1), pp. 5-32.

BRITTO, B., 2017. Actualización de las ecorregiones terrestres de Perú propuestas en el Libro Rojo de Plantas Endémicas del Perú. *Gayana.Botánica,* **74**(1), pp. 15-29.

BURY, J., MARK, B.G., CAREY, M., YOUNG, K.R., MCKENZIE, J.M., BARAER, M., FRENCH, A. and POLK, M.H., 2013. New geographies of water and climate change in Peru: Coupled natural and social transformations in the Santa River watershed. *Annals of the Association of American Geographers,* **103**(2), pp. 363-374.

BUSH, M.B., HANSELMAN, J.A. and GOSLING, W.D., 2010. Nonlinear climate change and Andean feedbacks: an imminent turning point? *Global Change Biology,* **16**(12), pp. 3223-3232.

CABRERA, A.L. and WILLINK, A., 1973. *Biogeografía de América latina.* Programa Regional de Desarrollo Científico y Tecnológico Washington DC.

CAI, W., MCPHADEN, M.J., GRIMM, A.M., RODRIGUES, R.R., TASCHETTO, A.S., GARREAUD, R.D., DEWITTE, B., POVEDA, G., HAM, Y. and SANTOSO, A., 2020. Climate impacts of the El Niño–southern oscillation on South America. *Nature Reviews Earth & Environment,* **1**(4), pp. 215-231.

CANEDO-ROSSO, C., HOCHRAINER-STIGLER, S., PFLUG, G., CONDORI, B. and BERNDTSSON, R., 2019. Drought risk in the Bolivian Altiplano associated with El Niño Southern Oscillation using satellite imagery data. *Natural Hazards and Earth System Sciences Discussion,* **2019**, pp. 1-21.

CARDENAS, T., NAOKI, K., LANDIVAR, C.M., STRUELENS, Q., GÓMEZ, M.I., MENESES, R.I., CAUVY-FRAUNIÉ, S., ANTHELME, F. and DANGLES, O., 2022. Glacier influence on bird assemblages in habitat islands of the high Bolivian Andes. *Diversity and Distributions,* **28**(2), pp. 242-256.

CASAGRANDA, E., NAVARRO, C., GRAU, H.R. and IZQUIERDO, A.E., 2019. Interannual lake fluctuations in the Argentine Puna: relationships with its associated peatlands and climate change. *Regional Environmental Change,* **19**(6), pp. 1737-1750.

CENEPRED, 2022-last update, Sistema de Información para la Gestión del Riesgo de Desastres del Peru2022].

CHÁVEZ, R.O., CHRISTIE, D.A., OLEA, M. and ANDERSON, T.G., 2019. A multiscale productivity assessment of high Andean Peatlands across the Chilean Altiplano using 31 years of landsat imagery. *Remote Sensing,* **11**(24), pp. 2955.

CHIMNER, R.A., BOURGEAU-CHAVEZ, L., GRELIK, S., HRIBLJAN, J.A., CLARKE, A.M.P., POLK, M.H., LILLESKOV, E.A. and FUENTEALBA, B., 2019. Mapping mountain peatlands and wet meadows using multi-date, multi-sensor remote sensing in the Cordillera Blanca, Peru. *Wetlands,* **39**(5), pp. 1057-1067.

COCHI-MACHACA, N., CONDORI, B., ROJAS-PARDO, A., ANTHELME, F., MENESES, R.I., WEEDA, C.E. and PEROTTO-BALDIVIESO, H.L., 2018. Effects of grazing pressure on plant species composition and water presence on bofedales in the Andes mountain range of Bolivia.

COOPER, D.J., KACZYNSKI, K., SLAYBACK, D. and YAGER, K., 2015. Growth and organic carbon production in peatlands dominated by Distichia muscoides, Bolivia, South America. *Arctic Antarctic and Alpine Research,* **47**(3), pp. 505-510.

COOPER, D.J., SUELTENFUSS, J., OYAGUE, E., YAGER, K., SLAYBACK, D., CABALLERO, E.M.C., ARGOLLO, J. and MARK, B.G., 2019. Drivers of peatland water table dynamics in the central Andes, Bolivia and Peru. *Hydrological Processes,* **33**(13), pp. 1913-1925.

DANGLES, O., RABATEL, A., KRAEMER, M., ZEBALLOS, G., SORUCO, A., JACOBSEN, D. and ANTHELME, F., 2017. Ecosystem sentinels for climate change? Evidence of wetland cover changes over the last 30 years in the tropical Andes. *Plos One,* **12**(5), pp. e0175814.

DIAZ, H.F., HOERLING, M.P. and EISCHEID, J.K., 2001. ENSO variability, teleconnections and climate change. *International Journal of Climatology: A Journal of the Royal Meteorological Society,* **21**(15), pp. 1845-1862.

DIRECCION GENERAL DE AGUAS DE CHILE, 2022. *Inventario Público de Cuencas Hidrográficas y Lagos.*

DOMIC, A., MENESES, R.I., YAGER, K. and BECK, S., 2019. Qué son los bofedales altoandinos? In: A. DOMIC, R.I. MENESES, K. YAGER and S. BECK, eds, *Bofedales Altoandinos. Un oasis en la Puna.* La Paz: Herbario Nacional de Bolivia, pp. 15-32.

EARLE, L.R., WARNER, B.G. and ARAVENA, R., 2003. *Rapid development of an unusual peat-accumulating ecosystem in the Chilean Altiplano.*

FONSECA, L.R., GODOY, M.J. and GUERRERO, O.A., 2012. Los modelos de Elevación Digital (DEM) y Los Sistemas de Información Geográfica Libres Como Herramientas en el Estudio Geomorfológico de Humedales Andinos. *Mapping,* **152**, pp. 82-88.

GARCÍA, C.L., TEICH, I., GONZALEZ-ROGLICH, M., KINDGARD, A.F., RAVELO, A.C. and LINIGER, H., 2019. Land degradation assessment in the Argentinean Puna: Comparing expert knowledge with satellite-derived information. *Environmental Science & Policy,* **91**, pp. 70-80.

GARCÍA, E. and LLEELLISH, M.A., 2012. Cartografiado de bofedales usando imágenes de satélite Landsat en una cuenca altoandina del Perú. *Revista de Teledetección,* **38**, pp. 92-108.

GARCIA, E. and OTTO, M., 2015. Caracterización ecohidrológica de humedales alto andinos usando imágenes de satélite multitemporales en la cabecera de cuenca del río Santa, Ancash, Perú. *Ecología Aplicada,* **14**(2), pp. 115-125.

GARCIA, J.L. and WILLEMS, B., 2015. Metodología para el Estudio de Bofedales en Cabeceras de Cuenca Usando Datos Imágenes de los Sensores TM, OLI a bordo de los Satélites Landsat-Caso Estudio: Bofedal Chunal, Cuenca Alta del río Chillón.: Avances. *Avances.Anais XVII Simpósio Brasileiro de Sensori.INPE.Recuperado de http://www.dsr.inpe.br/sbsr2015/files/p1122.pdf,* **1122**.

GARREAUD, R.D., 2009. The Andes climate and weather. *Advances in geosciences,* **22**, pp. 3-11.

GARREAUD, R., VUILLE, M. and CLEMENT, A.C., 2003. The climate of the Altiplano: observed current conditions and mechanisms of past changes. *Palaeogeography, Palaeoclimatology, Palaeoecology,* **194**(1-3), pp. 5-22.

GONZALES, R.K., QUENTA, E., MOLINA-RODRIGUEZ, J., DANGLES, O. and JACOBSEN, D., 2014. Propuesta metodológica para estimar la heterogeneidad ambiental, diversidad y estructura de comunidades acuáticas de pozas de agua en bofedales altoandinos. *Ecología en Bolivia,* **49**(3), pp. 56-72.

GORELICK, N., HANCHER, M., DIXON, M., ILYUSHCHENKO, S., THAU, D. and MOORE, R., 2017. Google Earth Engine: Planetary-scale geospatial analysis for everyone. *Remote Sensing of Environment,* **202**, pp. 18-27.

GRABHERR, G., GOTTFRIED, M. and PAULI, H., 2000. GLORIA: a global observation research initiative in alpine environments. *Mountain Research and Development,* **20**(2), pp. 190-191.

GRIFFITH, G.E., OMERNIK, J.M. and AZEVEDO, S.H., 1998. Ecological classification of the western hemisphere. *US Environmental Protection Agency, Corvallis, Oregon,* .

GUO, M., LI, J., SHENG, C., XU, J. and WU, L., 2017. A review of wetland remote sensing. *Sensors,* **17**(4), pp. 777.

HARTMAN, B.D., BOOKHAGEN, B. and CHADWICK, O.A., 2016. The effects of check dams and other erosion control structures on the restoration of Andean bofedal ecosystems. *Restoration Ecology,* **24**(6), pp. 761-772.

HASAN, S.H., AL-HAMEEDAWI, A.N. and ISMAEL, H.S., 2022Supervised Classification Model Using Google Earth Engine Development Environment for Wasit Governorate, *IOP Conference Series: Earth and Environmental Science* 2022, IOP Publishing, pp. 012051.

HRIBLJAN, J.A., COOPER, D.J., SUELTENFUSS, J., WOLF, E.C., HECKMAN, K.A., LILLESKOV, E. and CHIMNER, R.A., 2015. Carbon storage and long-term rate of accumulation in high-altitude Andean peatlands of Bolivia. *Mires and Peat.15: article 12.14 p.,* **15**(12),.

HRIBLJAN, J.A., SUAREZ, E., BOURGEAU-CHAVEZ, L., ENDRES, S., LILLESKOV, E.A., CHIMBOLEMA, S., WAYSON, C., SEROCKI, E. and CHIMNER, R.A., 2017. Multidate, multisensor remote sensing reveals high density of carbon-rich mountain peatlands in the páramo of Ecuador. *Global Change Biology,* **23**(12), pp. 5412-5425.

IZQUIERDO, A.E., FOGUET, J. and RICARDO GRAU, H., 2015. Mapping and spatial characterization of Argentine High Andean peatbogs. *Wetlands Ecology and Management,* **23**(5), pp. 963-976.

IZQUIERDO, A.E., FOGUET, J. and GRAU, H.R., 2016. "Hidroecosistemas" de la Puna y Altos Andes de Argentina. *Acta geológica lilloana,* **28**(2), pp. 390-402.

JARA, C., DELEGIDO, J., AYALA, J., LOZANO, P., ARMAS, A. and FLORES, V., 2019. Estudio de bofedales en los Andes ecuatorianos a través de la comparación de imágenes Landsat-8 y Sentinel-2. *Revista de teledetección,* (53), pp. 45-57.

JENSEN, J.R., 2009. *Remote sensing of the environment: An earth resource perspective 2/e.* Pearson Education India.

JOMELLI, V., FAVIER, V., RABATEL, A., BRUNSTEIN, D., HOFFMANN, G. and FRANCOU, B., 2009. Fluctuations of glaciers in the tropical Andes over the last millennium and palaeoclimatic implications: A review. *Palaeogeography, Palaeoclimatology, Palaeoecology,* **281**(3-4), pp. 269-282.

JORDAN, E., 1991. Die Gletscher der bolivianischen Anden. Eine photogrammetrisch-kartographische Bestandsaufnahme der Gletscher Boliviens als Grundlage für klimatische Deutungen und Potential für die wirtschaftliche Nutzung. *Erdwissenschaftliche Forschung, .*

KANDUS, P., MINOTTI, P.G., MORANDEIRA, N.S., GRIMSON, R., GONZÁLEZ TRILLA, G., GONZÁLEZ, E.B., SAN MARTÍN, L. and GAYOL, M.P., 2018. Remote sensing of wetlands in South America: status and challenges. *International Journal of Remote Sensing,* **39**(4), pp. 993-1016.

KATIA VILLARROEL, E., PACHECO MOLLINEDO, P.L., DOMIC, A.I., CAPRILES, J.M. and ESPINOZA, C., 2014. Local Management of Andean Wetlands in Sajama National Park, Bolivia. *Mountain Research and Development,* **34**(4), pp. 356-368.

KORNER, C., 2003. *Alpine Plant Life.* 2nd Edition edn. Berlin: Springer.

LAMB, S., 2004. *Devil in the Mountain: A Search for the Origin of the Andes.* Princeton University Press.

LIEBMANN, B. and MECHOSO, C.R., 2011. The south American monsoon system. *The global monsoon system: research and forecast.* World Scientific, pp. 137-157.

LÓPEZ, R.P. and ZAMBRANA-TORRELIO, C., 2006. Representation of Andean dry ecoregions in the protected areas of Bolivia: the situation in relation to the new phytogeographical findings. *Biodiversity & Conservation,* **15**(7), pp. 2163-2175.

LOZA HERRERA, S., MENESES, R. and ANTHELME, F., 2015. Comunidades vegetales de los bofedales de la Cordillera Real (Bolivia) bajo el calentamiento global. *Ecología en Bolivia,* **50**(1), pp. 39-56.

MALDONADO FONKÉN, M.S., 2014. An introduction to the bofedales of the Peruvian high Andes. *Mires and Peat,* **15**(5),.

MALDONADO, M., NAVARRO, G., ACOSTA, F. and FERREIRA, W., 2014. Clasificación y regionalización de los humedales del Sistema TDPS. In: M. POUILLY, X. LAZZARO, D. POINT and M. AGUIRRE, eds, *Línea base de conocimientos sobre los recursos hidrológicos e hidrobiológicos en el sistema TDPS con enfoque en la cuenca del Lago Titicaca.* Quito: IRD - UICN, pp. 97-133.

MANDANICI, E. and BITELLI, G., 2016. Preliminary comparison of sentinel-2 and landsat 8 imagery for a combined use. *Remote Sensing,* **8**(12), pp. 1014.

MARK, B.G., 2008. Tracing tropical Andean glaciers over space and time: Some lessons and transdisciplinary implications. *Global and Planetary Change,* **60**(1-2), pp. 101-114.

MARK, B.G., FRENCH, A., BARAER, M., CAREY, M., BURY, J., YOUNG, K.R., POLK, M.H., WIGMORE, O., LAGOS, P., CRUMLEY, R., MCKENZIE, J.M. and LAUTZ, L., 2017. *Glacier loss and hydro-social risks in the Peruvian Andes.*

MATTEUCCI, S.D., MORELLO, J., RODRIGUEZ, A. and SILVA, M., 2012. Ecorregión Puna. *Ecorregiones y Complejos Ecosistemicos Argentinos: Buenos Aires, Orientacion Grafica SRL,* , pp. 87-127.

MAZZARINO, M. and FINN, J.T., 2016. An NDVI analysis of vegetation trends in an Andean watershed. *Wetlands Ecology and Management,* **24**(6), pp. 623-640.

MENESES, R.I., 1997. *Estudio de la vegetación en la zona minera de Milluni (provincia Murillo, departamento
de La Paz).*, Universidad Mayor de San Andrés.

MENESES, R.I., STEPHAN, G. and ANTHELME, F., 2015. *La Cordillera Real y sus plantas.* IRD; 9Herbario Nacional de Bolivia.

MENESES, R., ORTUÑO, T., LOZA HERRERA, S., DOMIC, A., PALABRAL-AGUILERA, A. and ZEBALLOS, G., 2015. Bofedales Altoandinos. In: I. MOYA, R. MENESES and J. SARMIENTO, eds, *Historia Natural de un Valle en los Andes: La Paz.* 2nd Edition edn. Museo Nacional de Historia Natural, pp. 190-205.

MITSCH, W. and GOSSELINK, J., 2015. *Wetlands.* 5th Edition edn. New Jersey: Wiley.

MOREAU, S., BOSSENO, R., GU, X.F. and BARET, F., 2003. Assessing the biomass dynamics of Andean bofedal and totora high-protein wetland grasses from NOAA/AVHRR. *Remote Sensing of Environment,* **85**(4), pp. 516-529.

MOREAU, S. and LE TOAN, T., 2003. Biomass quantification of Andean wetland forages using ERS satellite SAR data for optimizing livestock management. *Remote Sensing of Environment,* **84**(4), pp. 477-492.

MORRONE, J.J., 2002. Presentación sintética de un nuevo esquema biogeográfico de América Latina y el Caribe. *Proyecto de Red Iberoamérica de Biogeografía y Entomología Sistemática PrIBES,* , pp. 267-275.

NAVARRO, C., 2020. *Respuesta funcional de las vegas de la puna argentina a la interacción entre cambios climáticos y cambios de uso del suelo*, Universidad Nacional de Tucumán.

NAVARRO, G. and MALDONADO, M., 2011. *Geografía Ecológica de Bolivia. Vegetación y Ambientes Acuáticos.* 5a Edición edn. Santa Cruz de la Sierra: Fundación Simón I. Patiño.

OLSON, D.M., DINERSTEIN, E., WIKRAMANAYAKE, E.D., BURGESS, N.D., POWELL, G.V., UNDERWOOD, E.C., D'AMICO, J.A., ITOUA, I., STRAND, H.E. and MORRISON, J.C., 2001. Terrestrial Ecoregions of the World: A New Map of Life on EarthA new global map of terrestrial ecoregions provides an innovative tool for conserving biodiversity. *Bioscience,* **51**(11), pp. 933-938.

OTTO, M., HÖPFNER, C., CURIO, J., MAUSSION, F. and SCHERER, D., 2016. Assessing vegetation response to precipitation in northwest Morocco during the last decade: an application of MODIS NDVI and high resolution reanalysis data. *Theoretical and applied climatology,* **123**(1-2), pp. 23-41.

OTTO, M., SCHERER, D. and RICHTERS, J., 2011. Hydrological differentiation and spatial distribution of high altitude wetlands in a semi-arid Andean region derived from satellite data. *Hydrology and Earth System Sciences,* **15**(5), pp. 1713.

OTTO, M. and GIBBONS, R.E., 2017. Potential Effects of Projected Decrease in Annual Rainfall on Spatial Distribution of High Andean Wetlands in Southern Peru. *Wetlands,* **37**(4), pp. 647-659.

OYAGUE, E. and COOPER, D.J., 2020. Peatlands of the Central Andes Puna, South America. *Wetland Science & Practice,* , pp. 255-260.

OZESMI, S.L. and BAUER, M.E., 2002. Satellite remote sensing of wetlands. *Wetlands Ecology and Management,* **10**(5), pp. 381-402.

PAHLEVAN, N., CHITTIMALLI, S.K., BALASUBRAMANIAN, S.V. and VELLUCCI, V., 2019. Sentinel-2/Landsat-8 product consistency and implications for monitoring aquatic systems. *Remote Sensing of Environment,* **220**, pp. 19-29.

PAUCA-TANCO, A., RAMOS-MAMANI, C., LUQUE-FERNÁNDEZ, C.R., TALAVERA-DELGADO, C., VILLASANTE-BENAVIDES, J.F., QUISPE-TURPO, J.P. and VILLEGAS-PAREDES, L., 2020. Análisis espacio temporal y climático del humedal altoandino de Chalhuanca (Perú) durante el periodo 1986-2016. *Revista de Teledetección,* (55), pp. 105-118.

PHAN, T.N., KUCH, V. and LEHNERT, L.W., 2020. Land cover classification using Google Earth Engine and random forest classifier—The role of image composition. *Remote Sensing,* **12**(15), pp. 2411.

PHILANDER, S.G.H., 1983. El Nino southern oscillation phenomena. *Nature,* **302**(5906), pp. 295-301.

POLK, M.H., YOUNG, K.R., BARAER, M., MARK, B.G., MCKENZIE, J.M., BURY, J. and CAREY, M., 2017. *Exploring hydrologic connections between tropical mountain wetlands and glacier recession in Peru's Cordillera Blanca.*

POLK, M.H., MISHRA, N.B., YOUNG, K.R. and MAINALI, K., 2020. Greening and browning trends across Peru's diverse environments. *Remote Sensing,* **12**(15), pp. 2418.

POSTIGO, J.C., YOUNG, K.R. and CREWS, K.A., 2008. Change and continuity in a pastoralist community in the high Peruvian Andes. *Human Ecology,* **36**(4), pp. 535-551.

PRIETO, G., ALZÉRRECA, H., LAURA, J., LUNA, D. and LAGUNA, S., 2001. Características y distribución de los bofedales en el ámbito boliviano del sistema TDPS. *Uso pastoril en humedales altoandinos,* , pp. 13.

QUENTA HERRERA, E., JACOBSEN, D., CASAS, J. and DANGLES, O., 2018. Environmental and spatial filters of zooplankton metacommunities in shallow pools in high-elevation peatlands in the tropical Andes. *Freshwater Biology,* **63**(5), pp. 432-442.

QUENTA, E., MOLINA-RODRIGUEZ, J., GONZALES, K., REBAUDO, F., CASAS, J., JACOBSEN, D. and DANGLES, O., 2016. Direct and indirect effects of glaciers on aquatic biodiversity in high Andean peatlands. *Global Change Biology,* **22**(9), pp. 3196-3205.

RABATEL, A., FRANCOU, B., SORUCO, A., GOMEZ, J., CACERES, B., CEBALLOS, J.L., BASANTES, R., VUILLE, M., SICART, J.-., HUGGEL, C., SCHEEL, M., LEJEUNE, Y., ARNAUD, Y., COLLET, M., CONDOM, T., CONSOLI, G., FAVIER, V., JOMELLI, V., GALARRAGA, R., GINOT, P., MAISINCHO, L., MENDOZA, J., MENEGOZ, M., RAMIREZ, E., RIBSTEIN, P., SUAREZ, W., VILLACIS, M. and WAGNON, P., 2013. Current state of glaciers in the tropical Andes: a multi-century perspective on glacier evolution and climate change. *Cryosphere,* **7**(1), pp. 81-102.

RIVAS-MARTÍNEZ, S., NAVARRO, G., PENAS, A. and COSTA, M., 2011. Biogeographic map of South America. A preliminary survey. *International Journal of Geobotanical Research,* **1**(1), pp. 21-40.

ROCCHIO, L.E., CONNOT, P., YOUNG, S., RAMSAYER, K., OWEN, L., BOUCHARD, M. and BARNES, C., 2018. No title. *Landsat benefiting society for fifty years,* .

ROJO, V., ARZAMENDIA, Y., PÉREZ, C., BALDO, J. and VILA, B.L., 2019. Spatial and temporal variation of the vegetation of the semiarid Puna in a pastoral system in the Pozuelos Biosphere Reserve. *Environmental monitoring and assessment,* **191**(10), pp. 1-18.

Ruthsatz B. Vegetation and ecology of the high Andean peatlands of Bolivia. Phytocoenologia. 2012 DEC 31;42(3-4):133-79.

SEIMON, T.A., SEIMON, A., YAGER, K., REIDER, K., DELGADO, A., SOWELL, P., TUPAYACHI, A., KONECKY, B., MCALOOSE, D. and HALLOY, S., 2017. Long-term monitoring of tropical alpine habitat change, Andean anurans, and chytrid fungus in

the Cordillera Vilcanota, Peru: Results from a decade of study. *Ecology and evolution,* **7**(5), pp. 1527-1540.

SIEBEN, E.J., 2019. Zonal and azonal vegetation revisited: how is wetland vegetation distributed across different zonobiomes. *Austral Ecology,* **44**(3), pp. 449-460.

SORUCO, A., VINCENT, C., FRANCOU, B. and GONZALEZ, J.F., 2009. Glacier decline between 1963 and 2006 in the Cordillera Real, Bolivia. *Geophysical Research Letters,* **36**(3),.

SOTO, J., ROMÁN-FIGUEROA, C. and PANEQUE, M., 2019. A Model for Estimating the Vegetation Cover in the High-Altitude Wetlands of the Andes (HAWA). *Land,* **8**(1), pp. 20.

SQUEO, F.A., TRACOL, Y., LÓPEZ, D., GUTIÉRREZ, J.R., CORDOVA, A.M. and EHLERINGER, J.R., 2006. ENSO effects on primary productivity in Southern Atacama desert. *Advances in Geosciences,* **6**, pp. 273-277.

SQUEO, F.A., WARNER, B.G., ARAVENA, R. and ESPINOZA, D., 2006. Bofedales: high altitude peatlands of the central Andes. *Revista Chilena De Historia Natural,* **79**(2), pp. 245-255.

SUHET, 2015. *Sentinel-2 User Handbook.*

TAPIA MOLINA, G., 2014. Inventario de cuencas, subcuencas y subsubcuencas de Chile.

THIBEAULT, J.M., SETH, A. and GARCÍA, M., 2010. Changing climate in the Bolivian Altiplano: CMIP3 projections for temperature and precipitation extremes. *Journal of Geophysical Research: Atmospheres,* **115**(D8),.

THOMPSON, L.G., DAVIS, M.E., MOSLEY-THOMPSON, E., SOWERS, T.A., HENDERSON, K.A., ZAGORODNOV, V.S., LIN, P., MIKHALENKO, V.N., CAMPEN, R.K. and BOLZAN, J.F., 1998. A 25,000-year tropical climate history from Bolivian ice cores. *Science,* **282**(5395), pp. 1858-1864.

TOOTH, S., 2015. Google Earth as a resource. *Geography,* **100**(1), pp. 51-56.

TOVAR NARVÁEZ, A., 2018. Definiciones conceptuales de los ecosistemas del Perú.

TRENBERTH, K.E., 1997. The definition of el nino. *Bulletin of the American Meteorological Society,* **78**(12), pp. 2771-2778.

TUCKER, C.J., 1979. Red and photographic infrared linear combinations for monitoring vegetation. *Remote Sensing of Environment,* **8**(2), pp. 127-150.

VALOIS, R., SCHAFFER, N., FIGUEROA, R., MALDONADO, A., YÁÑEZ, E., HEVIA, A., YÁNEZ CARRIZO, G. and MACDONELL, S., 2020. Characterizing the water storage capacity and hydrological role of mountain peatlands in the arid andes of North-Central Chile. *Water,* **12**(4), pp. 1071.

VEETTIL, B.K. and KAMP, U., 2017. Remote sensing of glaciers in the tropical Andes: a review. *International Journal of Remote Sensing,* **38**(23), pp. 7101-7137.

VEETTIL, B.K., WANG, S., DE SOUZA, S.F., BREMER, U.F. and SIMÕES, J.C., 2017. Glacier monitoring and glacier-climate interactions in the tropical Andes: A review. *Journal of South American Earth Sciences,* **77**, pp. 218-246.

VINING, B.R., STEINMAN, B.A., ABBOTT, M.B. and WOODS, A., 2019. Paleoclimatic and archaeological evidence from Lake Suches for highland Andean refugia during the arid middle-Holocene. *The Holocene,* **29**(2), pp. 328-344.

VRHR and UICN, 2010. *Manual de procedimientos de delimitación y codificación de unidades hidrográficas de Bolivia.* Ministerio de Medio Ambiente y Agua.

WANG, D., WAN, B., QIU, P., SU, Y., GUO, Q., WANG, R., SUN, F. and WU, X., 2018. Evaluating the performance of sentinel-2, landsat 8 and pléiades-1 in mapping mangrove extent and species. *Remote Sensing,* **10**(9), pp. 1468.

WASHINGTON-ALLEN, R.A., RAMSEY, R.D., NORTON, B.E. and WEST, N.E., 1998. Change detection of the effect of severe drought on subsistence agropastoral communities on the Bolivian Altiplano. *International Journal of Remote Sensing,* **19**(7), pp. 1319-1333.

WHITE-NOCKLEBY, C., PRIETO, M., YAGER, K. and MENESES, R.I., 2021. Understanding Bofedales as Cultural Landscapes in the Central Andes. *Wetlands,* **41**(8), pp. 1-14.

YAGER, K., PRIETO, M. and MENESES, R.I., 2021. Reframing Pastoral Practices of Bofedal Management to Increase the Resilience of Andean Water Towers. *Mountain Research and Development,* **41**(4), pp. A1-A9.

YAGER, K., VALDIVIA, C., SLAYBACK, D., JIMENEZ, E., MENESES, R.I., PALABRAL, A., BRACHO, M., ROMERO, D., HUBBARD, A. and PACHECO, P., 2019. Socio-ecological dimensions of Andean pastoral landscape change: bridging traditional ecological knowledge and satellite image analysis in Sajama National Park, Bolivia. *Regional Environmental Change,* , pp. 1-17.

ZEBALLOS, G., SORUCO, Á, CUSICANQUI, D., JOFFRÉ, R. and RABATEL, A., 2014. Uso de imágenes satelitales, modelos digitales de elevación y sistemas de información geográfica para caracterizar la dinámica espacial de glaciares y humedales de alta montaña en Bolivia. *Ecología en Bolivia,* **49**(3), pp. 14-26.

ZIMMER, A., MENESES, R.I., RABATEL, A., SORUCO, A., DANGLES, O. and ANTHELME, F., 2018. Time lag between glacial retreat and upward migration alters tropical alpine communities. *Perspectives in Plant Ecology, Evolution and Systematics,* **30**, pp. 89-102.

ZOROGASTÚA-CRUZ, P., 2012. Dinámica de los bofedales en el altiplano peruano-boliviano. *Revista Latinoamericana de Recursos Naturales,* **8**(2), pp. 63-75.

Appendix A. Google Earth Engine Codes

A

```
var roi = ee.FeatureCollection('users/project/CORDILLERA_REAL_polygons');
Map.centerObject(roi, 10);
```

B

```
function maskS2clouds(image) {
  var qa = image.select('QA60');
  var cloudBitMask = 1 << 10;
  var cirrusBitMask = 1 << 11;
  var mask = qa.bitwiseAnd(cloudBitMask).eq(0)
      .and(qa.bitwiseAnd(cirrusBitMask).eq(0));
  return image.updateMask(mask).divide(10000);
}
```

C

```
 var collection = ee.ImageCollection('COPERNICUS/S2_SR')
                  .filterDate('2021-01-01', '2021-12-31')
                  .filter(ee.Filter.lt('CLOUDY_PIXEL_PERCENTAGE',15))
                  .map(maskS2clouds);
var composite = collection.mean();
var image2 = composite.clipToCollection(roi);
```

D

```
 var puntos =
ee.FeatureCollection('users/project/CORDILLERA_REAL_PUNTOS_2021_v2');
Map.addLayer(puntos, {}, "GPS_POINTS");
```

E

```
var bands = ['B2', 'B3', 'B4', 'B5', 'B6', 'B7', 'B8', 'B8A', 'B11', 'B12']
var label = 'Class'
var points = ee.FeatureCollection(puntos);
var training = image2.select(bands).sampleRegions({
   'collection': points,
   'properties': ['Class'],
   'scale': 10
});
```

F

```
var withRandom = training.randomColumn('random');
var split = 0.8;
var trainingPartition = withRandom.filter(ee.Filter.lt('random', split));
var testingPartition = withRandom.filter(ee.Filter.gte('random', split));
```

Figure 42. A continued figure. Script for the random forest classification. A) definition of the study area as the region of interest (roi) variable. B) script to mask out the pixels with cloud coverage. C) Definition of the Sentinel 2 satellite imagery collection and selection of the range of dates for and cloud masking function. D) Definition of the fieldwork based

points with the categories for the supervised classification. E) Definition of the bands to be used for prediction, loading of the training points, and overlay of the points on the imagery to get training. F) Addition of a column of random uniforms to the training dataset and random selection of 20% of the data for testing. G) Training process with 80% of the data. H) Classification of the test FeatureCollection. I) Create a confusion matrix representing resubstitution accuracy. J) Classification of the image. K) Get a confusion matrix representing resubstitution accuracy. Obtention of sample from the polygons and classification of the validation data. L) Obtention of a confusion matrix representing expected accuracy. M) Visualization and downloading of the result.

Figure 28 continued.

G

```
var trainedClassifier = ee.Classifier.smileRandomForest({
 'numberOfTrees': 30,
 'minLeafPopulation': 1,
 'seed': 0
 });
var trained = trainedClassifier.train(trainingPartition, label, bands);
```

H

```
var test = testingPartition.classify(trained);
```

I

```
var ConfusionMatrix80 = trained.confusionMatrix();
```

J

```
var result = image2.select(bands).classify(trained);
print('Matrix80:', ConfusionMatrix80);
```

K

```
var trainAccuracy = trained.confusionMatrix();
var validation = image2.select(bands).sampleRegions({
      'collection': points,
      'properties': ['Class'],
     'scale': 10
      }).filter(ee.Filter.neq('B2', null));
var validated = validation.classify(result);
```

L

```
var testaccuracy = validated.errorMatrix('Class', 'classification');
print('Validation error matrix: ', trained.confusionMatrix());
print('Validation overall accuracy: ', trained.confusionMatrix().accuracy());
```

M

```
var vizParams2 = {'Class':['1', '2', '3', '4', '5', '6'], 'palette': [  '006600', '3C7E18', '71EE5C', 'FFFF00',
'BFBFBF', '9BC2E6'], 'min': 1,'max': 6,};
Map.addLayer(result, vizParams2, 'result');
print(puntos);
Export.image.toDrive({
                    image: result,
                    description: 'Download',
                    folder: 'Random_Forest',
                    fileNamePrefix: 'Random_Forest_ROI',
                    region: roi.geometry(),
                    scale: 10,
                    maxPixels: 1e12,
                    fileFormat: 'GeoTIFF',
                    });
```

Appendix B. NDVI time series

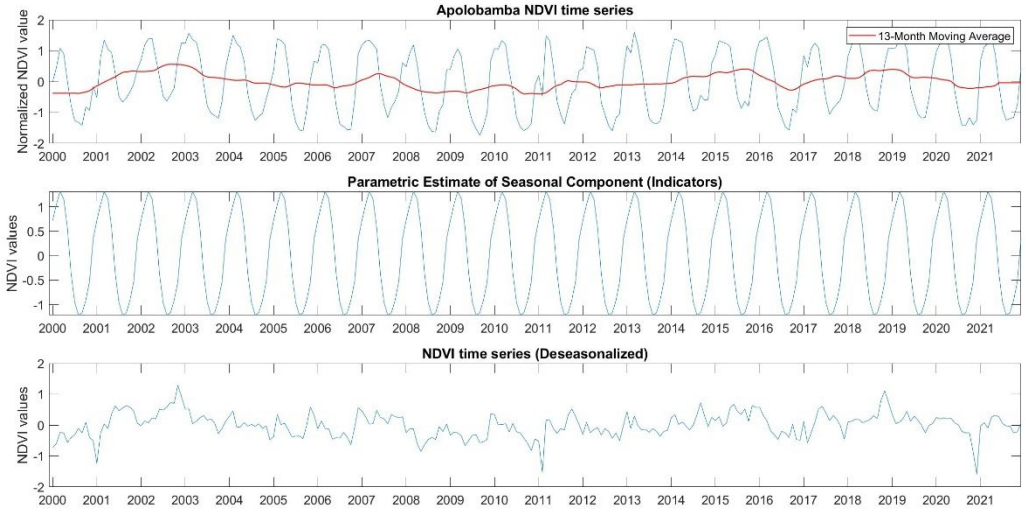

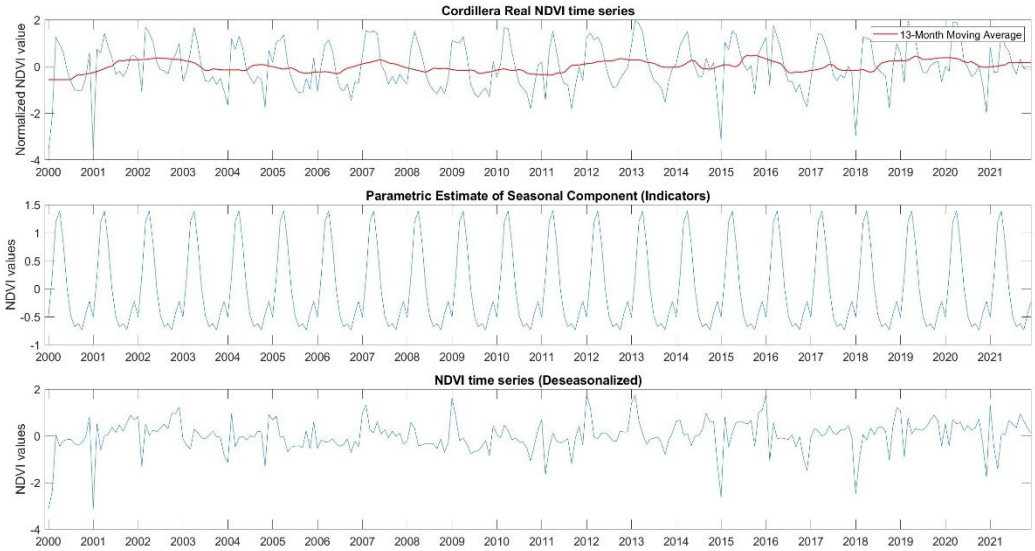

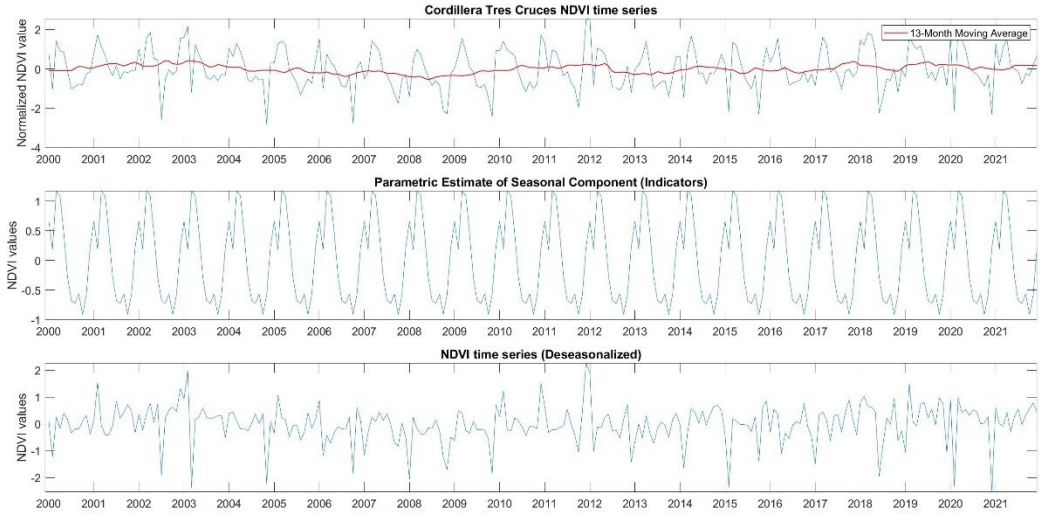
Cordillera Tres Cruces NDVI time series
Normalized NDVI value
13-Month Moving Average
Parametric Estimate of Seasonal Component (Indicators)
NDVI values
NDVI time series (Deseasonalized)
NDVI values
2000 2001 2002 2003 2004 2005 2006 2007 2008 2009 2010 2011 2012 2013 2014 2015 2016 2017 2018 2019 2020 2021

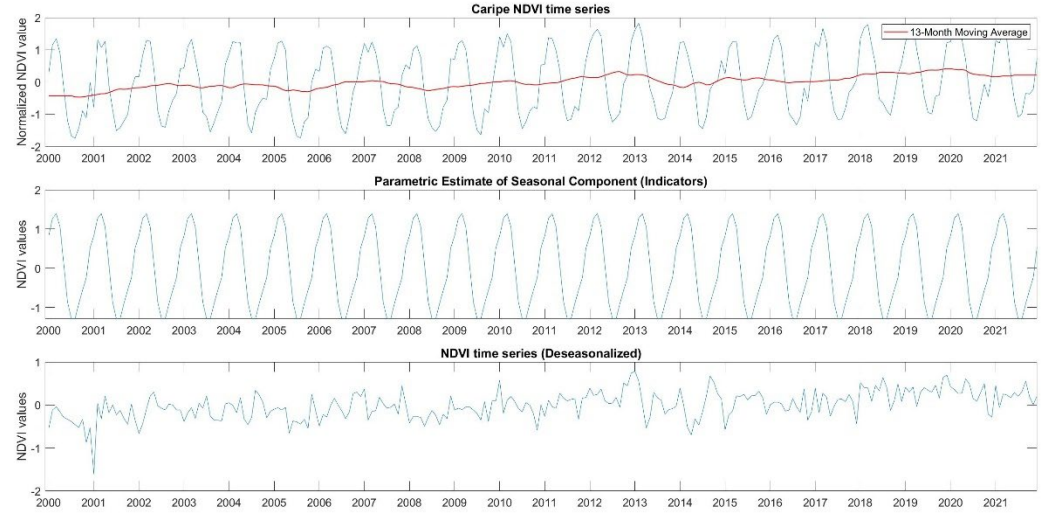
Caripe NDVI time series
Normalized NDVI value
13-Month Moving Average
Parametric Estimate of Seasonal Component (Indicators)
NDVI values
NDVI time series (Deseasonalized)
NDVI values
2000 2001 2002 2003 2004 2005 2006 2007 2008 2009 2010 2011 2012 2013 2014 2015 2016 2017 2018 2019 2020 2021

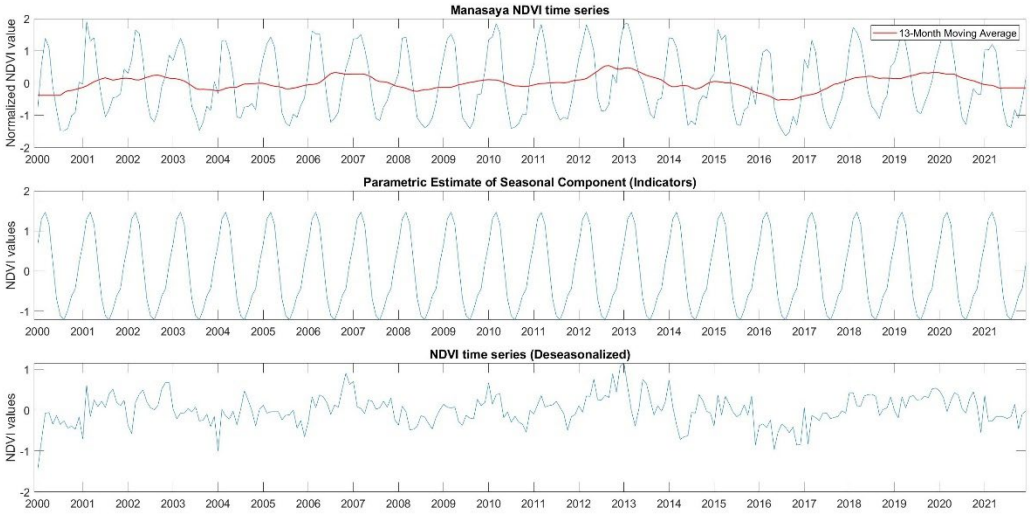
Manasaya NDVI time series
Normalized NDVI value
13-Month Moving Average
Parametric Estimate of Seasonal Component (Indicators)
NDVI values
NDVI time series (Deseasonalized)
NDVI values
2000 2001 2002 2003 2004 2005 2006 2007 2008 2009 2010 2011 2012 2013 2014 2015 2016 2017 2018 2019 2020 2021

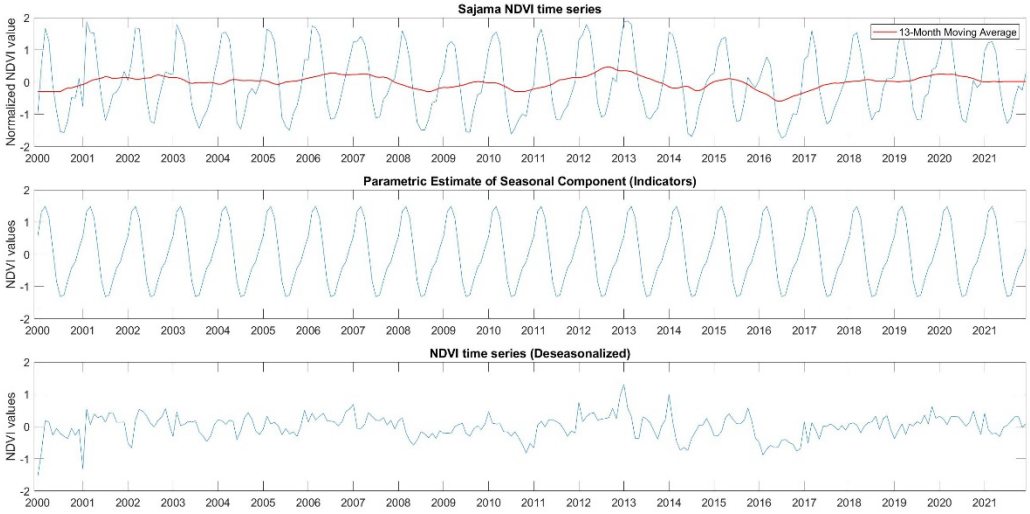
Sajama NDVI time series
Normalized NDVI value
13-Month Moving Average
Parametric Estimate of Seasonal Component (Indicators)
NDVI values
NDVI time series (Deseasonalized)
NDVI values
2000 2001 2002 2003 2004 2005 2006 2007 2008 2009 2010 2011 2012 2013 2014 2015 2016 2017 2018 2019 2020 2021

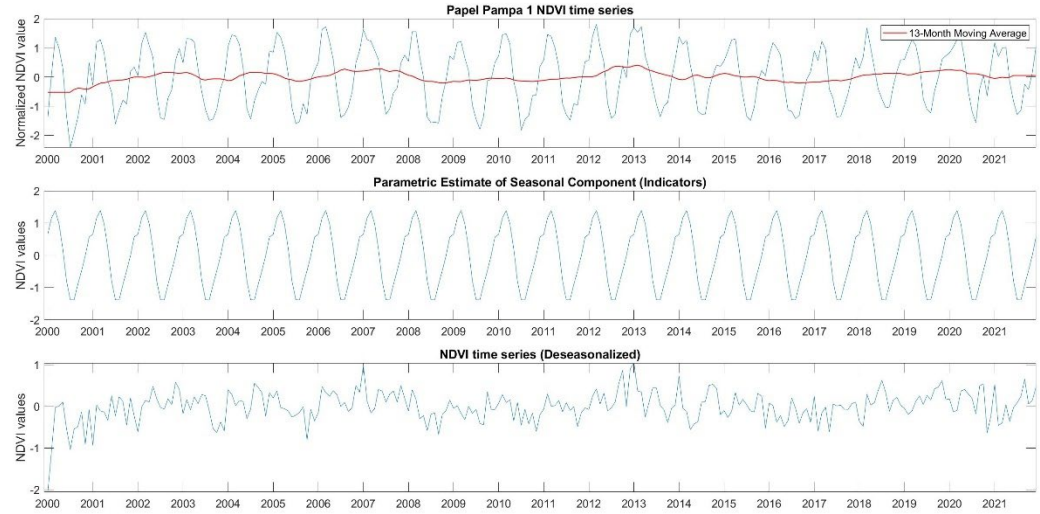
Papel Pampa 1 NDVI time series
Normalized NDVI value
13-Month Moving Average
Parametric Estimate of Seasonal Component (Indicators)
NDVI values
NDVI time series (Deseasonalized)
NDVI values
2000 2001 2002 2003 2004 2005 2006 2007 2008 2009 2010 2011 2012 2013 2014 2015 2016 2017 2018 2019 2020 2021

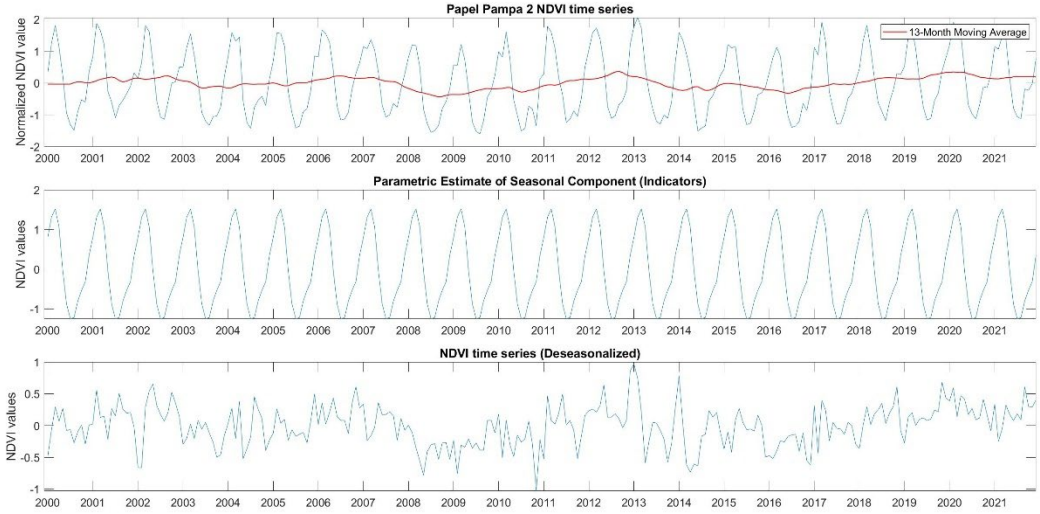
Papel Pampa 2 NDVI time series
Normalized NDVI value
13-Month Moving Average
Parametric Estimate of Seasonal Component (Indicators)
NDVI values
NDVI time series (Deseasonalized)
NDVI values
2000 2001 2002 2003 2004 2005 2006 2007 2008 2009 2010 2011 2012 2013 2014 2015 2016 2017 2018 2019 2020 2021

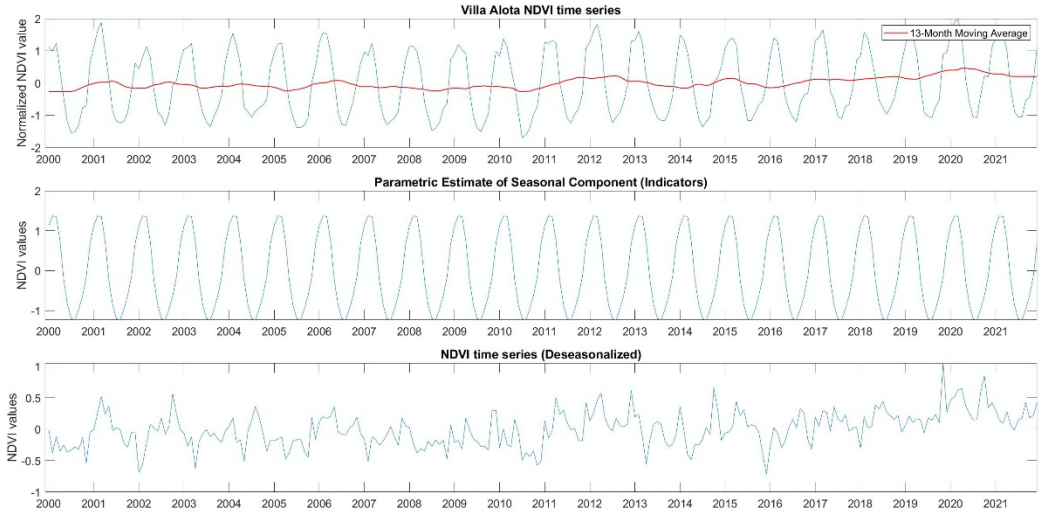
Villa Alota NDVI time series
Normalized NDVI value
13-Month Moving Average
Parametric Estimate of Seasonal Component (Indicators)
NDVI values
NDVI time series (Deseasonalized)
NDVI values
2000 2001 2002 2003 2004 2005 2006 2007 2008 2009 2010 2011 2012 2013 2014 2015 2016 2017 2018 2019 2020 2021

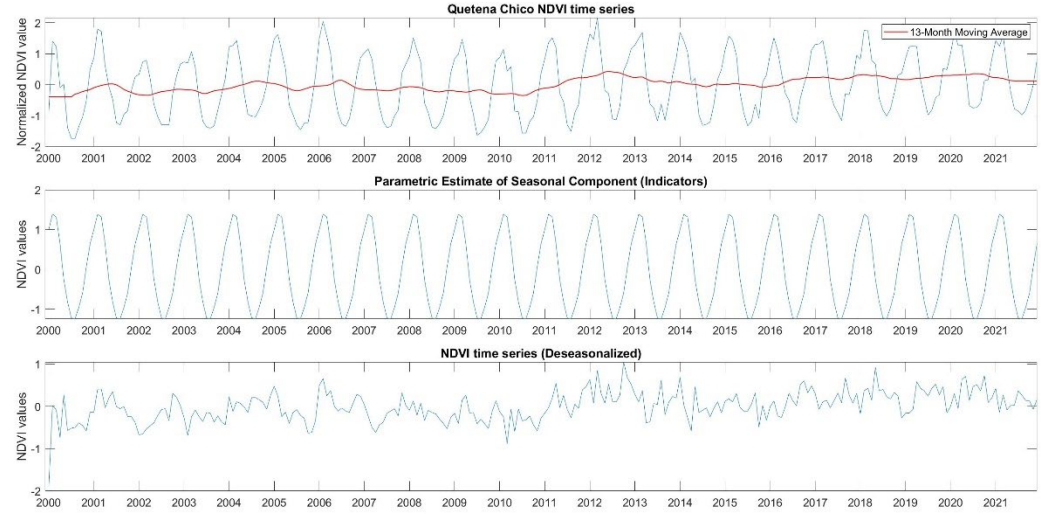
Quetena Chico NDVI time series
Normalized NDVI value
13-Month Moving Average
Parametric Estimate of Seasonal Component (Indicators)
NDVI values
NDVI time series (Deseasonalized)
NDVI values
2000 2001 2002 2003 2004 2005 2006 2007 2008 2009 2010 2011 2012 2013 2014 2015 2016 2017 2018 2019 2020 2021

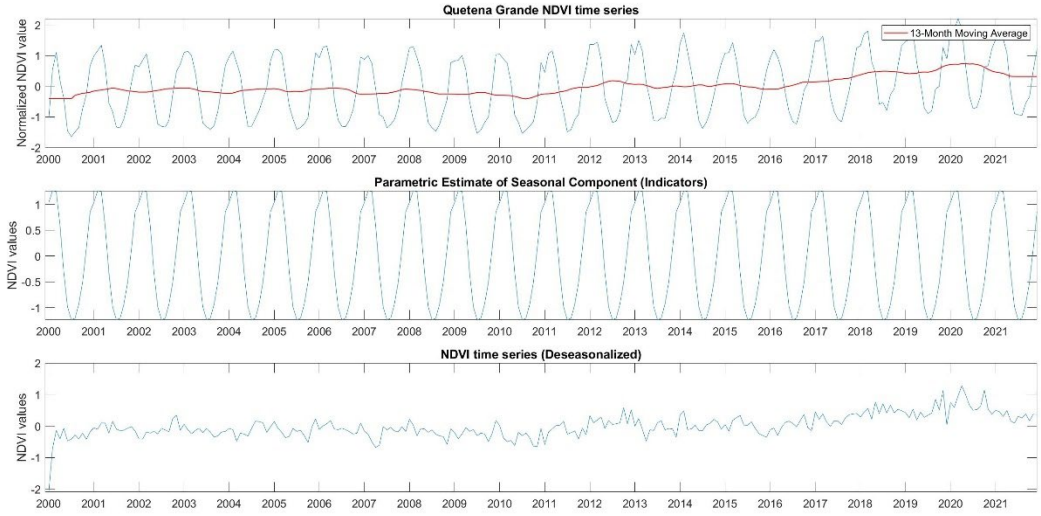
Quetena Grande NDVI time series
13-Month Moving Average
Normalized NDVI value
Parametric Estimate of Seasonal Component (Indicators)
NDVI values
NDVI time series (Deseasonalized)
NDVI values
2000
2001
2002
2003
2004
2005
2006
2007
2008
2009
2010
2011
2012
2013
2014
2015
2016
2017
2018
2019
2020
2021

Appendix C. Normalized NDVI, Temperature, and Precipitation

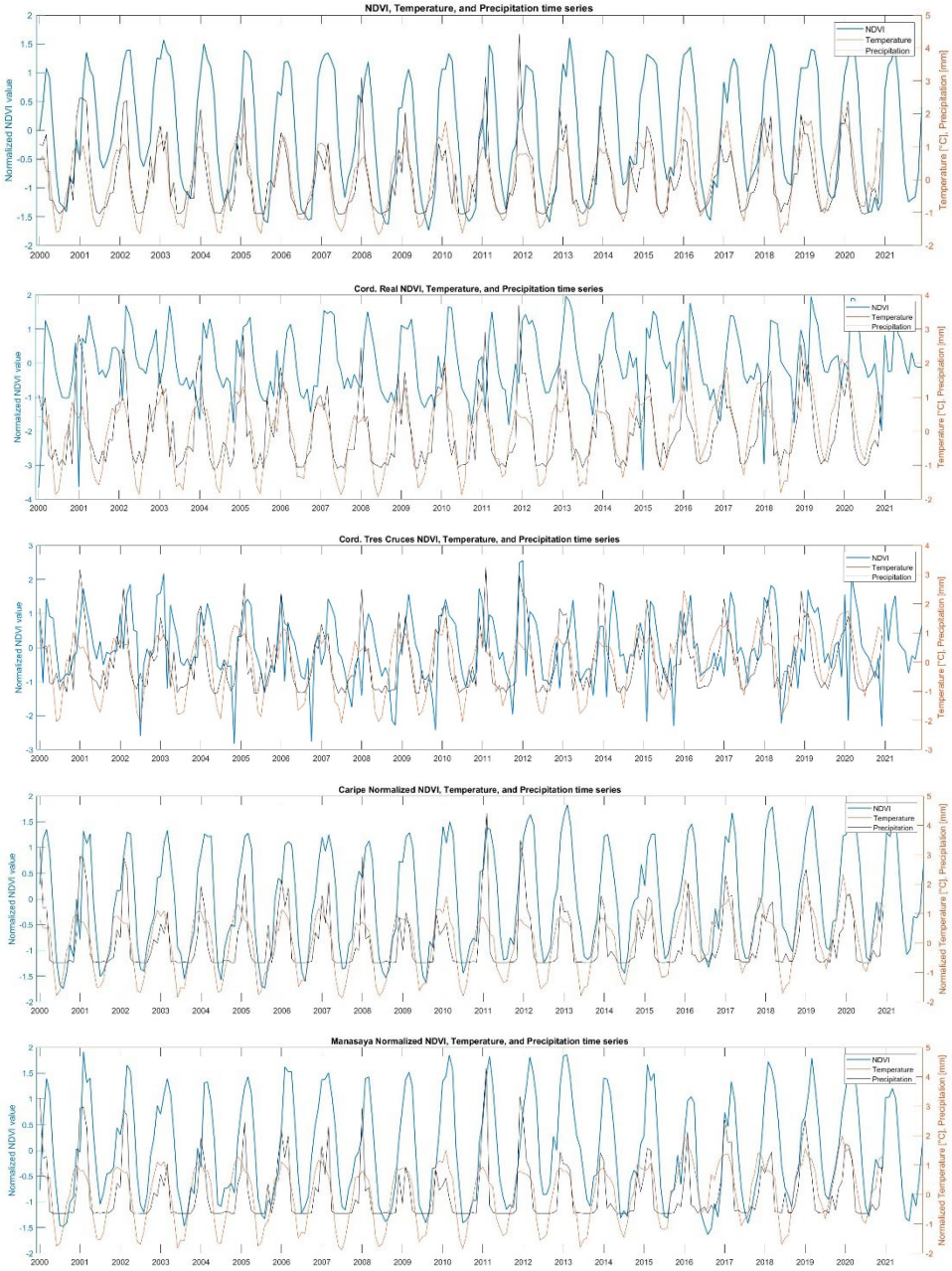

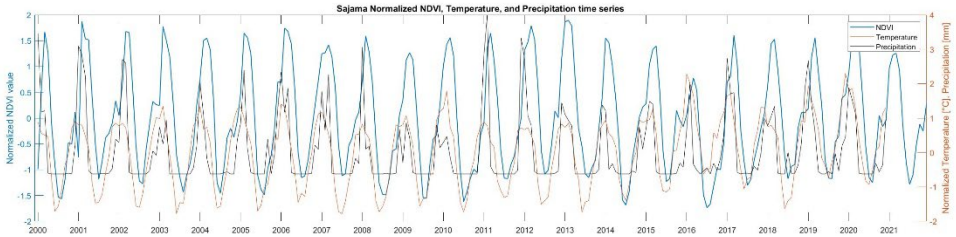
Sajama Normalized NDVI, Temperature, and Precipitation time series
NDVI
Temperature
Precipitation
Normalized NDVI value
Normalized Temperature [°C], Precipitation [mm]

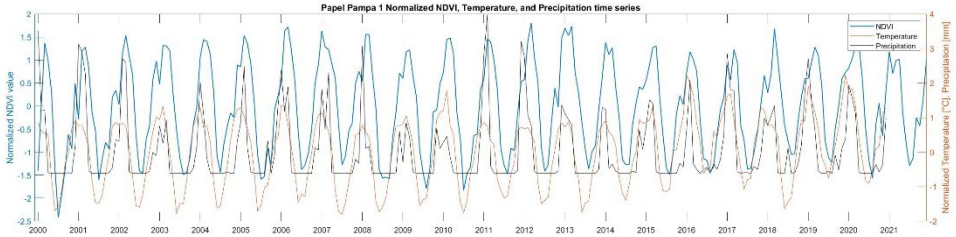
Papel Pampa 1 Normalized NDVI, Temperature, and Precipitation time series
NDVI
Temperature
Precipitation
Normalized NDVI value
Normalized Temperature [°C], Precipitation [mm]

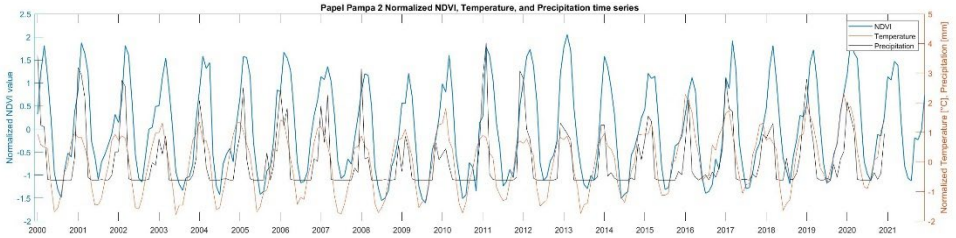
Papel Pampa 2 Normalized NDVI, Temperature, and Precipitation time series
NDVI
Temperature
Precipitation
Normalized NDVI value
Normalized Temperature [°C], Precipitation [mm]

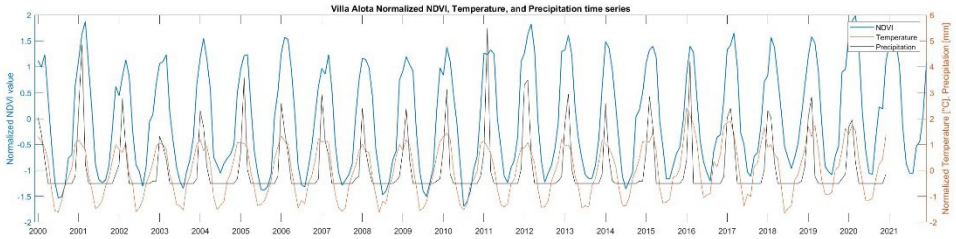
Villa Alota Normalized NDVI, Temperature, and Precipitation time series
NDVI
Temperature
Precipitation
Normalized NDVI value
Normalized Temperature [°C], Precipitation [mm]

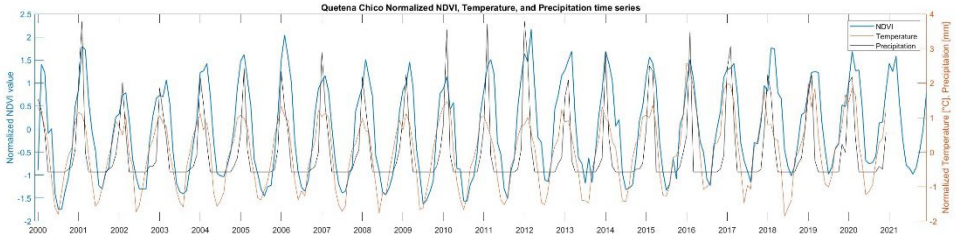
Quetena Chico Normalized NDVI, Temperature, and Precipitation time series
NDVI
Temperature
Precipitation
Normalized NDVI value
Normalized Temperature [°C], Precipitation [mm]

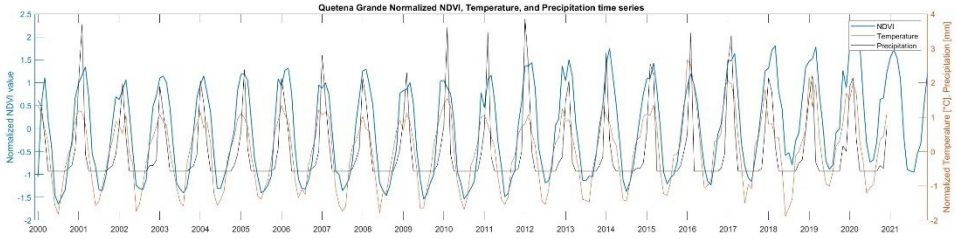
Quetena Grande Normalized NDVI, Temperature, and Precipitation time series
NDVI
Temperature
Precipitation
Normalized NDVI value
Normalized Temperature [°C], Precipitation [mm]